
REINFORCEMENT LEARNING WITH EXOGENOUS STATES AND REWARDS

A PREPRINT

George Trimponias*
Amazon
Luxembourg
trimpog@amazon.lu

Thomas G. Dietterich*
Collaborative Robotics and Intelligent Systems (CoRIS) Institute
Oregon State University, Corvallis, OR 97331 USA
tgd@cs.orst.edu

March 24, 2023

ABSTRACT

Exogenous state variables and rewards can slow reinforcement learning by injecting uncontrolled variation into the reward signal. This paper formalizes exogenous state variables and rewards and shows that if the reward function decomposes additively into endogenous and exogenous components, the MDP can be decomposed into an exogenous Markov Reward Process (based on the exogenous reward) and an endogenous Markov Decision Process (optimizing the endogenous reward). Any optimal policy for the endogenous MDP is also an optimal policy for the original MDP, but because the endogenous reward typically has reduced variance, the endogenous MDP is easier to solve. We study settings where the decomposition of the state space into exogenous and endogenous state spaces is not given but must be discovered. The paper introduces and proves correctness of algorithms for discovering the exogenous and endogenous subspaces of the state space when they are mixed through linear combination. These algorithms can be applied during reinforcement learning to discover the exogenous space, remove the exogenous reward, and focus reinforcement learning on the endogenous MDP. Experiments on a variety of challenging synthetic MDPs show that these methods, applied online, discover large exogenous state spaces and produce substantial speedups in reinforcement learning.

Keywords: Reinforcement learning, exogenous state variables, Markov Decision Processes, Markov Reward Processes, causal discovery

1 Introduction

In many practical settings, the actions of an agent have only a limited effect on the environment. For example, in a wireless cellular network, the cell tower base stations have many parameters that must be dynamically controlled to optimize network performance. We can formulate this as a Markov Decision Process (MDP) in which the reward function is the negative of the number of users who are suffering from low bandwidth. However, this reward is heavily influenced by exogenous factors such as the number, location, and behavior of the cellular network customers. Customer demand varies stochastically as a function of exogenous factors (news, sporting events, traffic accidents). In addition, atmospheric conditions can affect the capacity of each wireless channel. This high degree of stochasticity can confuse reinforcement learning algorithms, because during exploration, the benefit of trying action a in state s is hard to determine because the change in reward is obscured by the exogenous components of the reward. Many trials are required to average away these exogenous components so that the effect of the action can be measured. For temporal difference algorithms, such as Q Learning, the learning rate needs to be very small. For policy gradient algorithms, the number of Monte Carlo trials required to estimate the gradient grows very large (or equivalently, the step size must be very small). In this paper, we analyze this setting and develop algorithms for automatically detecting and removing the effects of exogenous state variables. This accelerates reinforcement learning (RL).

*Equal contributions

The first part of the paper defines exogenous state variables based on a causal foundation. It then introduces Exogenous State MDPs, which capture a broad class of MDPs with exogenous states. We characterize the space of all Exogenous State MDPs in terms of constraints on the structure of the corresponding two-time step dynamic Bayesian network. The paper analyzes the properties of exogenous subspaces of the state space and proves that every Exogenous State MDP has a unique maximal exogenous subspace that contains all other exogenous subspaces. The paper then shows that, under the assumption that the reward function decomposes additively into exogenous and endogenous components, the Bellman equation for the original MDP decomposes into two equations: one for an exogenous Markov reward process (Exo-MRP) and the other for an endogenous MDP (Endo-MDP). Importantly, every optimal policy for the Endo-MDP is an optimal policy for the full MDP.

In the second part of the paper, we identify one condition—based on the covariance between the endogenous and exogenous returns—under which solving the Endo-MDP is faster (in sample complexity) than solving the full MDP. To do this, we derive dynamic programming updates for the covariance between the H -horizon returns of the Exo-MRP and the Endo-MDP, which may be of independent interest.

The third part of the paper formulates the problem of discovering the Exo/Endo Decomposition assuming we have access to a sufficiently large and representative sample of $\langle s, a, r, s' \rangle$ tuples recorded from MDP trajectories. The problem is formalized as a constrained optimization problem where the objective is to find an exogenous subspace that minimizes the variance of the endogenous reward subject to conditional mutual information constraints that enforce the Exogenous State MDP structure. We introduce and study several variations of this constrained optimization problem. For the case of linear subspaces, the mutual information constraints can be replaced by constraints on a quantity called the conditional correlation coefficient (CCC), and this yields practical algorithms. This section concludes with a discussion of the conditions that the MDP and the exploration policy should satisfy such that the sample of $\langle s, a, r, s' \rangle$ tuples is sufficient for identifying violations of the conditional mutual information constraints and ensure that the variables in the discovered exogenous subspace are causally exogenous.

The fourth part of the paper introduces two algorithms for solving the conditional correlation formulation and studies their soundness and correctness. One algorithm solves a series of global optimization problems, and the other is a stepwise algorithm that identifies one exogenous dimension at a time. We prove the correctness of the global algorithm, and we develop some insights into when the stepwise algorithm works well.

Finally, the fifth part of the paper articulates a set of research questions and executes experiments to answer those questions. The main finding is that the Exo/Endo decomposition algorithms can discover large exogenous subspaces that yield substantial speedups in reinforcement learning for the high-performing PPO actor-critic algorithm. The experiments also study the sensitivity of our algorithms to their hyperparameters and suggest a practical strategy for setting them. We also explore the behavior of the algorithms on MDPs with nonlinear rewards, nonlinear dynamics, and discrete states. Connections to previous work are interleaved throughout the paper.

2 MDPs with Exogenous States and Rewards

We study discrete time stationary MDPs with stochastic rewards and stochastic transitions [Puterman, 1994, Sutton and Barto, 1998]; the state and action spaces may be either discrete or continuous. Notation: state space \mathcal{S} , action space \mathcal{A} , reward distribution $R: \mathcal{S} \times \mathcal{A} \mapsto \mathcal{P}(\mathbb{R})$ (where $\mathcal{P}(\mathbb{R})$ is the space of probability distributions over the real numbers), transition function $P: \mathcal{S} \times \mathcal{A} \mapsto \mathcal{P}(\mathcal{S})$ (where $\mathcal{P}(\mathcal{S})$ is the space of probability distributions over \mathcal{S}), starting state distribution $P_0 \in \mathcal{P}(\mathcal{S})$, and discount factor $\gamma \in (0, 1]$. We assume that for all $(s, a) \in \mathcal{S} \times \mathcal{A}$, $R(s, a)$ has expected value $m(s, a)$ and finite variance $\sigma^2(s, a)$. We denote random variables by capital letters (S , A , etc.) and their corresponding values by lower case letters (s , a , etc.). Table 1 summarizes the notation employed in this paper.

Let the state space \mathcal{S} take the form $\mathcal{S} = \times_{i=1}^d \mathcal{S}_i$, where \mathcal{S}_i defines the domain of the i^{th} state variable. In our problems the domain of each variable is either the real numbers or a finite, discrete set of values. Each state $s \in \mathcal{S}$ can then be written as a d -tuple of the values of these state variables $s = (s_1, \dots, s_d)$, with $s_i \in \mathcal{S}_i$. We refer to s_i as the value of the i^{th} state variable. We denote by $S_t = \times_{i=1}^d S_{t,i}$ the random vector for the state at time t . Similarly, A_t is the random variable for the action at time t , and R_t is the random variable for the reward at time t . In some formulas, instead of indexing by time, we will use “prime” notation. For example, S and S' denote the current and next states, respectively (and analogously for A and A' , R and R'). When it is clear from the context, we will also refer to S_i as the i -th state variable. In the terminology of Koller and Friedman [2009], S_i is a “template variable” that refers to the family of random variables that correspond to \mathcal{S}_i at all time steps: $\{S_{1,i}, S_{2,i}, \dots, S_{H,i}\}$.

We are interested in problems where the set of state variables S can be decomposed into endogenous and exogenous sets E and X . In the simplest case, this can be accomplished by variable selection. Following the notation of Efroni et al. [2022a], define an index set \mathcal{I} as a subset of $[d] = \{1, \dots, d\}$ and $\mathcal{I}^c = [d] \setminus \mathcal{I}$ as its complement. The variable

Symbol	Meaning
endo, exo	endogenous, exogenous
CMI	Conditional Mutual Information
CCC	Conditional Correlation Coefficient
$\mathcal{S}, \mathcal{E}, \mathcal{X}, \mathcal{A}$	State, Endo State, Exo State, and Action Spaces
S/S'	Random Vector for Current/Next State
s, a, r	Realizations of the State, Action, and Reward
S_i, S'_i, s_i	The i^{th} component of \mathcal{S}, S, s
$\mathbf{S}, \mathbf{S}', \mathbf{A}, \mathbf{R}$	Observational data for state, next state, action, reward
$\mathcal{P}(\mathcal{B})$	Space of probability distributions over space \mathcal{B}
$S = (E, X)$	Decomposition of \mathcal{S} into endo and exo sets E and X
\subseteq, \subset	Subset of, Strict (proper) subset of
$[d]$	The set $\{1, \dots, d\}$
$\mathcal{I}, \mathcal{I}^c$	Index set ($\subseteq [d]$), Complement of \mathcal{I} ($= [d] \setminus \mathcal{I}$)
$S[\mathcal{I}], S'[\mathcal{I}], s[\mathcal{I}]$	$(S_i)_{i \in \mathcal{I}}, (S'_i)_{i \in \mathcal{I}}, (s_i)_{i \in \mathcal{I}}$
$I(A; B C)$	CMI of random vectors A and B given C
$A \perp\!\!\!\perp B C$	Conditional independence of A and B given C
\mathbb{R}, \mathbb{R}^d	Set of real numbers, Real d -dimensional vector space
$\mathbb{R}^{m \times n}$	The vector space of $m \times n$ matrices over \mathbb{R}
$S \stackrel{W}{=} [E, X]$	Linear decomposition of S into endo/exo parts E and X via W
$\mathcal{A} + \mathcal{B}, \mathcal{A} \oplus \mathcal{B}$	Sum (Direct Sum) of vector spaces \mathcal{A} and \mathcal{B}
$\mathcal{A} \subseteq \mathcal{B}, \mathcal{A} \subset \mathcal{B}$	\mathcal{A} is a vector subspace (proper subspace) of vector space \mathcal{B}
\mathcal{A}^\perp	Orthogonal complement of subspace \mathcal{A} of vector space \mathcal{S}
$\dim(\mathcal{A})$	Dimension of vector subspace \mathcal{A}
$\mathbb{I}_n, \mathbf{0}^{m \times n}$	Identity matrix of size n , Matrix of zeros of size $m \times n$
W_{exo}	Matrix that defines the linear exogenous subspace
$\text{tr}(A), A^\top, \det(A)$	Trace of matrix A , Transpose of A , Determinant of A
$\ u\ _2$	Euclidean norm of vector u
Σ_{AA}, Σ_{AB}	Covariance matrix of A , Cross-covariance matrix of A, B
$\mathcal{N}(\mu, \sigma^2)$	Gaussian distribution with mean μ and variance σ^2

Table 1: Symbols and Abbreviations.

selection formulation aims to discover an index set \mathcal{I} so that the state vector $S = \times_{i=1}^d S_i$ can be decomposed into two disjoint sets of state variables $X = \times_{i \in \mathcal{I}} S_i = S[\mathcal{I}]$ and $E = \times_{i \in \mathcal{I}^c} S_i = S[\mathcal{I}^c]$. We will also denote the corresponding exo and endo state spaces as $\mathcal{X} = \times_{i \in \mathcal{I}} \mathcal{S}_i = \mathcal{S}[\mathcal{I}]$ and $\mathcal{E} = \times_{i \in \mathcal{I}^c} \mathcal{S}_i = \mathcal{S}[\mathcal{I}^c]$.

In many problems, the given state variables do not neatly separate into endogenous and exogenous subsets. Instead, we must discover a mapping $\xi : U \mapsto V$ such that the first d_{exo} dimensions of $\xi(S)$ provide the exogenous state variables, and the remaining $d - d_{exo}$ dimensions give the endogenous state variables. In this paper, we will be interested in the case where ξ is a full-rank linear transformation. In general, we will argue that ξ should be a diffeomorphism so that no information in the original space \mathcal{S} is lost in the new space $\xi(\mathcal{S})$.

2.1 Exogenous State Variables

The notion of exogeneity is fundamentally causal: a variable is exogenous if it is impossible for our actions to affect its value. We formalize this in terms of Pearl’s do-calculus.

Definition 1 (Causally-Exogenous Variables). *A set of state variables $X = S[\mathcal{I}]$ is causally exogenous for MDP \mathcal{M} with causal graph \mathcal{G} if and only if for all times $t < H$, graph \mathcal{G} encodes the conditional independence*

$$P(X_{t+1}, \dots, X_H | X_t, \text{do}(A_t = a_t)) = P(X_{t+1}, \dots, X_H | X_t) \quad \forall a_t \in \mathcal{A}. \quad (1)$$

Causal exogeneity is a qualitative property that depends only on the structure of the causal graph \mathcal{G} and not on the parameters of the probability distributions associated with each node.

Consider any state decomposition of S based on an index set $\mathcal{I} \subseteq [d]$, so that $X = S[\mathcal{I}]$ and $E = S[\mathcal{I}^c]$. Assuming the MDP is stationary, its causal graph can be described by the 2-timestep Dynamic Bayesian Network shown in Figure 1, which includes all possible edges between X , E , and actions A at the current time step and X' and E' in the next

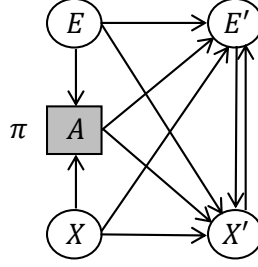


Figure 1: A fully-connected dynamic Bayesian network for state decomposition $S = (E, X)$ (reward function not shown).

time step. We have included diachronic edges (from one time step to the next) and synchronic edges (within a single time step). At most one of the two synchronic edges connecting X' and E' can be present in an MDP. In this diagram, E , X , E' , and X' denote sets of state variables, and if there is an edge between two nodes $U \rightarrow V$, it means there exists at least one edge between one variable in U and one variable in V .

We now derive a condition on the structure of the DBN causal graph that is sufficient to ensure that the variables in X are exogenous.

Theorem 1 (Full Exogenous DBN). *Any DBN with a causal graph matching the structure of Figure 2 and any DBN graph obtained by deleting edges from this structure, when unrolled for H time steps, yields an MDP for which X is causally exogenous. We call the state decomposition $S = (E, X)$ a full exo/endo decomposition with exogenous set X .*

Proof. Figure 3 shows the DBN causal graph unrolled over the H -step horizon. To obtain the result, we will apply Rule 3 of the do-calculus to remove the $\text{do}(A_t)$ action. We will treat $A_0, \dots, A_{t-1}, A_{t+1}, \dots, A_{H-1}$ as random variables distributed according to (possibly stochastic) policy π . We must show that the result holds for all possible policies.

Rule 3 states that for any causal graph \mathcal{G}

$$P(F \mid \text{do}(G), \text{do}(H), J) = P(F \mid \text{do}(G), J), \text{ if } F \perp\!\!\!\perp H \mid G \cup J \text{ in } \tilde{\mathcal{G}},$$

where $\tilde{\mathcal{G}}$ is the graph obtained by first deleting all edges pointing into G and then deleting all arrows pointing into H , if H is not an ancestor of J .

Consider the query $P(X_{t+1}, \dots, X_H \mid X_t, \text{do}(A_t))$ and apply Rule 3 with the following bindings: $F \leftarrow X_{t+1}, \dots, X_H$, $G \leftarrow \emptyset$, $H \leftarrow A_t$, and $J \leftarrow X_t$; in that case, $\tilde{\mathcal{G}}$ will be the same as \mathcal{G} , except that the incoming edges to A_t from X_t and E_t are removed.

Now apply the d -separation procedure to $\tilde{\mathcal{G}}$ by forming the graph of all variables mentioned in the query $P(X_{t+1}, \dots, X_H \mid X_t)$ and their ancestors. This ancestral graph contains only the singleton node A_t and the Markov chain $P(X_0) \cdot P(X_1 \mid X_0) \cdots P(X_{t+1} \mid X_t) \cdots P(X_H \mid X_{H-1})$. The fact that A_t is disconnected from the Markov chain establishes that $X_{t+1}, \dots, X_H \perp\!\!\!\perp A_t \mid X_t$. Applying Rule 3 gives the result. Note that the policy π plays no role in the derivation. Hence, the result applies for any possible policy.

Deleting edges from the DBN graph cannot introduce new ancestors, so X remains exogenous under edge deletion. \square

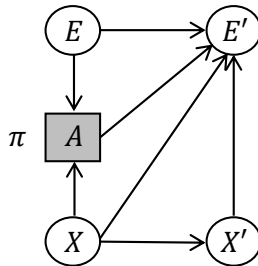


Figure 2: Restricted dynamic Bayesian network sufficient to establish that X is exogenous. We call this the “full setting” because it includes the synchronic edge from X' to E' .

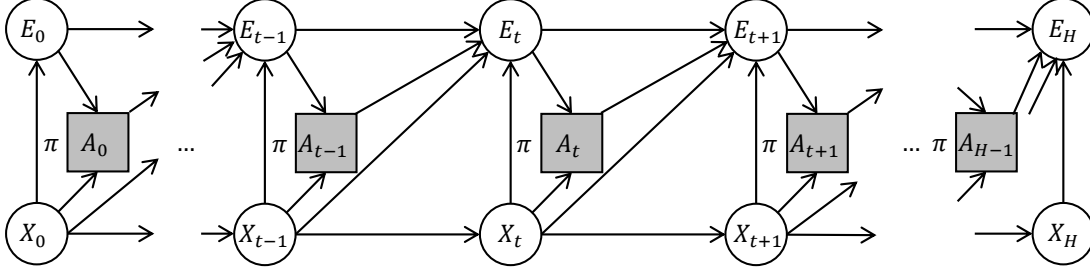


Figure 3: Unrolled state transition diagram for the full exo DBN.

Next, we examine some properties of exo/endo decompositions.

We first note that it is possible for an MDP with exogenous state variables to accept multiple exo/endo decompositions. In Figure 4, the decompositions $(X_1 = \{S_2\}, E_1 = \{S_1, S_3\})$ and $(X_2 = \{S_1, S_2\}, E_2 = \{S_3\})$ are both valid decompositions, since they match the full DBN template of Figure 2. This shows that the set E in an exo/endo decomposition (E, X) may contain additional exogenous state variables not in X .

Theorem 2 (Union of Exo/Endo Decompositions). *Assume an MDP accepts two full exo/endo decompositions (E_1, X_1) and (E_2, X_2) . Define the union of the two decompositions as the state decomposition (E, X) with $X = X_1 \cup X_2$ and $E = E_1 \cap E_2$. Then (E, X) is a full exo/endo decomposition with exo state set X .*

Proof. Because X_1 is exogenous, there are no edges from any of the remaining state variables E_1 and no edges from the action A to any variable in X_1 . Similarly, there are no edges from nodes in E_2 or A to nodes in X_2 . Hence, the union $X = X_1 \cup X_2$ also has no incoming edges from E_1 , E_2 , or A , and therefore has no incoming edges from E . This shows that the decomposition (E, X) satisfies the conditions of Theorem 1. \square

On the other hand, not every subset of exogenous state variables can yield a valid exo/endo decomposition.

Theorem 3 (Exogenous Subsets). *Let (X, E) be a full exo/endo decomposition and X_1 and X_2 be non-empty, disjoint proper subsets of X , $X_1 \cap X_2 = \emptyset$, such that their disjoint union gives back X : $X_1 \cup X_2 = X$. Then $(X_1, X_2 \cup E)$ is not necessarily a valid full exo/endo decomposition.*

Proof. By example. In Figure 4, the decomposition $X_3 = \{S_1\}, E_3 = \{S_2, S_3\}$ is not a valid full exo/endo decomposition due to the link from E_3 to X_3 (specifically the link $S_2' \rightarrow S_1'$). \square

For an MDP with exogenous state variables, we will be interested in the exo/endo decomposition where the exo set X is as large as possible. This is formalized in the next definition:

Definition 2 (Maximal Exo/Endo Decomposition). *Given an MDP, the full exo/endo decomposition (E, X) is maximal if there is no other full exo/endo decomposition (\tilde{E}, \tilde{X}) with $|\tilde{X}| > |X|$. We denote the maximal decomposition as (E_m, X_m) and call X_m the maximal exo set.*

Corollary 1 (Uniqueness of Maximal Exo/Endo Decomposition). *The maximal exo/endo decomposition of any MDP is unique.*

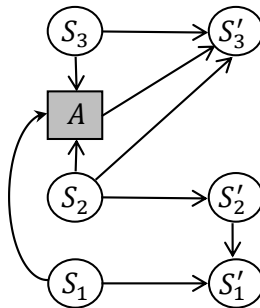


Figure 4: State transition diagram of MDP with 3 state variables.

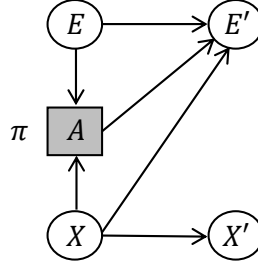


Figure 5: The Diachronic Exogenous State MDP.

Proof. By contradiction. Suppose that there are two distinct maximal decompositions (E_1, X_1) and (E_2, X_2) . By Theorem 2, their union would be a full exo/endo decomposition with an exo state set of higher cardinality. This contradicts the assumption that (E_1, X_1) and (E_2, X_2) were maximal. \square

Corollary 2 (Containment for Maximal Exo/Endo Decomposition). *For the maximal exo/endo decomposition (E_m, X_m) , it holds that $X_m \supseteq X$, where X is the exo set of any full exo/endo decomposition (E, X) .*

Proof. By contradiction. Suppose there exists a decomposition (E, X) so that $X \not\subseteq X_m$. By Theorem 2, we could take the union of (E, X) and (E_m, X_m) to get a new full exo/endo decomposition with exo set $X \cup X_m \supset X$ of higher cardinality than X . \square

In our work, we specifically focus on MDPs with exogenous state variables that match the full exogenous DBN.

Definition 3 (Exogenous State MDP). *Any MDP whose structure matches Figure 2 or any subset of its edges is called an exogenous state MDP with exo set X .*

We will analyze two types of exogenous state MDPs: The *full setting* shown in Figure 2 and the *diachronic setting* where the edge $X' \rightarrow E'$ is removed, as shown in Figure 5. Note that in the full setting, the MDP dynamics can be factored as follows

$$P(E', X' | E, X, A) = P(X' | X) \cdot P(E' | E, X, A, X'). \quad (2)$$

Similarly, in the diachronic setting, the MDP dynamics can be factored as

$$P(E', X' | E, X, A) = P(X' | X) \cdot P(E' | E, X, A). \quad (3)$$

It is useful to draw a distinction between state variables that are *causally* exogenous and state variables that are *statistically* exogenous.

Definition 4 (Statistically-Exogenous Variables). *A set of state variables $X = S[\mathcal{I}]$ is statistically exogenous in MDP \mathcal{M} if the transition probability distribution $P(E', X' | E, X, A)$ can be factored according to either (2) or (3).*

In reinforcement learning, we typically start with an MDP for which we do not know anything about the causal graph beyond the fact that it defines an MDP. However, by collecting data and fitting a model of the transition probabilities, we may infer that the MDP dynamics satisfy (2) or (3). In such cases, we can conclude that X is statistically exogenous but we cannot infer that X is causally exogenous. In Section 3.4, we will discuss additional assumptions required to conclude that a set of state variables that are statistically exogenous are also causally exogenous. In Appendix A, we provide a structural characterization of exogenous state variables and MDPs with exogenous state variables, and show that under certain conditions the maximal exo set contains all exogenous state variables, with the exception of some edge cases.

2.2 Additive Reward Decomposition

In this paper, we identify and analyze a case where reinforcement learning can be accelerated even when the exogenous variables are all relevant to the policy, the dynamics, and the reward. This case arises when the reward function can be decomposed additively into two functions, R_{exo} , which only depends on X , and R_{end} , which can depend on both X and E .

Definition 5 (Additively Decomposable Exogenous State MDP). *An Additively Decomposable Exogenous State MDP is an Exogenous State MDP whose reward function can be decomposed into the sum of two terms*

$$R(x, e, a) = R_{exo}(x) + R_{end}(x, e, a),$$

where $R_{exo}: \mathcal{X} \mapsto \mathcal{P}(\mathbb{R})$ is the exogenous reward function and $R_{end}: \mathcal{E} \times \mathcal{X} \times \mathcal{A} \mapsto \mathcal{P}(\mathbb{R})$ is the endogenous reward function. If the reward function is defined as a distribution over $\mathcal{S} \times \mathcal{A} \times \mathcal{S}$, we instead consider the decomposition $R(x, e, a, x', e') = R_{exo}(x, x') + R_{end}(x, e, a, x', e')$.

Let $m_{exo}(x)$ and $\sigma_{exo}^2(x) < \infty$ be the mean and variance of the exogenous reward distribution in state x . Similarly, let $m_{end}(e, x, a)$ and $\sigma_{end}^2(e, x, a) < \infty$ be the mean and variance of the endogenous reward distribution for state-action pair (e, x, a) .

Theorem 4. For any Additively Decomposable Exogenous State MDP with exo set X , the H -step finite-horizon Bellman optimality equation can be decomposed into two separate equations, one for a Markov Reward Process involving only X and R_{exo} and the other for an MDP (the endo-MDP) involving only R_{end}

$$V(e, x; h) = V_{exo}(x; h) + V_{end}(e, x; h) \quad (4)$$

$$V_{exo}(x; h) = m_{exo}(x) + \gamma \mathbb{E}_{x' \sim P(x'|x)} [V_{exo}(x'; h - 1)] \quad (5)$$

$$V_{end}(e, x; h) = \max_a m_{end}(e, x, a) + \mathbb{E}_{x' \sim P(x'|x); e' \sim P(e'|e, x, a)} [V_{end}(e', x'; h - 1)]. \quad (6)$$

Proof. We consider the diachronic setting; the full setting can be shown similarly by replacing $P(e' | x, e, a)$ by $P(e' | x, x', e, a)$.

Proof by induction on the horizon H . Note that the expectations could be either sums (if \mathcal{S} is discrete) or integrals (if \mathcal{S} is continuous).

Base case: $H = 1$; we take one action and terminate.

$$V(e, x; 1) = m_{exo}(x) + \max_a m_{end}(e, x, a).$$

The base case is established by setting $V_{exo}(x; 1) = m_{exo}(x)$ and $V_{end}(e, x; 1) = \max_a m_{end}(e, x, a)$.

Recursive case: $H = h$.

$$V(e, x; h) = m_{exo}(x) + \max_a \{m_{end}(e, x, a) + \mathbb{E}_{x' \sim P(x'|x); e' \sim P(e'|e, x, a)} [V_{exo}(x'; h - 1) + V_{end}(e', x'; h - 1)]\}.$$

Distribute the expectation over the sum in brackets and simplify. We obtain

$$V(e, x; h) = m_{exo}(x) + \gamma \mathbb{E}_{x' \sim P(x'|x)} [V_{exo}(x'; h - 1)] + \max_a \{m_{end}(e, x, a) + \gamma \mathbb{E}_{x' \sim P(x'|x); e' \sim P(e'|e, x, a)} [V_{end}(e', x'; h - 1)]\}.$$

The result is established by setting

$$\begin{aligned} V_{exo}(x; h) &= m_{exo}(x) + \gamma \mathbb{E}_{x' \sim P(x'|x)} [V_{exo}(x'; h - 1)] \\ V_{end}(e, x; h) &= \max_a \{m_{end}(e, x, a) + \gamma \mathbb{E}_{x' \sim P(x'|x); e' \sim P(e'|e, x, a)} [V_{end}(e', x'; h - 1)]\}. \end{aligned}$$

□

Corollary 3. Any optimal policy for the endo-MDP of Equation (6) is an optimal policy for the full exogenous state MDP.

Proof. Because $V_{exo}(s; H)$ does not depend on the policy, the optimal policy can be computed simply by solving the endo-MDP. □

We will refer to Equations (4), (5) and (6) as the Exo/Endo Decomposition of the full MDP. In the remainder of this paper, unless stated otherwise, we will work with the full setting because it is more general.

Bray (2019) proves a result similar to Theorem 4. He also identifies conditions under which value iteration and policy iteration for a fully-specified Endo-MDP can be accelerated by computing the eigenvector decomposition of the endogenous transition matrix. While such techniques are useful for MDP planning with a known transition matrix, we do not know how to exploit them in reinforcement learning where the MDP is unknown. In other related work, McGregor et al. (2017) show how to remove known exogenous state variables in order to accelerate the Model Free Monte Carlo algorithm [Fonteneau et al., 2012]. Their experiments obtain substantial improvements in policy evaluation and reinforcement learning.

2.3 Variance Analysis of the Exo/Endo Decomposition

Suppose we are given the decomposition of the state space into exogenous and endogenous sets. Under what conditions would reinforcement learning on the endogenous MDP be more efficient than on the original MDP? To explore this question, let us consider the problem of estimating the value of a fixed policy π in a given start state s_0 via Monte Carlo trials of length H . We will compare the sample complexity of estimating $V^\pi(s_0; H)$ on the full MDP to the sample complexity of estimating $V_{end}^\pi(s_0; H)$ on the Endogenous MDP. Of course most RL algorithms must do more than simply estimate $V^\pi(s_0; H)$ for fixed π , but the difficulty of estimating $V^\pi(s_0; H)$ is closely related to the difficulty of fitting a value function approximator or estimating the gradient in a policy gradient method.

Define $B^\pi(s_0; H)$ to be a random variable for the H -step cumulative discounted return of starting in state s_0 and choosing actions according to π for H steps. The expected value of $B^\pi(s_0; H)$ is the value function $V^\pi(s_0; H)$. To compute a Monte Carlo estimate of $V^\pi(s_0; H)$, we will generate N realizations b_1, \dots, b_N of $B^\pi(s_0; H)$ by executing N H -step trajectories in the MDP, each time starting in s_0 .

Theorem 5. For any $\epsilon > 0$ and any $0 < \delta < 1$, let $\hat{V}^\pi(s_0; H) = N^{-1} \sum_{i=1}^N b_i$ be the Monte Carlo estimate of the expected H -step return of policy π starting in state s_0 . If

$$N \geq \frac{\text{Var}[B^\pi(s_0; H)]}{\delta \epsilon^2}$$

then

$$P[|\hat{V}^\pi(s_0; H) - V^\pi(s_0; H)| > \epsilon] \leq \delta.$$

Proof. This is a simple application of the Chebychev Inequality,

$$P(|X - \mathbb{E}[X]| > \epsilon) \leq \frac{\text{Var}[X]}{\epsilon^2},$$

with $X = \hat{V}^\pi(s_0; H)$. The variance of the mean of N iid random variables is the variance of any single variable divided by N . Hence $\text{Var}[\hat{V}^\pi(s_0; H)] = \text{Var}[B^\pi(s_0; H)]/N$. To obtain the result, plug this into the Chebychev inequality, set the rhs equal to δ , and solve for N . \square

Now let us consider the Exo/Endo decomposition of the MDP. Let $B_{exo}^\pi(s_0; H)$ denote the H -step return of the exogenous MRP and $B_{end}^\pi(s_0; H)$ denote the return of the endogenous MDP. Then $B_x^\pi(s_0; H) + B_e^\pi(s_0; H)$ is a random variable denoting the cumulative H -horizon discounted return of the original, full MDP. Let $\text{Var}[B^\pi(s_0; H)]$ be the variance of $B^\pi(s_0; H)$ and $\text{Cov}[B_{exo}^\pi(s_0; H), B_{end}^\pi(s_0; H)]$ be the covariance between the exogenous and endogenous returns.

Theorem 6. The Chebychev upper bound on the number of Monte Carlo trials required to estimate $V^\pi(s_0; H)$ using the endogenous MDP will be reduced compared to the full MDP iff $\text{Var}[B_{exo}^\pi(s_0; H)] > -2 \text{Cov}[B_{exo}^\pi(s_0; H), B_{end}^\pi(s_0; H)]$.

Proof. From Theorem 5, we know that the sample size bound using the endogenous MDP will be less than the required sample size using the full MDP when $\text{Var}[B_{end}^\pi(s_0; H)] < \text{Var}[B_{exo}^\pi(s_0; H) + B_{end}^\pi(s_0; H)]$. The variance of the sum of two random variables is

$$\text{Var}[B_{exo}^\pi(s_0; H) + B_{end}^\pi(s_0; H)] = \text{Var}[B_{exo}^\pi(s_0; H)] + \text{Var}[B_{end}^\pi(s_0; H)] + 2\text{Cov}[B_{exo}^\pi(s_0; H), B_{end}^\pi(s_0; H)].$$

Hence,

$$\text{Var}[B_{end}^\pi(s_0; H)] < \text{Var}[B_{exo}^\pi(s_0; H) + B_{end}^\pi(s_0; H)]$$

if and only if

$$\text{Var}[B_{exo}^\pi(s_0; H)] > -2\text{Cov}[B_{exo}^\pi(s_0; H), B_{end}^\pi(s_0; H)].$$

\square

To evaluate this covariance condition, we need to compute the variance and covariance of the H -step returns. In Appendix C, we derive dynamic programming formulas for these quantities. The dynamic programs allow us to check the covariance condition of Theorem 6 in every state, including the start state s_0 , so that we can decide whether to solve the original MDP or the endo-MDP. Some special cases are easy to verify. For example, if the mean exogenous reward $m_{exo}(s) = 0$, for all states, then the covariance condition reduces to $\sigma_{exo}^2(s) > 0$.

Algorithm 1 Practical RL with the Exo/Endo Decomposition

```

1: Inputs: Decomposition steps  $L$ , Exogenous reward update steps  $M$ , Policy update steps  $K$ , Total steps  $N$ 
2: Datasets: RL training tuples  $D$ , Exogenous reward examples  $D_{exo}$ 
3: //Phase 1
4: Initialize policy and/or value networks randomly
5: for  $i = 1$  to  $L$  do
6:   Run RL to collect a new transition  $\langle s_i, a_i, r_i, s'_i \rangle$  and add it to  $D$ 
7:   if  $i \bmod K == 0$  then
8:     Update the policy using last  $K$  observations with observed rewards  $r_i$ 
9:   end if
10: end for
11: Run a state decomposition algorithm (see Section 4) on  $D$  to compute the exogenous state mapping  $\xi_{exo}$ 
12: Let  $D_{exo} \{(\xi_{exo}(s_i), r_i)\}_{i=1}^L$  be the exogenous reward training set
13: Fit the exogenous reward function  $\hat{m}_{exo}$  to  $D_{exo}$ 
14: Update  $D$  by replacing each tuple  $\langle s_i, a_i, r_i, s'_i \rangle$  by  $\langle s_i, a_i, r_i - \hat{m}_{exo}(\xi_{exo}(s_i)), s'_i \rangle$ 
15: //Phase 2
16: for  $i = L + 1$  to  $N$  do
17:   Run RL to collect a new transition  $\langle s_i, a_i, r_i, s'_i \rangle$ 
18:   Add  $(\xi_{exo}(s_i), r_i)$  to  $D_{exo}$ 
19:   Add  $\langle s_i, a_i, r_i - \hat{m}_{exo}(\xi_{exo}(s_i)), s'_i \rangle$  to  $D$ 
20:   if  $i \bmod K == 0$  then
21:     Update the policy using last  $K$  observations in  $D$ 
22:   end if
23:   if  $i \bmod M == 0$  then
24:     Update the estimate of the exogenous reward function  $\hat{m}_{exo}$  with the last  $M$  observations in  $D_{exo}$ 
25:   end if
26: end for

```

3 Decomposing an Exogenous State MDP: Optimization Formulations

We now turn our attention to discovering the exogenous variables (or exogenous subspace) of an MDP from data collected during exploration. Our overall strategy is shown in Algorithm 1. We assume we are applying an online reinforcement learning algorithm, such as PPO or Q-learning. As it interacts with the environment, it collects $\langle s_t, a_t, r_t, s_{t+1} \rangle$ experience tuples into a dataset D . After L tuples have been collected, we apply an exogenous space discovery algorithm (see Section 4) to find a function ξ_{exo} , so that $x_t = \xi_{exo}(s_t)$ computes the exogenous state x_t from state s_t . By applying ξ_{exo} to each s_t of the experience tuples, we assemble a supervised training set D_{exo} of the form $\{(x_t, r_t)\}$. We then solve a regression problem to predict as much of the reward r_t from x_t as possible. The resulting fitted function \hat{m}_{exo} is our estimate of the mean of the exogenous reward function. Because of the additive decomposition, we can therefore estimate the endogenous rewards as $\hat{r}_{end,t} := r_t - \hat{m}_{exo}(x_t)$. We then convert the set of experience tuples into modified tuples $\langle s_t, a_t, \hat{r}_{end,t}, s_{t+1} \rangle$ by replacing the original reward r_t values with our estimate of the endogenous reward and resume running the online reinforcement learning algorithm. Depending on the algorithm, we may need to re-initialize the data structures using the modified experience tuples. In any case, as the algorithm collects additional full experience tuples $\langle s_t, a_t, r_t, s_{t+1} \rangle$, each is converted to an experience tuple for the endo-MDP by replacing r_t by $\hat{r}_{end,t}$. In our experiments, we find that there is some benefit to repeating the reward regression at regular intervals, so we also add $(\xi_{exo}(s_i), r_i)$ to D_{exo} at each time step. However, we do not observe similar benefits from rerunning the exogenous space discovery algorithm, especially when the state transition function is linear, so we only execute it once.

The heart of our approach is the exogenous state discovery problem. This is easiest to discuss for the case where we are given a fixed set of state variables and our goal is to determine which state variables are exogenous and which are endogenous. Within this variable selection setting, we formulate the discovery problem as one of finding a set of variables that minimizes the residuals of the fitted exogenous reward function \hat{m}_{exo} subject to the constraint that the variables are exogenous. We formulate the exogeneity constraint in terms of conditional mutual information for both the full and the diachronic DBN structures. Then we present two variations of the optimization formulation. The first variation solves the discovery problem jointly by selecting the exogenous features that minimize the residuals of the exogenous reward regression. The second variation takes a hierarchical approach in which we first select the maximal exogenous subspace and then perform the reward regression. We will show that this two-phase algorithm finds the same

solution as the joint optimization. This is the approach adopted in Algorithm 1, because it allows us to repeat the reward regressions without recomputing the exogenous subspace.

After presenting these ideas in the context of exogenous variable selection, we then consider the most general formulation in which the exo-endo decomposition is defined by a diffeomorphism that maps from a continuous state space to a space that separates the exogenous and endogenous subspaces.

Finally, we study a practical special case in which the exogenous and endogenous spaces are defined by a linear mapping. In this setting, we show how to approximate the mutual information constraints by constraints on the conditional correlation coefficients. In Section 4, we will then present two algorithms for solving the linear formulation.

3.1 Variable Selection Formulation

The variable selection formulation aims to discover an index set \mathcal{I} with the following two properties:

- \mathcal{I} decomposes the set of state variables $S = \times_{i=1}^d S_i$ into two disjoint sets $X = \times_{i \in \mathcal{I}} S_i$ and $E = \times_{i \in \mathcal{I}^c} S_i$ that satisfy the structure of Figure 2 or Figure 5.
- The squared error of the exogenous reward regression, $\sum_t [\hat{m}_{exo}(x_t) - r_t]^2$ is minimized, where \hat{m}_{exo} regresses r_t onto $X = \times_{i \in \mathcal{I}} S_i$.

How can we state the first property in a form suitable for constrained optimization? We can express the required structure in terms of two conditional mutual information (CMI) constraints. The full setting can be enforced by the constraint

$$I(X'; [E, A] | X) = 0, \quad (7)$$

where $X = S[\mathcal{I}]$ and $E = S[\mathcal{I}^c]$. This says that if we know the value of X , then the combination of the endogenous state variables and the action carries no additional information about X' , the value of the exogenous state in the next time step. Note that this does not constrain the synchronic link $X' \rightarrow E'$.

To remove the synchronic link and enforce the diachronic structure, we can strengthen the conditional mutual information constraint as follows

$$I(X'; [E, A, E'] | X) = 0 \quad (8)$$

This says that given the exogenous state X , X' carries no information about E , A , or E' .

Note that our discovery algorithms will be evaluating these conditional mutual information constraints on the finite sample of tuples collected from exploring the MDP. Below, we will discuss the conditions that must be satisfied by the MDP and the exploration policy to ensure the soundness of these conditional mutual information computations.

3.1.1 Coupled Formulation

We can now formalize the exogenous space discovery problem for the full setting as follows

$$\begin{aligned} \mathcal{I}^*, \hat{m}_{exo}^* = & \arg \min_{\mathcal{I} \subseteq [d], \hat{m}_{exo}: \mathcal{X} \mapsto \mathbb{R}} \mathbb{E}[(\hat{m}_{exo}(X) - R)^2] \\ & \text{subject to } I(X'; [E, A] | X) = 0, X = S[\mathcal{I}], E = S[\mathcal{I}^c]. \end{aligned} \quad (9)$$

For the diachronic setting, we must use the stronger CMI constraint of Equation (8) instead.

3.1.2 Hierarchical Formulation

Formulation (9) is coupled—that is, it simultaneously involves the exo/endo state decomposition and the exogenous reward regression. The following gives an alternative hierarchical formulation that decouples the optimization of the state representation from the reward regression

$$\hat{m}_{exo}^* = \arg \min_{\hat{m}_{exo}: \mathcal{X}^* \mapsto \mathbb{R}} \mathbb{E}[(\hat{m}_{exo}(X) - R)^2], \text{ where } X^* = S[\mathcal{I}^*] \text{ and} \quad (10)$$

$$\mathcal{I}^* = \arg \max_{\mathcal{I} \subseteq [d]} |\mathcal{I}| \quad (11)$$

$$\text{subject to } I(X'; [E, A] | X) = 0, X = S[\mathcal{I}], E = S[\mathcal{I}^c]. \quad (12)$$

Formulation (10)-(12) breaks the coupled problem into two subproblems: Subproblem (11)-(12) computes the maximal exo/endo decomposition, while subproblem (10) computes the best exogenous reward estimator corresponding to the

previously-computed exo/endo decomposition. The formulation is hierarchical, since we first compute the exo/endo state representation and subsequently fit the exogenous reward function. Our ultimate goal is still to solve the coupled formulation; the hierarchical formulation serves as a computationally simpler proxy. How do the two formulations relate? Let $\mathcal{I}_{coupled}$ be the solution to the coupled formulation and \mathcal{I}_{hier} be the solution to the hierarchical formulation. The containment property of Corollary 2 implies that $\mathcal{I}_{coupled} \subseteq \mathcal{I}_{hier}$, since the maximal exo set of (11)-(12) contains the exo set of any other exo/endo decomposition, including the endo/exo decomposition of (9). It is possible that $\mathcal{I}_{coupled} \subset \mathcal{I}_{hier}$ if there are exogenous variables that carry no information about the exogenous reward function R_{exo} . The hierarchical formulation will include those variables in the reward regression, and this may increase the variance of the estimated \hat{m}_{exo} , because the regression will need to fit zero-valued weights for these irrelevant variables. The variance can be addressed in the usual way by employing L_1 regularization when fitting \hat{m}_{exo} . Hence in practice (and in the limit of infinite data), the two formulations will produce the same solution.

3.2 Continuous Formulation

In the continuous formulation, we assume that the state space $\mathcal{S} \subseteq \mathbb{R}^d$ is an open subset $U \subseteq \mathbb{R}^d$. Each $s \in \mathcal{S}$ is thus a d -dimensional real-valued vector. The discovery problem is to find a mapping $\xi : U \mapsto V$ where $V \subseteq \mathbb{R}^d$ is also an open set such that the endogenous and exogenous state spaces can be readily extracted. Without loss of generality, we stipulate that the first d_{exo} components in $\xi(\mathcal{S})$ define the exogenous state, while the remaining $d_{end} = d - d_{exo}$ components define the endogenous state. Hence, $\mathcal{I} = [d_{exo}]$, so that $\mathcal{X} = \xi(\mathcal{S})[\mathcal{I}]$ and $\mathcal{E} = \xi(\mathcal{S})[\mathcal{I}^c]$.

What conditions must the mapping ξ satisfy? It is desirable that the mapping preserve probability densities so that the resulting exo/endo MDP is equivalent to the original MDP. A natural choice is the class of *diffeomorphisms* [Tu, 2010]. A diffeomorphism from an open subset $U \subseteq \mathbb{R}^d$ to an open subset $V \subseteq \mathbb{R}^d$ is defined as a bijective map $\xi : U \mapsto V$ so that both ξ and its inverse ξ^{-1} are continuously differentiable. We denote the class of such diffeomorphisms from U to any possible open set V as \mathfrak{X}_U^d .

Diffeomorphisms have several important properties. From an information theoretic point of view, they do not lose any information about the original random variables. In particular, by using the change of variables formula, we can analytically write the probability density function of the transformation ξ using the probability density of \mathcal{S} and the Jacobian of the transformation. Assuming the density of \mathcal{S} is $p_S(s' | s, a)$, the density $p_Z(z' | z, a)$ for the transformed variables $Z = f(S)$ is given by

$$p_Z(z' | z, a) = p_S(f^{-1}(z') | f^{-1}(z), a) \cdot |\det(J_{f^{-1}}(z'))|,$$

where $J_{f^{-1}}(z')$ is the Jacobian matrix of the inverse transformation f^{-1} and $\det(\cdot)$ is the determinant. In particular, $\int_U p_S(s' | s, a) ds' = \int_V p_Z(z' | z, a) dz' = 1$. Hence, the original MDP defined on \mathcal{S} can be transformed into an equivalent MDP defined on the transformation $\xi(\mathcal{S})$. An implication of the above is that mutual information between two random vectors is preserved under diffeomorphisms [Kraskov et al., 2004]. This result can be extended to the conditional mutual information. As a result, independence and conditional independence are also preserved under diffeomorphisms, as they correspond to the special case of zero mutual or conditional mutual information.

With these assumptions, the coupled formulation takes the following form

$$\begin{aligned} \xi^*, \hat{m}_{exo}^*, d_{exo}^* &= \arg \min_{\xi \in \mathfrak{X}_S^d, \hat{m}_{exo} : \mathcal{X} \mapsto \mathbb{R}, d_{exo} \in \{0, \dots, d\}} \mathbb{E}[(\hat{m}_{exo}(X) - R)^2] \\ &\text{subject to } I(X'; [E, A] | X) = 0, \\ &\text{where } \mathcal{I} = [d_{exo}], \mathcal{X} = \xi(\mathcal{S})[\mathcal{I}], \text{ and } \mathcal{E} = \xi(\mathcal{S})[\mathcal{I}^c]. \end{aligned} \quad (13)$$

This formulation jointly optimizes the diffeomorphic state transformation and the exogenous reward function, so that the latter best fits the observed reward. Notice that the optimal d_{exo} is unknown, so the formulation for the optimal decomposition must consider all possible values for d_{exo} .

Similarly, we can define the hierarchical formulation

$$\hat{m}_{exo}^* = \arg \min_{\hat{m}_{exo} : \mathcal{X}^* \mapsto \mathbb{R}} \mathbb{E}[(\hat{m}_{exo}(X^*) - R)^2], \text{ where } \mathcal{X}^* = S[\mathcal{I}^*], \mathcal{I}^* = [d_{exo}^*], \text{ and} \quad (14)$$

$$\xi^*, d_{exo}^* = \arg \max_{\xi \in \mathfrak{X}_S^d, d_{exo} \in \{0, \dots, d\}} d_{exo} \quad (15)$$

$$\text{subject to } I(X'; [E, A] | X) = 0, \quad (16)$$

$$\text{where } \mathcal{I} = [d_{exo}], \mathcal{X} = \xi(\mathcal{S})[\mathcal{I}], \text{ and } \mathcal{E} = \xi(\mathcal{S})[\mathcal{I}^c]. \quad (17)$$

Equations (15)-(17) first compute the diffeomorphic state transformation so that the corresponding exo/endo decomposition is valid and has the highest possible number of exogenous state variables. Equation (14) subsequently estimates the exogenous reward function.

As before, we can replace the CMI constraint in these formulations with the stronger version from Equation (8) to enforce the diachronic DBN structure.

The diffeomorphic formulation provides a general framework for continuous state variables. However, diffeomorphic transformations do not usually accept a simple parameterization. They can in principle be represented by invertible neural networks [Ardizzone et al., 2019, Behrmann et al., 2021] or normalizing flows [Rezende and Mohamed, 2015, Kobayev et al., 2021]. Particular care must be taken to ensure that the corresponding mappings are not just bijective but also continuously differentiable with a continuously differentiable inverse. This can be very restrictive in practice. Recent work by Koenen et al. [2021] relaxes the definition of a diffeomorphism to allow for mappings that are bijective and continuously differentiable almost everywhere, with a set of critical points of Lebesgue measure 0. The new class of transformations, named Lebesgue-diffeomorphisms or \mathcal{L} -diffeomorphisms, is consistent with several types of normalizing flows and can thus replace the more rigid class of diffeomorphisms.

3.3 Linear Formulation

We now introduce a tractable formulation for the general class of continuous diffeomorphisms from Section 3.2. Concretely, we consider the *general linear group* $GL(d, \mathbb{R})$ of *invertible linear transformations* in vector space \mathbb{R}^d .

Instead of directly defining the full state transformation ξ , we start by defining a linear mapping ξ_{exo} from the full state space to the exogenous state space. We then define the endogenous state space as its orthogonal complement. Let ξ_{exo} be specified by a matrix $W_{exo} \in \mathbb{R}^{d \times d_{exo}}$ with $0 \leq d_{exo} \leq d$, where d_{exo} is the dimension of subspace \mathcal{X} . Given a state s , its projected exogenous state is $W_{exo}^\top \cdot s$. The endogenous subspace is the orthogonal complement of \mathcal{X} of dimension $d_{end} = d - d_{exo}$, written $\mathcal{E} = \mathcal{X}^\perp$ and defined by some matrix W_{end} . The endogenous state e contains the components of s in subspace \mathcal{E} . In the linear setting, \mathcal{E} and \mathcal{X} are vector subspaces of vector space \mathcal{S} , and we can write $\mathcal{S} = \mathcal{E} \oplus \mathcal{X}$, with $\dim(\mathcal{S}) = \dim(\mathcal{E}) + \dim(\mathcal{X})$. We will use the notation

$$\mathcal{S} \stackrel{W}{=} [E, X],$$

to denote the state-space decomposition defined by $W = (W_{exo}, W_{end})$. The matrix W is invertible with rank d , and hence, defines a linear diffeomorphism.

Let $P \in \mathcal{P}(\mathcal{S})$ denote a probability distribution over the state space. We can map this distribution into a distribution \tilde{P} in the decomposed state space through the change of variables formula:

$$\tilde{P}(X = x, E = e) = \frac{1}{|\det(W)|} P(S = W^{-1}[x, e]). \quad (18)$$

The marginal distributions $\tilde{P}(X)$ and $\tilde{P}(E)$ can be computed by marginalizing in the original space. For example,

$$\tilde{P}(X = x) = \frac{1}{|\det(W)|} \int_e P(S = W^{-1}[x, e]) de.$$

In the remainder of the paper, we will simply write $P(X)$ and $P(E)$ for the probability distributions in the transformed space.

For computational convenience, we impose the requirement that the columns of W_{exo} consist of *orthonormal* vectors, so that $W_{exo}^\top \cdot W_{exo} = \mathbb{I}_{d_{exo}}$. Linear decomposition theory [Friedberg et al., 2002] then tells us that the exogenous state can be represented in the original d -dimensional basis as $x = \xi_{exo}(s) = W_{exo} \cdot W_{exo}^\top \cdot s$, and the endogenous state $e = \xi_{end}(s) = s - x = s - W_{exo} \cdot W_{exo}^\top \cdot s$. Under this approach, $\xi_{exo}(s) + \xi_{end}(s) = x + e = s$. Every state $s \in \mathcal{S}$ can be written uniquely in this way (i.e., this is a direct sum) for a given exogenous projection matrix W_{exo} . Of course, like W_{exo} , the endogenous matrix W_{end} can also be expressed using orthonormal components.

Because diffeomorphisms preserve mutual information [Kraskov et al., 2004], the conditional mutual information constraint holds in the mapped state space

$$I(W_{exo} \cdot S'; [W_{end} \cdot S, A] | W_{exo} \cdot S) = 0$$

if and only if it holds in the original space,

$$I(X'; [E, A] | X) = 0.$$

Note that it is possible for two different matrices W_{exo} and W'_{exo} to satisfy the conditional mutual information constraint if they are related by an invertible matrix $U \in \mathbb{R}^{d_{exo} \times d_{exo}}$ as $W_{exo} = W'_{exo} \cdot U$ (and similarly for W_{end}). Hence, when we solve the coupled (Equation (13)) or hierarchical (Equations (14)-(17)) formulations, the exogenous subspace is only

identified up to multiplication by an invertible matrix U . This can make it difficult to interpret the discovered subspace. One suggestion is to put M_{exo} into block-diagonal canonical form, so that to the extent possible, the coordinates of the mapped space are the same as in the original space.

To develop the linear formulations of the discovery problem, let us consider the database D of $\{(s_i, a_i, r_i, s'_i)\}_{i=1}^N$ sample transitions collected in Algorithm 1. We start by centering s_i and s'_i by subtracting off the mean of the observed states. Let $\mathbf{S} \in \mathbb{R}^{N \times d}$, $\mathbf{A} \in \mathbb{R}^{N \times k}$, $\mathbf{R} \in \mathbb{R}^{N \times 1}$, $\mathbf{S}' \in \mathbb{R}^{N \times d}$ be the matrices containing the observations of s_i, a_i, r_i , and s'_i , respectively. These are samples from the random variables S, A, R, S' , and we will estimate the expectations required in the optimization formulations (expected squared reward regression error and CMI values) from these samples. Given observation matrices \mathbf{S}, \mathbf{S}' , we can write the corresponding exogenous and endogenous states as $\mathbf{X} = \mathbf{S} \cdot W_{exo}$, $\mathbf{X}' = \mathbf{S}' \cdot W_{exo}$, $\mathbf{E} = \mathbf{S} - \mathbf{S} \cdot W_{exo} \cdot W_{exo}^\top$, and $\mathbf{E}' = \mathbf{S}' - \mathbf{S}' \cdot W_{exo} \cdot W_{exo}^\top$.

The exogenous reward regression problem takes a particularly simple form if we adopt linear regression. Let $\hat{\mathbf{X}} = \mathbf{S} \cdot W_{exo}$ be the matrix of estimated exogenous state vectors, and let w_R^* be the fitted coefficients of the linear regression. This coefficient vector can be computed as the solution of the usual least squares problem

$$w_R^* = \arg \min_{w_R \in \mathbb{R}^{d_{exo}}} \|\hat{\mathbf{X}} \cdot w_R - \mathbf{R}\|_2^2 = \arg \min_{w_R \in \mathbb{R}^{d_{exo}}} \{(\hat{\mathbf{X}} \cdot w_R - \mathbf{R})^\top \cdot (\hat{\mathbf{X}} \cdot w_R - \mathbf{R})\} = (\hat{\mathbf{X}}^\top \hat{\mathbf{X}})^{-1} \hat{\mathbf{X}}^\top \mathbf{R}. \quad (19)$$

This gives us the optimization objective for the linear formulation. Now let us consider how to express the conditional mutual information constraints.

Estimating mutual information (and conditional mutual information) has been studied extensively in machine learning. Recent work exploits variational bounds [Donsker and Varadhan, 1983, Nguyen et al., 2007, Nowozin et al., 2016, Barber and Agakov, 2003, Blei et al., 2017] to enable differentiable end-to-end estimation of mutual information with deep nets [Belghazi et al., 2018, Poole et al., 2019, Alemi et al., 2018, Hjelm et al., 2019, van den Oord et al., 2018]. Despite their promise, mutual information estimation by maximizing variational lower bounds is challenging due to inherent statistical limitations [McAllester and Stratos, 2020]. Alternative approaches for estimating the mutual information include k-nearest neighbors [Kraskov et al., 2004], ensemble estimation [Moon et al., 2017], jackknife estimation [Zeng et al., 2018], kernel density estimation [Kandasamy et al., 2015, Han et al., 2020], and Gaussian copula methods [Singh and Póczos, 2017]. All of these require substantial computation, and some of them also require delicate hyperparameter tuning. Extending them to estimate conditional mutual information raises additional challenges.

We have chosen instead to replace conditional mutual information with a quantity we call the conditional correlation coefficient (CCC). To motivate the CCC, assume that variables X, Y, Z are distributed according to a multivariate Gaussian distribution. In this case, it is known [Baba et al., 2004] that X and Y are conditionally independent given Z , if and only if

$$\Sigma_{XY} - \Sigma_{YZ} \Sigma_{ZZ}^{-1} \Sigma_{XZ} = \mathbf{0},$$

where Σ_{AA} is the covariance matrix of A and Σ_{AB} is the cross-covariance matrix of A and B . We can normalize the above expression to obtain the normalized cross-covariance matrix

$$V(X, Y, Z) = \Sigma_{XX}^{-1/2} (\Sigma_{XY} - \Sigma_{XZ} \Sigma_{ZZ}^{-1} \Sigma_{ZY}) \Sigma_{YY}^{-1/2} = \mathbf{0}. \quad (20)$$

It is not hard to see that Equation (20) holds if and only if

$$\text{tr}(V^\top(X, Y, Z) \cdot V(X, Y, Z)) = 0,$$

where $\text{tr}(\cdot)$ is the trace function. We call the quantity $\text{tr}(V^\top(X, Y, Z) \cdot V(X, Y, Z))$ the *conditional correlation coefficient* (CCC), and we denote it by $CCC(X, Y | Z)$.² Because (20) involves matrix inversion, we apply Tikhonov regularization [Tikhonov and Arsenin, 1977] to all inverse matrices with a small positive constant $\lambda > 0$ for numerical stability. For instance, $\Sigma_{XX}^{-1/2}$ becomes $(\Sigma_{XX} + \lambda \cdot \mathbb{I}_n)^{-1/2}$, where n is the size of random vector X .

Of course, the equivalence of zero CCC and conditional independence does not necessarily hold outside of the multivariate Gaussian distribution. A more general approach, which inspired our CCC method, would be to employ kernel measures of conditional independence [Fukumizu et al., 2004, 2008]. These define normalized cross-covariance operators on reproducing kernel Hilbert spaces (RKHS) and establish that conditional independence holds if and only if the Hilbert-Schmidt norm of the operator is 0. Unfortunately, mapping our data into an RKHS would make the exogenous space discovery problem hard to optimize in terms of the underlying projection matrix W_{exo} . Instead, we directly optimize over the linearly projected data. Our experiments in Section 5 demonstrate that, despite being much simpler than kernel measures of conditional independence, our method can still provide useful results in MDPs with nonlinear dynamics.

²In Dietterich et al. [2018], we referred to this quantity as the Partial Correlation Coefficient (PCC), but this was an error. While the PCC can be used to determine conditional independence for Gaussians, it is a different quantity.

We can now express the coupled formulation of the exogenous subspace discovery problem for the full setting as follows

$$\begin{aligned}
& \min_{0 \leq d_{exo} \leq d, W_{exo} \in \mathbb{R}^{d \times d_{exo}}, w_R \in \mathbb{R}^{d_{exo}}} \|\mathbf{S} \cdot W_{exo} \cdot w_R - \mathbf{R}\|_2^2 \\
& \text{subject to } W_{exo}^\top W_{exo} = \mathbb{I}_{d_{exo}} \\
& CCC(\mathbf{S}'W_{exo}; [\mathbf{S} - \mathbf{S}W_{exo}W_{exo}^\top, \mathbf{A}] \mid \mathbf{S}W_{exo}) < \epsilon.
\end{aligned} \tag{21}$$

Note that we have relaxed the CCC constraint slightly to allow non-zero values less than a small constant ϵ .

To obtain a linear coupled formulation for the diachronic case, let

$$Y(W_{exo}) = [\mathbf{S} - \mathbf{S}W_{exo}W_{exo}^\top, \mathbf{S}' - \mathbf{S}'W_{exo}W_{exo}^\top, \mathbf{A}].$$

This creates a stacked matrix corresponding to $[\mathbf{E}, \mathbf{E}', \mathbf{A}]$. We can then write the CCC constraint for the diachronic case as

$$CCC(\mathbf{S}'W_{exo}; Y(W_{exo}) \mid \mathbf{S}W_{exo}) = 0.$$

This is the CCC equivalent of the diachronic CMI constraint of Equation (8).

The linear hierarchical formulation for the full case can be written as

$$\begin{aligned}
& \min_{w_R \in \mathbb{R}^{d_{exo}^*}} \|\mathbf{S} \cdot W_{exo}^* \cdot w_R - \mathbf{R}\|_2^2 \\
& \text{where} \\
& d_{exo}^*, W_{exo}^* = \arg \max_{d_{exo} \in \{0, \dots, d\}, W_{exo} \in \mathbb{R}^{d \times d_{exo}}} d_{exo} \\
& \text{subject to } W_{exo}^\top W_{exo} = \mathbb{I}_{d_{exo}} \\
& CCC(\mathbf{S}'W_{exo}; [\mathbf{S} - \mathbf{S}W_{exo}W_{exo}^\top, \mathbf{A}] \mid \mathbf{S}W_{exo}) < \epsilon.
\end{aligned} \tag{22}$$

Although we have written the outer objective in terms of linear regression, this is not essential. Once the optimal linear projection matrix $W_{exo}^* \in \mathbb{R}^{d \times d_{exo}^*}$ has been determined and the reward regression dataset D_{exo} has been constructed, any form of regression—including nonlinear neural network regression—can be employed.

3.4 Conditions Establishing Sound Inference

What conditions must hold so that the coupled or hierarchical optimization discovery formulations, when applied to the collected data D , find valid exo/endo decompositions? In this section, we address this question for “tabular” MDPs—that is, MDPs with finite, discrete state and action spaces. To find valid exo/endo decompositions, we need to ensure that the factorizations of Equations (2) or (3) hold in all states of the MDP. This means that our exploration policy needs to visit all states, and it needs to execute all possible actions in each state to verify that the action does not affect (either directly or indirectly) the exogenous variables. We formalize this as follows.

Consider an idealized version of Algorithm 1 that collects the tuple dataset D by executing a fixed exploration policy π_x for a large number of steps. We will require that π_x is fully randomized, according to the following definition:

Definition 6 (Fully Randomized Policy). *An exploration policy π_x is fully randomized for a tabular MDP with action space \mathcal{A} if π_x assigns non-zero probability to every possible action $a \in \mathcal{A}$ in every state $s \in \mathcal{S}$.*

We will also require that the structure of the MDP is such that a fully-randomized policy will visit every state $s \in \mathcal{S}$ infinitely often.

Definition 7 (Admissible MDP). *A tabular MDP is admissible if any fully-randomized policy will visit every state in the MDP infinitely often.*

Examples of admissible MDPs include episodic MDPs and ergodic MDPs. An episodic MDP begins each episode in a fixed start state s_0 and executes a policy until a terminal state is reached. Then it resets to the starting state. It must satisfy the requirement that all policies will reach a terminal state in a finite number of steps. The simplest episodic MDP always terminates after a fixed number of steps H , which is called the horizon time of the MDP. Note that if an episodic MDP contains states that are not reachable from the start state s_0 by *any* policy, then these must be deleted from the MDP in order to satisfy the definition of admissibility.

An ergodic MDP has the property that for all policies, every state is reachable from every other state in a finite number of steps, and the time between successive visits to any given state is aperiodic.

Theorem 7 (Soundness of Empirical Conditional Mutual Information). *Let \mathcal{M} be an admissible MDP, and let D be a set of $\langle s, a, r, s' \rangle$ tuples collected by executing fully-randomized policy π_x for n steps and recording the state, action, reward, and result state at each step. Let (X, E) be a proposed exo/endo decomposition of S . Let $\hat{P}(E, X, A, E', X')$ be the maximum-likelihood estimate of the joint distribution of the decomposed (S, A, S') triples, and let $\hat{I}(X'; E, A, E'|X)$ be the corresponding estimate of the conditional mutual information for the diachronic form. If $\lim_{n \rightarrow \infty} \hat{I}(X'; E, A, E'|X) = 0$ then (X, E) is a valid exo/endo decomposition of S .*

Proof. From the structure of an MDP, we know that the joint distribution $\hat{P}(E, A, E'X')$ can be factored as

$$\hat{P}(E, X, A, E'X') = \hat{P}(E, X)\hat{P}(A|E, X)\hat{P}(E', X'|E, X, A).$$

The first term is the empirical probability of visiting state $S = (E, X)$, the second term is the empirical estimate of π_x , and the third term is the estimated transition dynamics of the MDP. The empirical conditional mutual information can be written as

$$\hat{I}(X'; E, A, E'|X) = \sum_{E, X, A, E', X'} \hat{P}(E, X, A, E', X') \left[\log \frac{\hat{P}(X', E, A, E'|X)}{\hat{P}(X'|X)\hat{P}(E, A, E'|X)} \right].$$

If $\hat{I}(X'; E, A, E'|X) = 0$, then it is easy to show that the fraction inside the log must be equal to 1 for all (E, X, E', X', A) for which $\hat{P}(E, X, E', X', A) > 0$. As n gets large, this will hold for all possible state transitions. Hence,

$$\hat{P}(X', E, A, E'|X) = \hat{P}(X'|X)\hat{P}(E, A, E'|X). \quad (23)$$

From the structure of the MDP, we know the left-hand side of (23) can be rewritten as

$$\hat{P}(X', E, A, E'|X) = \hat{P}(X', E'|E, X, A)\hat{P}(A|E, X)\hat{P}(E|X).$$

By applying the chain rule of conditional probability, we can rewrite the right-hand side of (23) as

$$\hat{P}(X'|X)\hat{P}(E, A, E'|X) = \hat{P}(X'|X)\hat{P}(E'|E, X, A)\hat{P}(A|E, X)\hat{P}(E|X).$$

Substituting these into (23) gives

$$\hat{P}(X', E'|E, X, A)\hat{P}(A|E, X)\hat{P}(E|X) = \hat{P}(X'|X)\hat{P}(E'|E, X, A)\hat{P}(A|E, X)\hat{P}(E|X).$$

Because the MDP is admissible and π_x is fully randomized, then for n sufficiently large,

$$\begin{aligned} \hat{P}(A|E, X) &> 0 \quad \forall E, X, A \\ \hat{P}(E|X) &> 0 \quad \forall E, X. \end{aligned}$$

Hence, we can cancel them from both sides of the equation to obtain

$$\hat{P}(X', E'|E, X, A) = \hat{P}(X'|X)\hat{P}(E'|E, X, A).$$

As $n \rightarrow \infty$, all estimates will converge to their true values, and we will obtain

$$P(X', E'|E, X, A) = P(X'|X)P(E'|E, X, A), \quad (24)$$

which is the factorization for the diachronic Exogenous State MDP. This proves that (X, E) is a valid exo/endo decomposition of the diachronic form.

Because we know the exploration policy π_x , we could replace $\hat{P}(A|E, X)$ by $\pi_x(A|E, X)$ throughout this derivation. Note also that $P(E', X'|E, X, A)$ will be zero for states $S' = (E', X')$ that cannot be directly reached from (E, X) by any action A . This is not a problem, because the conditional mutual information formula is only concerned with the terms where $P(E, X, A, E', X') > 0$. \square

An analogous theorem and proof can easily be provided for Exogenous State MDPs of the full form.

For purposes of computing a valid exo/endo decomposition that respects the full or diachronic factorization, this theorem suffices. But it only shows that the variables in X are statistically exogenous. We might also wish to prove that they are causally exogenous according to Definition 1. To apply this definition, we need a causal graph. To infer the structure of a causal graph from observational data, we can make the following faithfulness assumption [Spirtes et al., 2000].

Assumption 1 (Faithfulness). *The set of conditional independencies exhibited by the observed distribution $P(S'|S, A)$ is exactly the set of conditional independencies entailed by the causal graph of the MDP.*

Corollary 4. *If the conditions of Theorem 7 hold, the underlying structural causal model has the structure of a stationary MDP, and the causal model satisfies the faithfulness assumption, then the set X satisfies the causal definition of exogeneity in Definition 1.*

Proof. From the assumptions (faithfulness, MDP structure, and Theorem 7), we know that every probabilistic dependency (and independency) implied by the structure of the causal graph will be exhibited by the observed data D .

Consider the diachronic setting first. Assume that any of the links $E \rightarrow X$, $A \rightarrow X$ or $E' \rightarrow X$ were present in the causal graph \mathcal{G} . In that case, variables E , A , E' are not d -separated from X' given X . But then faithfulness would imply that $X' \not\perp\!\!\!\perp E, A, E' \mid X$, which is a contradiction. Hence the causal graph has the form of Figure 5.

For the full setting, we can similarly show the links $A \rightarrow X$ and $E \rightarrow X$ must be missing. What about link $E' \rightarrow X'$? Assume that such a link indeed exists in \mathcal{G} . Consider any state variable E'_i in set E' , so that the link $E'_i \rightarrow X'$ is present. If either link $A \rightarrow E'_i$ or $E \rightarrow E'_i$ is present, then there is a directed path from A (or E) to X' through E'_i . But in that case variables A (or E) and X' are not d -separated given X , so the faithfulness assumption implies that $X' \not\perp\!\!\!\perp A \mid X$ (or $X' \not\perp\!\!\!\perp E \mid X$), which is a contradiction. What if there is no link from A or E to E'_i ? In that case, we can immediately see that both X and E'_i are causally exogenous. Hence the causal graph has the form of Figure 2.

In summary, if the conditional mutual information $I(X'; E, A, E' \mid X)$ is zero, then the factorization in (24) matches the structure of the causal graph \mathcal{G} , and the set X satisfies the causal definition of exogeneity. \square

Note that if the faithfulness assumption does not hold, then the set X may contain variables that coincidentally satisfy the factorization of (24) but are not causally exogenous. However, if X is a maximal set of exogenous variables, then we know that it contains all of the causally exogenous variables (and possibly others).

In our experiments, we initialize our chosen reinforcement learning algorithm, PPO, to implement a fully-randomized policy. However, as PPO is an on-policy RL algorithm, the policy gradually departs from full randomization, and we lose any guarantee that all states will be visited and all actions exercised. Consequently, the resulting exogenous sets X may not be valid.

4 Algorithms for Decomposing an MDP into Exogenous and Endogenous Components

This section introduces two practical algorithms for addressing the exogenous subspace discovery problem. The first algorithm, GRDS (Global Rank Descending Scheme), is based on the linear hierarchical formulation of Equation (22). It initializes d_{exo} to d and decreases d_{exo} one dimension at a time until it can find a W_{exo} matrix whose CCC is near zero. We refer to it as a ‘‘global’’ scheme, because it must solve a series of global manifold optimization problems. The second algorithm, SRAS (Stepwise Rank-Ascending Scheme), starts with $d_{exo} := 0$ and constructs the W_{exo} matrix by adding one column at a time as long as it can keep CCC near zero. SRAS only needs to solve one-dimensional manifold optimization problems, so it has the potential to be faster.

4.1 GRDS: Global Rank Descending Scheme

Algorithm 2 gives the pseudo-code for the global rank descending scheme, GRDS. GRDS solves the inner objective (Equation (22)) by iterating from $d_{exo} := d$ down to zero. Instead of treating the $CCC < \epsilon$ condition as a constraint, we put CCC into the objective and minimize it (line 6). If the optimization finds a W_{exo} with $CCC < \epsilon$, we know that this gives the maximum value, d_{exo}^* . Hence, we can halt and return W_{exo} as the solution.

One might hope that we could use a more efficient search procedure, such as binary search, to find d_{exo}^* . Unfortunately, because not all subsets of the maximal exogenous subspace are valid decompositions (Theorem 3), it is possible for an exogenous subset with $\hat{d} < d_{exo}^*$ to violate the $CCC < \epsilon$ constraint.

The orthonormality constraint in the minimization (line 6) forces the weight matrix W_{exo} to lie on a Stiefel manifold [Stiefel, 1935]. Hence, line 6 seeks to minimize a function on a manifold, a problem to which we can apply familiar tools for Euclidean spaces such as gradient descent, steepest descent and conjugate gradient. Several optimization algorithms exist for optimizing on Stiefel manifolds [Jiang and Dai, 2015, Absil et al., 2007, Edelman et al., 1999]. Manifold optimization on a Stiefel manifold has previously been considered by Bach and Jordan [2003] in the context of Independent Component Analysis, but in their case the linearly projected data are subsequently mapped to a Reproducing Kernel Hilbert Space (RKHS).

Algorithm 2 GRDS: Global Rank-Descending Scheme

```

1: Inputs: A database of transitions  $\{(s_i, a_i, s'_i)\}_{i=1}^N$  provided as matrices  $\mathbf{S}, \mathbf{A}, \mathbf{S}'$ 
2: Output: The exogenous state projection matrix  $W_{exo}^*$ 
3: for  $d_{exo} = d$  down to 1 do
4:   Set  $Y(W_{exo}) \leftarrow [\mathbf{S} - \mathbf{S}W_{exo}W_{exo}^\top, \mathbf{S}' - \mathbf{S}'W_{exo}W_{exo}^\top, \mathbf{A}]$  for the diachronic setting
5:   or  $Y(W_{exo}) \leftarrow [\mathbf{S} - \mathbf{S}W_{exo}W_{exo}^\top, \mathbf{A}]$  for the full setting
6:   Solve the following optimization problem
           
$$W_{exo}^* := \arg \min_{W_{exo} \in \mathbb{R}^{d \times d_{exo}}} CCC(\mathbf{S}'W_{exo}; Y(W_{exo}) \mid \mathbf{S}W_{exo})$$

           
$$\text{subject to } W_{exo}^\top W_{exo} = \mathbb{I}_{d_{exo}}$$

7:   Set  $CCC \leftarrow CCC(\mathbf{S}'W_{exo}^*; Y(W_{exo}^*) \mid \mathbf{S}W_{exo}^*)$ 
8:   if  $CCC < \epsilon$  then
9:     return  $W_{exo}^*$ 
10:  end if
11: end for
12: return null projection  $\mathbf{0}$ 

```

4.2 Analysis of the Global Rank-Descending Scheme

In this section, we study the properties of the global rank-descending scheme. We assume that we fit the exo reward function using linear regression (19), since this simplifies our analysis. Directly analyzing Algorithm 2 is hard, because it (i) uses the CCC objective as a proxy for conditional independence, (ii) involves estimation errors due to having a finite number of samples, and (iii) involves approximations in the optimization (both from numerical errors and from the ϵ threshold). To side-step these challenges, we consider an *oracle variant* of our setting, where we have access to the true joint distribution $P(S, A, S')$ and perfect algorithms for solving all optimization problems (including the exo reward linear regression). Access to $P(S, A, S')$ is equivalent to having an infinite training sample collected by visiting all states and executing all actions so that estimation errors vanish when computing the conditional mutual information and the expected value of the residual error in (19).

Under this oracle setting, we prove that the global rank-descending scheme returns the unique exogenous subspace of maximum rank. In practice, if we have a sufficiently representative sample of $\langle s, a, s', r \rangle$ tuples and the CCC captures conditional independence reasonably well, we can hope that our methods will still give useful results.

Algorithm 3 shows the oracle version of GRDS. It is identical to GRDS except that the optimization step of minimizing the CCC is replaced by the following feasibility problem:

$$\begin{aligned}
& \text{Find } W_{exo} \in \mathbb{R}^{d \times d_{exo}} \text{ such that:} \\
& W_{exo}^\top W_{exo} = \mathbb{I}_{d_{exo}} \\
& I(S'W_{exo}; [S - SW_{exo}W_{exo}^\top, A] \mid SW_{exo}) = 0.
\end{aligned} \tag{25}$$

Theorem 8. *The Oracle-GRDS algorithm returns a matrix W_{exo} such that*

- (a) *the subspace \mathcal{X} defined by W_{exo} and the subspace \mathcal{E} defined as the orthogonal complement of \mathcal{X} form a valid exo/endo decomposition of the full form;*
- (b) *the subspace \mathcal{X} has maximal dimension over all valid exo/endo decompositions; and*
- (c) *the subspace \mathcal{X} is unique and contains all other exogenous subspaces $\tilde{\mathcal{X}}$ that could form valid exo/endo decompositions.*

Proof. To prove property (a), first note that we can define the joint distribution $P(X = W_{exo}W_{exo}^\top s, E = s - W_{exo}W_{exo}^\top s) = P(S = s)$, because each column of W_{exo} is a unit vector and they are orthogonal. Because W_{exo} is a feasible solution to the manifold optimization Problem 25 and the conditional mutual information is zero, we know from Theorem 7 that $P(S'|S, A)$ factors as $P(X'|X)P(E'|X, E, A, X')$. Hence, it is a valid exo/endo decomposition according to Theorem 1.

Algorithm 3 Oracle-GRDS for the Full Setting

-
- 1: **Input:** Joint distribution $P(S, A, S')$ corresponding a fully-randomized policy controlling an admissible exogenous state MDP with maximal exogenous subspace \mathcal{X} defined by W_{exo}^*
 - 2: **Output:** Matrix \hat{W}_{exo}^*
 - 3: **for** $d_{exo} = d$ **down to** 1 **do**
 - 4: Solve the following system of equations for $W_{exo} \in \mathbb{R}^{d, d_{exo}}$:

$$\begin{aligned} W_{exo}^\top W_{exo} &= \mathbb{I}_{d_{exo}} \\ I(S'W_{exo}; [S - SW_{exo}W_{exo}^\top, A] | SW_{exo}) &= 0. \end{aligned}$$

- 5: **if** the above system is feasible with solution W_{exo} of rank d_{exo} **then**
 - 6: $\hat{W}_{exo}^* := W_{exo}$
 - 7: **return** \hat{W}_{exo}^*
 - 8: **end if**
 - 9: **end for**
 - 10: **return** null matrix $\mathbf{0}$
-

Property (b) follows from the fact that d_{exo} is the largest value that yields a feasible solution to Problem 25.

To establish property (c), we need to prove three lemmas, which are the vector space versions of Theorem 2, Corollary 1, and Corollary 2.

Lemma 1 (Union of Exo/Endo Decompositions). *Let $[\mathcal{X}_1, \mathcal{E}_1]$ and $[\mathcal{X}_2, \mathcal{E}_2]$ be two full exo/endo decompositions of an MDP \mathcal{M} with state space \mathcal{S} , where $\mathcal{X}_1 = \{W_1^\top s : s \in \mathcal{S}\}$ and $\mathcal{X}_2 = \{W_2^\top s : s \in \mathcal{S}\}$ and where $W_1^\top W_1 = \mathbb{I}_{d_1 \times d_1}$ and $W_2^\top W_2 = \mathbb{I}_{d_2 \times d_2}$, $1 \leq d_1, d_2 \leq d$. Let $\mathcal{X} = \mathcal{X}_1 + \mathcal{X}_2$ be the subspace formed by the sum of subspaces \mathcal{X}_1 and \mathcal{X}_2 , and let \mathcal{E} be its complement. It then holds that the state decomposition $S = [E, X]$ with $E \in \mathcal{E}$ and $X \in \mathcal{X}$ is a valid full exo/endo decomposition of \mathcal{S} .*

Proof. We wish to follow the same reasoning as in Theorem 2. To do this, we need to compute the linear subspaces equivalent to $\mathcal{X} = \mathcal{X}_1 + \mathcal{X}_2$ and $\mathcal{E} = \mathcal{E}_1 \cap \mathcal{E}_2$. Consider the following subspaces expressed in the original d -dimensional coordinate system:

$$\bar{\mathcal{X}} = \mathcal{X}_1 \cap \mathcal{X}_2 = \{W_2 W_2^\top W_1 W_1^\top s : s \in \mathbb{R}^d\} \quad (26)$$

$$\hat{\mathcal{X}}_1 = \mathcal{X}_1 \cap \mathcal{E}_2 = \{s \in \mathcal{X}_1 : W_2 W_2^\top s = 0\} \quad (27)$$

$$\hat{\mathcal{X}}_2 = \mathcal{X}_2 \cap \mathcal{E}_1 = \{s \in \mathcal{X}_2 : W_1 W_1^\top s = 0\} \quad (28)$$

$$\mathcal{X} = \mathcal{X}_1 + \mathcal{X}_2 = \bar{\mathcal{X}} \oplus \hat{\mathcal{X}}_1 \oplus \hat{\mathcal{X}}_2 \quad (29)$$

$$\mathcal{E} = \mathcal{X}^\perp = \{s \in \mathbb{R}^d : W_1 W_1^\top s = 0 \wedge W_2 W_2^\top s = 0\} \quad (30)$$

Equation (26) defines the intersection of the two subspaces \mathcal{X}_1 and \mathcal{X}_2 , because $W_1 W_1^\top$ is a projection matrix that projects s into \mathcal{X}_1 , and $W_2 W_2^\top$ is a projection matrix that projects $W_1 W_1^\top s$ into \mathcal{X}_2 . In Equation (27), we define $\hat{\mathcal{X}}_1$ as the set of points in \mathcal{X}_1 that are not in \mathcal{X}_2 , because $W_2 W_2^\top$ maps them to zero. Hence, they are also not in the intersection $\bar{\mathcal{X}}$. This implies that $\mathcal{X}_1 = \bar{\mathcal{X}} \oplus \hat{\mathcal{X}}_1$. Note that because \mathcal{E}_2 is defined as the points that $W_2 W_2^\top$ maps to zero, $\hat{\mathcal{X}}_1$ can also be expressed as $\mathcal{X}_1 \cap \mathcal{E}_2$. Similarly, $\hat{\mathcal{X}}_2 = \mathcal{X}_2 \cap \mathcal{E}_1$, and $\mathcal{X}_2 = \bar{\mathcal{X}} \oplus \hat{\mathcal{X}}_2$. We can therefore express $\mathcal{X}_1 + \mathcal{X}_2$ as the direct sum $\bar{\mathcal{X}} \oplus \hat{\mathcal{X}}_1 \oplus \hat{\mathcal{X}}_2$ (Equation (29)). Equation (30) defines \mathcal{E} as the set of points that are simultaneously in the orthogonal complements of both \mathcal{X}_1 and \mathcal{X}_2 . Either $\hat{\mathcal{X}}_1$ or $\hat{\mathcal{X}}_2$ may of course be the zero vector spaces, if one exogenous subspace is contained in the other.

Now we can define random variables that permit us to apply the proof of Theorem 2. Define random variables for the input spaces: $X_1 \in \mathcal{X}_1$, $E_1 \in \mathcal{E}_1$, $X_2 \in \mathcal{X}_2$, for the $(\mathcal{X}, \mathcal{E})$ decomposition. Similarly, define random variables for the output spaces: $X = (\bar{X}, \hat{X}_1, \hat{X}_2)$, where $\bar{X} \in \bar{\mathcal{X}}$, $\hat{X}_1 \in \hat{\mathcal{X}}_1$, and $\hat{X}_2 \in \hat{\mathcal{X}}_2$. Let $S \in \mathcal{S}$.

Because (X_1, E_1) is a valid decomposition, there can be no edges from E_1 or A to any variable in X_1 . Similarly, because (X_2, E_2) is a valid decomposition, there can be no edges from E_2 or A to any variable in X_2 . Consequently, there can be no edges from E and A to any subspace in X . This demonstrates that (X, E) is a valid full exo/endo decomposition of the state space. \square

Lemma 2 (Unique Maximal Subspace). *The maximal exo vector subspace \mathcal{X}_{max} defined by $W_{exo, max}$ is unique.*

Algorithm 4 Stepwise Rank Ascending Scheme: SRAS

```

1: Inputs: A database of transitions  $\{(s_i, a_i, r_i, s'_i)\}_{i=1}^N$ 
2: Output: The exogenous state projection matrix  $W_{exo}$ 
3: Initialize  $W_{exo} \leftarrow [], W_{temp} \leftarrow [], C_x \leftarrow [], k \leftarrow 0$ 
4: repeat
5:    $N \leftarrow$  orthonormal basis for the null space of  $C_x$ 
6:   Solve the following optimization problem
           
$$\hat{w} := \arg \min_{w \in \mathbb{R}^{(d-k) \times 1}} CCC(\mathbf{S}'[W_{temp}, N^\top w]; \mathbf{A} \mid \mathbf{S}[W_{temp}, N^\top w])$$

           subject to  $w^\top w = 1$ 
7:    $w_{k+1} \leftarrow N^\top \hat{w}$ 
8:    $C_x \leftarrow C_x \cup \{w_{k+1}\}$ 
9:    $CCC_{sim} \leftarrow CCC(\mathbf{S}'[W_{temp}, w_{k+1}]; \mathbf{A} \mid \mathbf{S}[W_{temp}, w_{k+1}])$ 
10:  if  $CCC_{sim} < \epsilon$  then
11:     $W_{temp} \leftarrow W_{temp} \cup \{w_{k+1}\}$ 
12:     $\mathbf{E} \leftarrow \mathbf{S} - \mathbf{S}W_{temp}W_{temp}^\top$ 
13:     $CCC_{full} \leftarrow CCC(\mathbf{S}'W_{temp}; [\mathbf{E}, \mathbf{A}] \mid \mathbf{S}W_{temp})$ 
14:    if  $CCC_{full} < \epsilon$  then
15:       $W_{exo} \leftarrow W_{temp}$ 
16:    end if
17:  end if
18:   $k \leftarrow k + 1$ 
19: until  $k = d$ 
20: return  $W_{exo}$ 

```

Proof. By contradiction. If there were 2 distinct maximal subspaces, then Lemma 1 would allow us to combine them to get an even larger exogenous vector subspace. This is a contradiction. \square

Lemma 3. Let $W_{exo,max}$ define the maximal exogenous vector subspace \mathcal{X}_{max} , and let W_{exo} define any other exogenous vector subspace \mathcal{X} . Then $\mathcal{X} \subseteq \mathcal{X}_{max}$.

Proof. By contradiction. If there were an exogenous subspace \mathcal{X} not contained within \mathcal{X}_{max} , then by Lemma 1 we could combine the 2 exo/endo decompositions to get an even larger exogenous subspace. This contradicts the assumption that \mathcal{X}_{max} is maximal. \square

These three lemmas establish property (c) and complete the proof of Theorem 8. \square

This concludes our analysis of the Oracle-GRDS for the full setting (Algorithm 3). The analysis can trivially be extended to the diachronic setting.

How well does this analysis carry over to the non-oracle GRDS algorithm? GRDS departs from the oracle version in three ways. First, GRDS employs the CCC in place of conditional mutual information (CMI). This may assign non-zero CCC values to W_{exo} matrices that actually have zero CMI. This will cause GRDS to under-estimate d_{exo} , the dimensionality of the exogenous state space. Second, GRDS only requires CCC to be less than a parameter ϵ . If ϵ is large, then GRDS may stop too soon and over-estimate d_{exo} . Hence, by introducing ϵ , GRDS is able to compensate somewhat for the failures of CCC. Third, the database of transitions is not infinite, so the value of CCC that GRDS computes may be too high or too low. This in turn may cause d_{exo} to be too small or too large. In our experiments, we will compare the estimated d_{exo} to our understanding of its true value.

4.3 Stepwise Algorithm SRAS

The global scheme computes the entire W_{exo} matrix at once. In this section, we introduce an alternative *stepwise* algorithm, the Stepwise Rank Ascending Scheme (SRAS, see Algorithm 4), which constructs the matrix W_{exo} incrementally by solving a sequence of small manifold optimization problems.

SRAS maintains the current partial solution W_{exo} , a temporary matrix W_{temp} that may be extended to update W_{exo} , a set of all candidate column vectors generated so far, C_x , and an orthonormal basis N for the null space of C_x . (N is a matrix with a number of columns equal to the dimension of the null space of C_x .) The set of candidate column vectors C_x contains all of the column vectors in W_{exo} and possibly some additional vectors that were rejected for violating the full CCC constraint, as we will discuss below.

Suppose we have already found the first k columns of $W_{exo} = [w_1, w_2, \dots, w_k]$. To ensure that the new column w_{k+1} is orthogonal to all k previous vectors, we restrict w_{k+1} to lie in the space defined by N by requiring it to have the form $w_{k+1} = N^T w$. This ensures that it is orthogonal to all columns of W_{exo} and to any additional vectors in C_x .

In Line 6, we compute a new candidate vector \hat{w} by solving a simplified CCC minimization problem on the $(d - k) \times 1$ -dimensional Stiefel manifold. Recall that the full objective $I(X'; [E, A] | X) = 0$ seeks to enforce the conditional independence $X' \perp\!\!\!\perp E, A | X$. This requires us to know X and E , whereas at this point in the algorithm, we only know a portion of X , and we therefore do not know E at all. We circumvent this problem by using the *simplified objective* $I(X'_k; A | X_1, \dots, X_k)$ (approximated via the CCC). This objective ensures that A has no effect on the exogenous variables X' in the next time step, which eliminates the edge $A \rightarrow X'$, but it does not protect against the possibility that A causes a change in some chain of endogenous variables that affect X in some subsequent time step. Hence, the simplified objective is a necessary but not sufficient condition for X to be a valid exogenous subspace. See Appendix B for a detailed discussion of this point.

Lines 7 and 8 compute the new candidate vector w_{k+1} by mapping \hat{w} into the null space defined by N and then adding it to C_x . In Line 9, we compute CCC_{sim} , the value of the simplified objective (which is the same as the value that minimized the objective in Line 6). In Line 10, we check whether this is less than ϵ . If not, we increment k and loop back to Line 5 and find another \hat{w} vector. But if $CCC_{sim} < \epsilon$, then in Lines 11-13, we compute the corresponding \mathbf{E} matrix and compute CCC_{full} , the CCC of the full objective. In Line 14, we check whether $CCC_{full} < \epsilon$. If so, then we have a valid new column to add to W_{exo} . If not, we increment k and loop back to Line 5.

Recall that not all subsets of the maximal exogenous subspace are themselves valid exogenous subspaces that satisfy the full CCC constraint (Theorem 3). Hence, it is important that SRAS does not terminate when adding a candidate vector to W_{exo} causes the full constraint to be violated. Note, however, that every subset of the maximal exogenous subspace must satisfy the simplified objective, because otherwise, the action variable is directly affecting one of the exogenous state variables.

To allow SRAS to continue making progress when the full constraint is violated, the algorithm maintains the matrix W_{temp} . This matrix contains all of the candidates that have satisfied the simplified objective. If a subsequent candidate w_{k+1} allows W_{temp} to satisfy the full constraint, then we set W_{exo} to W_{temp} and continue. The algorithm terminates when $k = d$.

The primary advantage of SRAS compared to GRDS is that the CCC minimization problems have dimension $(d - k) \times 1$. However, GRDS can halt as soon as it finds a W_{exo} that satisfies the full CCC objective, whereas SRAS must solve all d problems. We can introduce heuristics to terminate d early. For example, we can monitor the residual variance $\|\hat{\mathbf{X}} \cdot w_R - \mathbf{R}\|_2^2$ of the reward regression. This decreases monotonically as columns are added to W_{exo} , and when those decreases become very small, we can terminate SRAS. This can make SRAS very efficient when the exogenous subspace has low rank d_{exo} relative to the rank d of the full state space. In such cases, GRDS must solve $d - d_{exo} + 1$ large manifold optimization problems of dimension at least $d \times d_{exo}$, whereas SRAS must only solve d_{exo} problems of dimension $(d - k) \times 1$.

What can we say about the correctness of SRAS? First, in an oracle version of SRAS (where the MDP was admissible, the data were collected using a fully-randomized policy, and CMI was computed instead of CCC), the W_{exo} matrix returned by SRAS would define a valid exo/endo decomposition. This is because it would satisfy the full CMI constraint. However, it would not necessarily define the maximal exogenous subspace, because the w vectors found using the simplified objective and stored in W_{temp} might not be a subset of a satisfying W_{exo} matrix. Of course, because the actual SRAS algorithm introduces the CCC approximation and only requires the CCC to be less than ϵ , we do not have any guarantee that the W_{exo} matrix returned by SRAS defines a valid exogenous subspace. We now turn to experimental tests of the algorithms to see whether they produce useful results despite their several approximations.

5 Experimental Study

We conducted a series of experiments to understand the behavior of our algorithms. In addition to GRDS and SRAS, we defined a third algorithm, Simplified-GRDS that applies the simplified objective $CCC(S'W_{Exo}; A|SW_{exo})$ in Line 6 of Algorithm 2 but then still uses the full objective in Line 7. Like SRAS, Simplified-GRDS will always return a valid W_{exo} , but it may not be maximal.

In this section, we present experiments to address the following research questions:

- RQ1: Do our methods speed up reinforcement learning in terms of sample complexity? In terms of total CPU time?
- RQ2: Do our methods discover the correct maximal exogenous subspaces?
- RQ3: What is the best approach to reward regression? Single linear, repeated linear, or online neural network regression?
- RQ4: How do the algorithms behave when the MDPs are changed to have different properties: (a) rewards are nonlinear, (b) transition dynamics are nonlinear, (c) action space is combinatorial, and (d) states and actions are discrete?
- RQ5: How do the algorithms behave when the covariance condition is violated?
- RQ6: What are the risks and benefits of using the simplified objective in SRAS and Simplified-GRDS?
- RQ7: How should hyperparameters be set? How many training tuples should be collected before performing exogenous subspace discovery? When should reward regression begin and on what schedule?

5.1 Experimental Details

We compare five methods:

- *Baseline*: Reinforcement learning applied to the full reward (sum of exogenous and endogenous components)
- *GRDS*: The Global Rank Descending Scheme
- *Simplified-GRDS*: GRDS using the simplified objective
- *SRAS*: The Stepwise Rank Ascending Scheme
- *Endo Reward Oracle*: Reinforcement learning applied with the oracle endogenous reward.

As the reinforcement learning algorithm, we employ the PPO implementation from stable-baselines3 [Raffin et al., 2021] in PyTorch [Paszke et al., 2019], and we model the MDPs in the OpenAI Gym framework [Brockman et al., 2016]. We use the default PPO hyperparameters in stable-baselines3, which include a clip range of 0.2, a value function coefficient of 0.5, an entropy coefficient of 0, and a generalized advantage estimation (GAE) parameter of 0.95. The policy and value networks have two hidden layers of 64 tanh units each. For PPO optimization, we employ the default Adam optimizer [Kingma and Ba, 2015] in PyTorch with default hyperparameters $\beta_1 = 0.9$, $\beta_2 = 0.999$, $\text{eps} = 1 \times 10^{-5}$ and a default learning rate of $lr_{PPO} = 0.0003$. The batch size for updating the policy and value networks is 64 samples. The discount factor in the MDPs is set to $\gamma = 0.99$. The default number of steps between each policy update is $K = 1536$. The number of steps L after which we compute the exo/endo decomposition and the total number of training steps in the experiment N vary per experiment, but their default values are $L = 3000$ and $N = 6000$. We summarize all hyperparameters in Table 2.

In each experimental run, we maintain two instances of the Gym environment. Training is carried out in the primary instance. After every policy update, we copy the policy to the second instance and evaluate the performance of the policy (without learning) for 1000 steps. To reduce measurement variance, these evaluations always start with the same random seed.

To solve the manifold optimization problems, we apply the solvers implemented in the Pymanopt package [Townsend et al., 2016]. We use the Steepest Descent solver with line search with the default Pymanopt hyperparameters. For the CCC constraint, ϵ is set to 0.05. The Tikhonov regularizer inside the CCC is set to $\lambda = 0.01$. These hyperparameters were determined empirically via random search [Bergstra and Bengio, 2012].

To implement neural network reward regression, we use a separate neural network in sklearn [Buitinck et al., 2013] with 2 hidden layers of 50 and 25 units, respectively, and ReLU activations. We train with Adam using the default Adam coefficients. The learning rate is set by default to $lr_{reg} = 0.0003$ and the L2 regularization to 3×10^{-5} . The batch size is set to 256. During Phase 1, we train the net with the L collected samples until convergence (or a maximum number of 125 epochs). During Phase 2, we perform online learning by updating the neural net every $M = 256$ training steps with a single pass over the last 256 samples. Linear regression is computed using the standard least squares matrix solution without regularization.

We chose to use the default library hyperparameters for PPO, Adam optimization, and manifold optimization to enable a fair comparison of the different methods. Furthermore, for online reinforcement learning algorithms, it is not feasible to perform extensive hyperparameter searches because of the cost (and risk) of interacting in the real world. Algorithms

Used for	Description	Symbol	Default Value	Fixed
PPO	clipping parameter	-	0.2	Yes
	value function coefficient	-	0.5	Yes
	entropy coefficient	-	0	Yes
	GAE parameter	-	0.95	Yes
Policy & Value Nets	number of layers	-	2	Yes
	units per layer	-	64, 64	Yes
	activation function	-	tanh	Yes
PPO Optimization with Adam	Adam learning rate	lr_{PPO}	0.0003	Yes
	Adam coefficients	$\beta_1, \beta_2, \text{eps}$	0.9, 0.99, 1e-5	Yes
	batch size	-	64	Yes
	L2 regularization	-	0	Yes
Reinforcement Learning	discount factor	γ	0.99	Yes
	policy update steps	K	1536	Yes
	total training steps	N	60000	No
	steps for decomposition	L	3000	No
	steps for exo regression	M	256	Yes
Manifold Optimization	evaluation steps	-	1000	Yes
	CCC threshold	ϵ	0.05	Yes
Exo regression Net	Tikhonov regularizer	λ	0.01	Yes
	number of layers	-	2	Yes
	units per layer	-	50, 25	Yes
Exo Regression Optimization with Adam	activation function	-	relu	Yes
	Adam learning rate	lr_{regr}	0.0003	No
	Adam coefficients	$\beta_1, \beta_2, \text{eps}$	0.9, 0.99, 1e-8	Yes
	batch size	-	256	Yes
	L2 regularization	-	0.00003	Yes

Table 2: Hyperparameters for High-D setting.

that only perform well after extensive hyperparameter search are not usable in practice. Hence, we wanted to minimize hyperparameter tuning.

In all our MDPs, we use the default values in Table 2 for all hyperparameters except for the number of decomposition steps L and the number of training steps N . The former is the most critical hyperparameter; it is discussed in detail in Section 5.6. The latter is set to a number that is high enough for our methods to converge or be near the limit. Finally, in a few settings we found it beneficial to use a regression learning rate of 0.0006 instead of 0.0003 for better convergence.

For each setting, we report the values of the hyperparameters that are different from their default values. We run all experiments on a c5.4xlarge EC2 machine on AWS³.

5.2 Performance Comparison on High-Dimensional Linear Dynamical MDPs

To address RQ1 and RQ2, we define a set of high-dimensional MDPs with linear dynamics. Each MDP, by design, has m endogenous and n exogenous variables, so that $e_t \in \mathbb{R}^m$ and $x_t \in \mathbb{R}^n$. There is a single action variable a_t that takes 10 discrete values $(-1, -0.777, -0.555, \dots, 0, \dots, 0.555, 0.777, +1)$. The policy chooses one of these values at each time step. The exo and endo transition functions are

$$\begin{aligned}
 x_{t+1} &= M_{exo} \cdot x_t + \varepsilon_{exo} \\
 e_{t+1} &= M_{end} \cdot \begin{bmatrix} e_t \\ x_t \end{bmatrix} + M_a \cdot a_t + \varepsilon_{end},
 \end{aligned}$$

where $M_{exo} \in \mathbb{R}^{n \times n}$ is the transition function for the exogenous MRP; $M_{end} \in \mathbb{R}^{m \times m}$ is the transition function for the endogenous MDP involving e_t and x_t ; $M_a \in \mathbb{R}^m$ is the coefficient for the action a_t , and it is set to a vector of ones; $\varepsilon_{exo} \in \mathbb{R}^n$ is the exogenous noise, whose elements are distributed according to $\mathcal{N}(0, 0.09)$; and $\varepsilon_{end} \in \mathbb{R}^m$ is the endogenous noise, whose elements are distributed according to $\mathcal{N}(0, 0.04)$. The observed state vector $s_t \in \mathbb{R}^{m+n}$ is a linear mixture of the hidden exogenous and endogenous states defined as

$$s_t = M \cdot \begin{bmatrix} e_t \\ x_t \end{bmatrix},$$

³<https://aws.amazon.com/ec2/instance-types/c5/>.

where $M \in \mathbb{R}^{(m+n) \times (m+n)}$. The elements in M_{exo} , M_{end} , and M are generated according to $\mathcal{N}(0, 1)$ and then each row of each matrix is normalized to sum to 0.99 for stability⁴. The elements of the initial endo and exo states are randomly initialized from a uniform distribution over $[0, 1]$.

In our first set of experiments, the reward at time t is

$$R_t = R_{exo,t} + R_{end,t},$$

where $R_{exo,t} = -3 \cdot \text{avg}(x_t)$ is the exogenous reward and $R_{end,t} = e^{-|\text{avg}(e_t)-1|}$ is the endogenous reward, and $\text{avg}(\cdot)$ denotes the average over a vector’s elements. For this class of MDPs, the optimal policy seeks to drive the average of e_t to 1.

We experiment in total with 6 MDPs with different choices for the numbers n and m of the exogenous and endogenous variables, respectively: (i) 5-D state with $m = 2$ endo variables and $n = 3$ exo variables; (ii) 10-D state with $m = 5$ and $n = 5$; (iii) 20-D state with $m = 10$ and $n = 10$; (iv) 30-D state with $m = 15$ and $n = 15$; (v) 45-D state with $m = 22$ and $n = 23$; and (vi) 50-D state with $m = 25$ endo variables and $n = 25$ exo variables. For the 50-D setting, we use $N = 100000$ training steps and $L = 10000$ decomposition steps due to its higher dimensionality. Similarly, we use $N = 80000$ and $L = 5000$ for the 45-D MDP, and $L = 5000$ for the 30-D MDP. On the other hand, we set $N = 50000$ and $L = 2000$ for the 5-D MDP. For each MDP, we run 20 replications with different random seeds and report the average results and standard deviations.

5.2.1 RL Performance

To address RQ1, we report the performance for each of the 6 MDPs over 20 replications in Figure 6. In all 6 MDPs, all of our methods far-outperform the baseline. Indeed, in the 5-D and 10-D MDPs, the baseline does not show any sign of learning, and in the larger problems, the baseline’s performance has attained roughly half of the performance of our methods after 65 policy updates. A simple linear extrapolation of the baseline learning curve for the 50-D problem suggests that it will require 132 policy updates to attain the performance of the other methods. This is more than 3 times as long as the 40 updates our methods require. Hence, in terms of sample complexity, our methods are much more efficient than the baseline method.

On these MDPs, the Simplified-GRDS and SRAS methods are able to match the performance of the Endo Reward Oracle, which is given the correct endogenous reward from the very start. GRDS performs very well on all MDPs except for the 5-D one, where it is still able to outperform the baseline.

RQ1 also asks whether our methods are superior in terms of CPU time. Table 3 reports the CPU time required by the various methods. The Baseline and Endo Reward Oracle consume identical amounts of time, so the table only lists the Baseline CPU time. We observe that even the slowest of our methods (SRAS on the 50-D problem) requires only 45% more time than the Baseline. However, if we again extrapolate the baseline to 132 policy updates, where its performance would match our methods, that would require 2997 seconds of CPU time, which is 49% more than SRAS. Hence, even if there is zero cost to collecting training samples in the real world, our methods are still faster.

5.2.2 Rank of Discovered Exo Subspace

RQ2 asks whether our methods find the correct maximal exogenous subspaces. Our experiments revealed a surprise. Although we constructed the MDPs with the goal of creating an n -dimensional exogenous space and an m -dimensional endogenous space, our methods usually discover exogenous spaces with $n + m - 1$ dimensions. Upon further analysis, we realized that because the action variable is 1-dimensional, it can only affect a 1-dimensional subspace of the $n + m$ -dimensional state space. Consequently, the true maximal exogenous subspace has dimension $n + m - 1$. The results in Table 3 show that the Simplified-GRDS always finds an exogenous subspace of the correct dimension. The exogenous space computed by SRAS is sometimes slightly smaller on the smaller MDPs, and the space computed by GRDS is sometimes slightly smaller on the larger MDPs. We believe the failures of SRAS are due to the approximations that we discussed in Section 4.3. We suspect the failures of GRDS reflect failures of the manifold optimization to find the optimum in high-dimensional problems.

The fact that the exogenous space has dimension $n + m - 1$ explains the relative amount of CPU time consumed by the different algorithms. SRAS is often the slowest, because it must solve $n + m$ optimization problems whereas GRDS and Simplified-GRDS must only solve two (large) manifold optimization problems before terminating.

⁴Notice that all matrices M_{exo} , M_{end} , and M in our synthetic linear MDPs are stochastic. Future work could explore more general classes of MDPs.

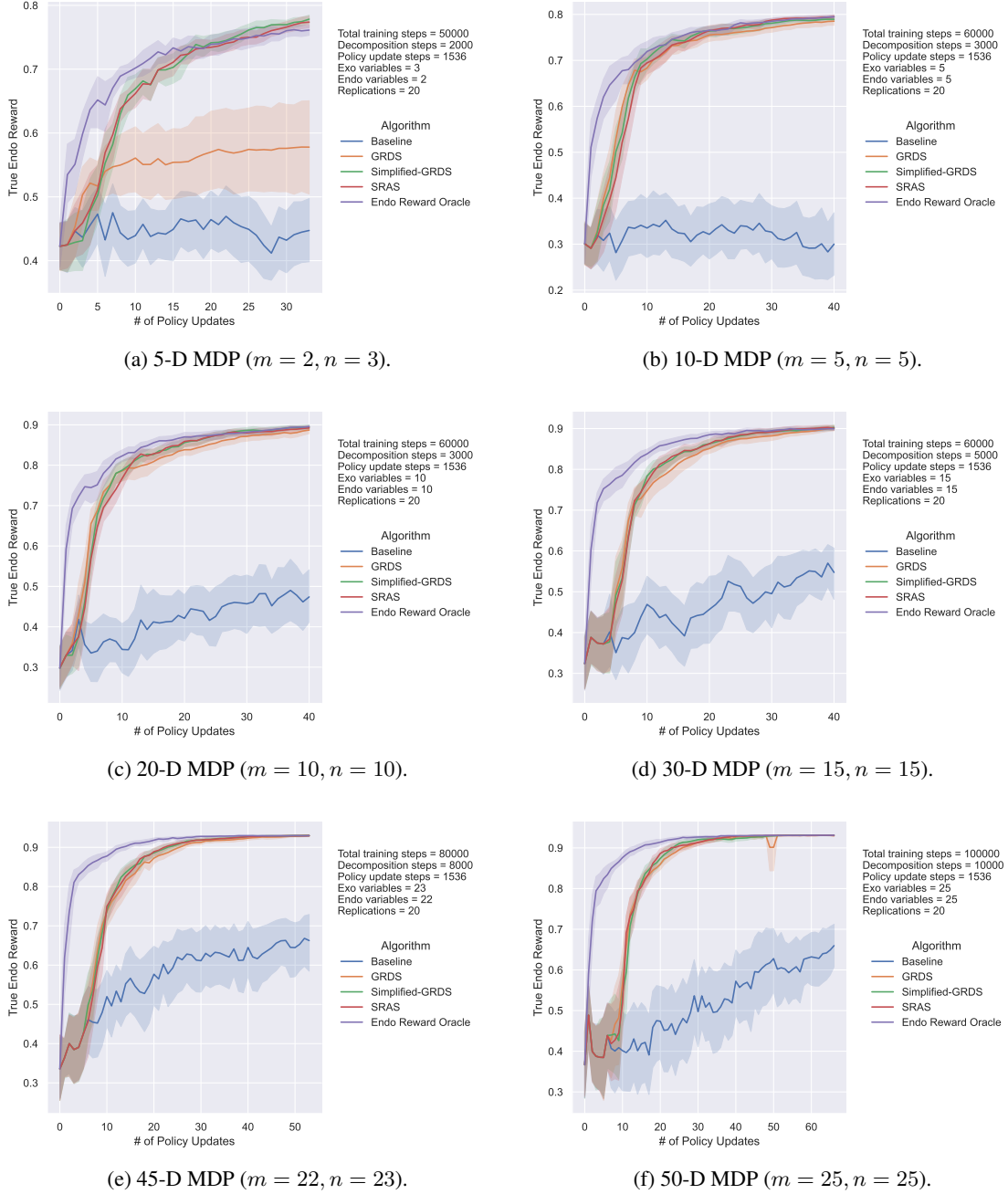


Figure 6: Comparison of various methods in high-D linear MDPs.

5.2.3 Comparison of Methods for Exo Reward Regression

We performed a second set of experiments to investigate how the type and configuration of exo reward regression affects the performance of our methods. We compare three reward regression configurations. The first configuration is *Single Linear Regression*, which fits a linear model for the exo reward and performs regression only once at the end of Phase 1 of Algorithm 1. The second configuration is *Repeated Linear Regression*. Like Single Linear Regression, it fits a linear model at the end of Phase 1. In addition, it re-fits the model in Phase 2 every 1,000 collected samples using all transition data so far. Note that this is different from online Algorithm 1, which updates the exogenous reward function in Phase 2 every M observations using only the last M observations in D_{exo} . The goal was to understand whether regular regression with all observed transition data can perform better than a single linear regression at the end of Phase 1. The third configuration is *Online Neural Net Regression* which fits a neural network to the exo reward data. At the

Total State Variables	Exo State Variables	Endo State Variables	Method	Exo Subspace Rank	Total Time (secs)	Decomposition Time (secs)
5	3	2	Baseline	-	245.9±14.7	-
			GRDS	4.0±4.0	294.9±113.0	6.3±4.6
			Simplified-GRDS	4.0±0.0	297.0±115.4	9.6±5.0
			SRAS	3.95±0.22	297.1±113.3	14.0±14.0
10	5	5	Baseline	-	345.3±10.48	-
			GRDS	8.65±0.48	413.5±148.0	22.6±18.0
			Simplified-GRDS	9.0±0.0	413.7±144.4	13.1±9.1
			SRAS	8.75±0.54	434.3±157.6	34.2±46.7
20	10	10	Baseline	-	450.2±34.8	-
			GRDS	18.1±1.18	525.3±167.9	41.8±47.8
			Simplified-GRDS	19.0±0.0	513.6±141.3	8.6±4.4
			SRAS	18.4±0.66	562.4±188.5	86.0±72.3
30	15	15	Baseline	-	509.9±43.0	-
			GRDS	28.25±1.22	597.5±185.6	56.9±84.1
			Simplified-GRDS	29.0±0.0	584.3±136.9	12.5±6.0
			SRAS	27.9±1.58	688.9±276.5	177.5±234.9
45	23	22	Baseline	-	895.4±159.3	-
			GRDS	43.4±0.86	1041.7±287.6	84.9±154.2
			Simplified-GRDS	44.0±0.0	1006.3±207.8	13.3±8.4
			SRAS	44.0±0.0	1323.4±716.1	605.1±538.7
50	25	25	Baseline	-	1472.4±126.0	-
			GRDS	48.45±0.86	1659.6±282.7	81.7±105.8
			Simplified-GRDS	49.0±0.0	1634.5±239.1	15.7±9.2
			SRAS	49.0±0.0	2009.2±840.3	667.8±616.9

Table 3: Average and standard deviation for rank of discovered exo subspace, total execution time, and decomposition time for the linear MDPs.

end of Phase 1, we perform reward regression until convergence. During Phase 2, we then perform a single epoch every 256 steps.

We plot RL performance over the 20 replications in Figure 6 on two MDPs: (i) the 10-D state MDP (Figures 7a-7b) and (ii) the 50-D state MDP (Figures 7c-7d). We compare the three regression methods applied to GRDS and SRAS. The results show that Online Neural Net Regression generally outperforms Single and Repeated Linear Regression, even though the exo reward function $R_{exo,t}$ is a linear function of the exo state. We speculate that this is because it is continually incorporating new data, which in turn may allow PPO to make more progress. Repeated Linear Regression also incorporates new data, but at a slower rate. Furthermore, when applied to SRAS, it becomes unstable and exhibits high variance. We speculate that this may be because it is only fitting to the most recent 1000 data points. Future work might consider training on all accumulated data and imposing strong regularization to improve stability.

Based on the superior performance of online neural network regression, we adopt it as the default reward regression method in the remainder of our experiments.

5.3 Exploring Modifications of the MDPs

To address RQ4, we now study the performance of our methods when they are applied to MDPs that depart in various ways from the linear dynamical MDPs studied thus far:

- Rewards are nonlinear functions of the state,
- Transition dynamics are nonlinear,
- The action space is combinatorial, and
- The states and actions are discrete.

5.3.1 Nonlinear Exogenous Reward Functions

Because we have adopted online neural network reward regression, we expect that our methods should be able to fit nonlinear exogenous reward functions. We consider the high-D linear setting of Section 5.2 with $m = n = 15$. We perform exo/endo decomposition after $L = 5000$ steps and train for a total of $N = 80000$ steps. We found it

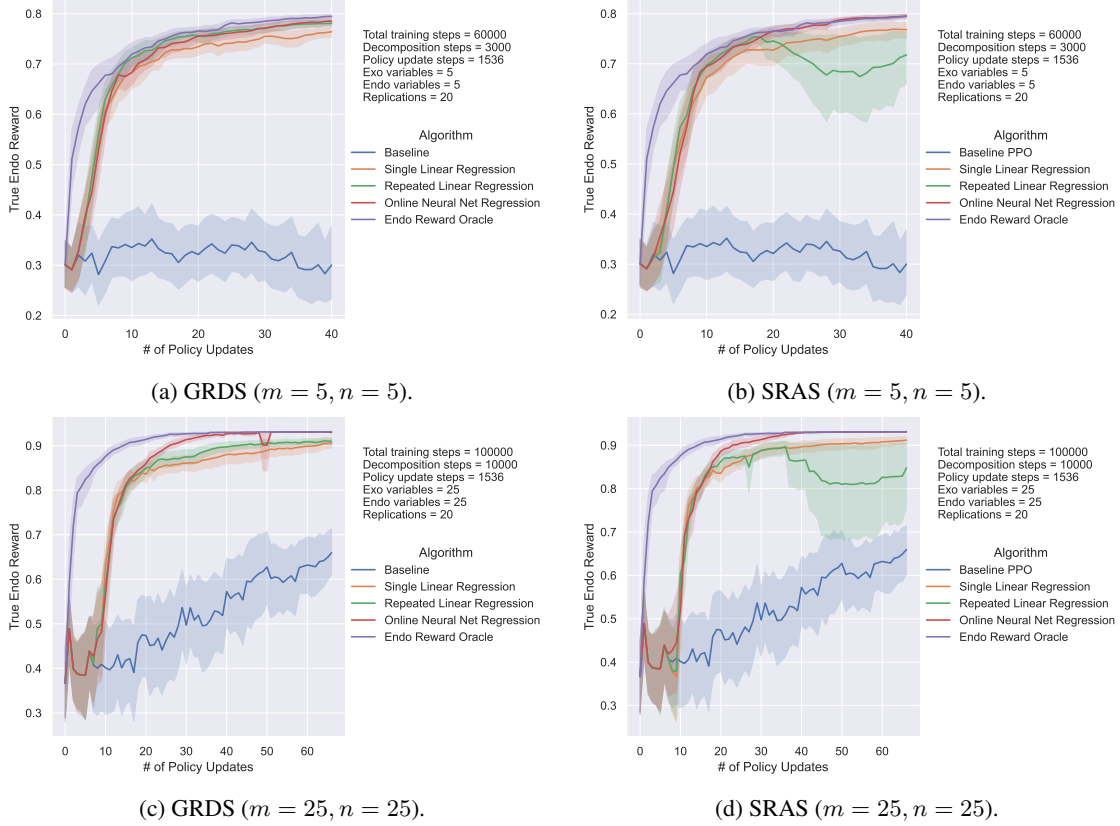


Figure 7: Impact of the type of exo reward regression on RL performance.

beneficial to use a learning rate for the exogenous reward regression of 0.0006 instead of the default 0.0003; the higher learning rate can help the exogenous reward neural net to adapt faster. We perform 20 replications with different seeds. Furthermore, we replace the linear exogenous reward function $R_{exo,t}$ by the following four choices:

- $R_{exo,t}^1 = \text{clip}(6 \cdot (\text{avg}(x_t) + \frac{1}{3} \cdot \text{avg}(x_t^2) - \frac{2}{15} \cdot \text{avg}(x_t^3)), -5.0, 5.0)$, a 3^{rd} degree polynomial.
- $R_{exo,t}^2 = -3 \cdot e^{-|\text{avg}(x_t)|^{1.5}}$, a function of $\text{avg}(x_t)$ with a single mode.
- $R_{exo,t}^3 = -3 \cdot (e^{-|\text{avg}(x_t+1.5)|^2} - e^{-|\text{avg}(x_t-1.5)|^2})$, a function of $\text{avg}(x_t)$ with two modes.
- $R_{exo,t}^4 = -3 \cdot (e^{-|\text{avg}(x_t+1)|^2} + \frac{3}{2} \cdot e^{-|\text{avg}(x_t-1.5)|^2} - \frac{5}{3} e^{-|\text{avg}(x_t)|^2})$, a function of $\text{avg}(x_t)$ with three modes.

Figures 8a-8d plot the results.

We generally observe that all methods match the Endo Reward Oracle’s performance and outperform the baseline by a large margin. This confirms that the nonlinear reward regression is able to fit these nonlinear reward functions. As we have observed before, the RL performance of SRAS is a bit unstable, perhaps because it is not always able to detect the maximal exogenous subspace. The Simplified-GRDS method also shows a tiny bit of instability.

Table 4 reports the average rank of the discovered exogenous subspaces. The true exogenous space has rank 29, but the exogenous reward only depends on 15 of those dimensions. The Simplified-GRDS method is most consistently able to find the true rank, whereas SRAS and GRDS struggle to capture that last dimension.

5.3.2 Nonlinear State Transition Dynamics

So far, we have considered MDPs with linear state transitions for the endogenous and exogenous states. It is a natural question whether our algorithms can handle more general MDPs. In this section, we provide experimental results on a more general class of nonlinear MDPs. Even though we lack a rigorous theoretical understanding, our results hint at the potential of the CCC objective to discover useful exo/endo state decompositions even when the dynamics are nonlinear.

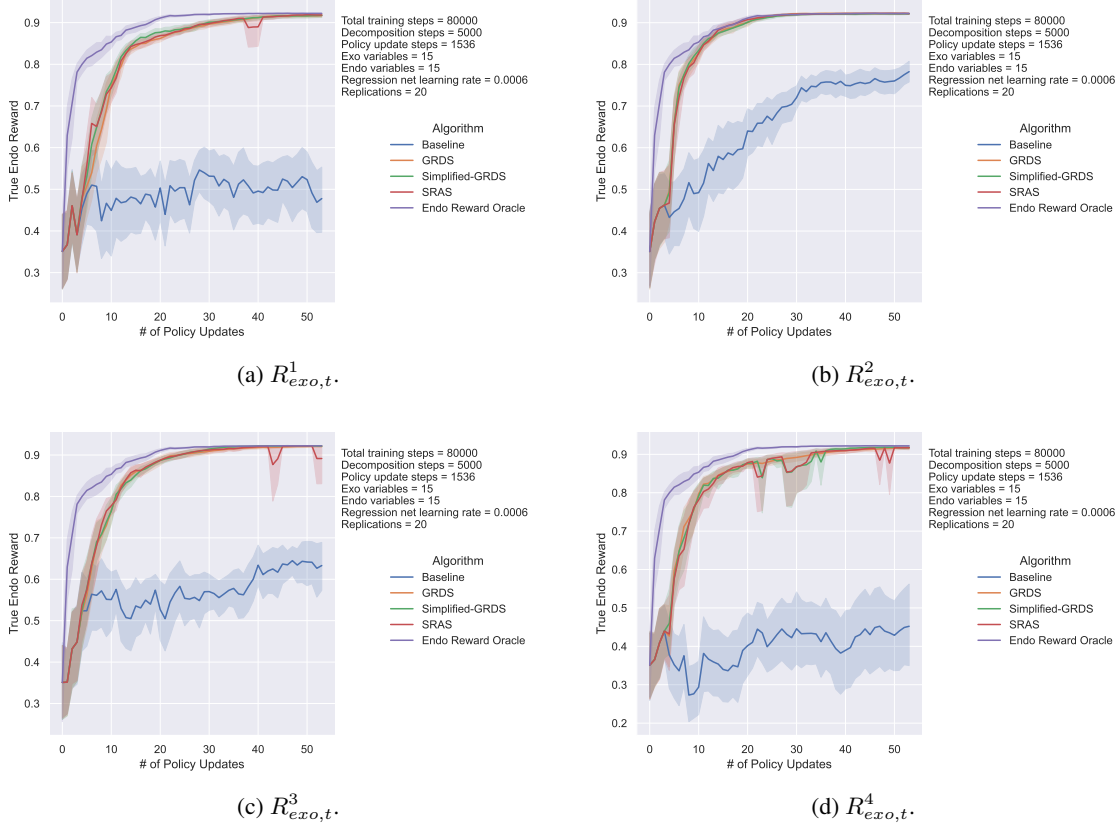


Figure 8: RL performance for MDPs with nonlinear exo reward functions.

Exo Reward Function	Method	Exo Subspace Rank	Total Time (secs)	Decomposition Time (secs)
$R^1_{exo,t}$	Baseline	-	1520.0±153.0	-
	GRDS	28.05±1.02	1874.6±357.3	155.8±122.1
	Simplified-GRDS	29.0±0.0	1808.6±278.7	40.5±11.3
	SRAS	27.95±1.56	1914.4±510.3	251.8±249.5
$R^2_{exo,t}$	Baseline	-	1510.9±136.2	-
	GRDS	28.3±0.9	1860.4±359.9	150.3±155.1
	Simplified-GRDS	29.0±0.0	1797.8±264.4	31.9±7.7
$R^3_{exo,t}$	Baseline	-	1518.1±146.4	-
	GRDS	28.0±1.0	1879.6±340.0	150.3±118.1
	Simplified-GRDS	29.0±0.0	1818.0±262.2	28.6±8.5
$R^4_{exo,t}$	Baseline	-	1513.8±103.7	-
	GRDS	28.35±0.79	1849.8±366.1	123.2±111.5
	Simplified-GRDS	28.35±0.79	1812.0±268.9	37.1±11.3
	SRAS	29.0±0.0	1926.7±560.5	307.4±320.7

Table 4: Average and standard deviation for rank of discovered exo subspace, total execution time, and decomposition time for the MDPs with nonlinear exo rewards.

In the experiments in this section, we introduce nonlinear dynamics, but we still configure the exogenous and endogenous state spaces so that they are linear projections of the full state space. We study the following three MDPs, which are defined according to the recipe in Section 5.2 with the following modifications:

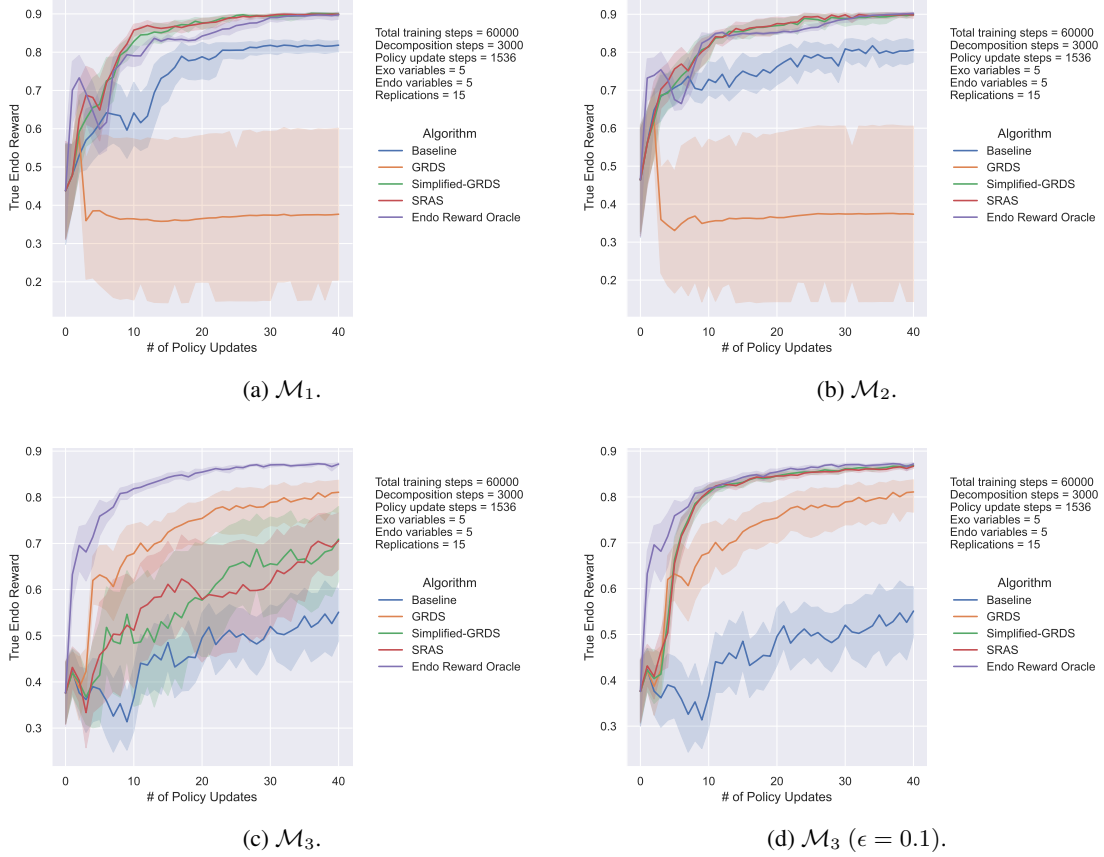


Figure 9: RL performance for MDPs with nonlinear state transitions.

- \mathcal{M}_1 is a 10-D MDP with $m = n = 5$ and a single action variable. The exo and endo state transitions are

$$x_{t+1} = \text{clip}(M_{exo} \cdot x_t + \frac{1}{3} \cdot N_{exo} \cdot x_t^2 - \frac{2}{15} \cdot K_{exo} \cdot x_t^3, -4, 4) + \varepsilon_{exo}$$

$$e_{t+1} = M_{end} \cdot \begin{bmatrix} e_t \\ x_t \end{bmatrix} + M_a \cdot a_t + \varepsilon_{end},$$

where M_{exo}, m_e, M_a and $\varepsilon_{exo}, \varepsilon_{end}$ are defined as in Section 5.2. Furthermore, the two matrices $N_{exo} \in \mathbb{R}^{n,n}$ and $K_{exo} \in \mathbb{R}^{n,n}$ are generated following the same procedure as M_{exo} . \mathcal{M}_1 has nonlinear exogenous dynamics but linear endogenous dynamics.

- \mathcal{M}_2 is exactly the same as \mathcal{M}_1 except that the endogenous transition function now has a nonlinear dependence on the action:

$$e_{t+1} = M_{end} \cdot \begin{bmatrix} e_t \\ x_t \end{bmatrix} + M_a \cdot a_t + N_a \cdot a_t^2 + \varepsilon_{end}.$$

The entries in $N_a \in \mathbb{R}^m$ are sampled from the uniform distribution over $[0.5, 1.5)$.

- \mathcal{M}_3 is a 10-D MDP with $m = n = 5$ and a single action variable. The exogenous and endogenous state transitions functions are

$$x_{t+1} = \text{clip}(5 \cdot \text{sign}(x_t) \cdot \sqrt{|x_t|} - \sin(x_t), -2, 2) + \varepsilon_{exo}$$

$$e_{t+1} = M_{end} \cdot \begin{bmatrix} e_t \\ x_t \end{bmatrix} + \sin(3 \cdot a_t) + \varepsilon_{end}.$$

The entries in the noise vectors ε_{exo} and ε_{end} are sampled from $\mathcal{N}(0, 0.16)$ and $\mathcal{N}(0, 0.09)$, respectively. Like $\mathcal{M}_2, \mathcal{M}_3$'s exo and endo transition functions are both nonlinear.

Figures 9a-9c plot the RL performance over 15 replications with different seeds and Table 5 reports the ranks of the discovered exogenous subspaces. Consider first MDPs \mathcal{M}_1 and \mathcal{M}_2 . The Simplified-GRDS and SRAS algorithms

MDP	Exo/Endo State Variables	Method	Exo Subspace Rank	Total Time (secs)	Decomposition Time (secs)
\mathcal{M}_1	5/5	Baseline	-	665.3±39.9	-
		GRDS	9.0±0.0	890.4±140.6	55.0±34.0
		Simplified-GRDS	9.0±0.0	906.7±154.6	72.2±19.8
		SRAS	9.0±0.0	951.2±253.2	172.8±73.2
\mathcal{M}_2	5/5	Baseline	-	717.0±30.3	-
		GRDS	9.0±0.0	959.5±137.1	61.9±41.2
		Simplified-GRDS	9.0±0.0	981.2±138.0	85.0±18.1
		SRAS	9.0±0.0	1019.8±271.9	187.4±72.6
\mathcal{M}_3 ($\epsilon = 0.05$)	5/5	Baseline	-	768.2±50.1	-
		GRDS	7.67±1.44	1033.0±241.2	125.8±126.7
		Simplified-GRDS	3.60±3.28	988.1±160.4	38.7±19.0
		SRAS	3.47±3.36	1081.3±370.7	168.8±70.7
\mathcal{M}_3 ($\epsilon = 0.1$)	5/5	Baseline	-	768.2±50.1	-
		GRDS	7.67±1.44	1033.0±241.2	125.8±126.7
		Simplified-GRDS	9.0±0.0	918.3±129.7	17.7±4.6
		SRAS	9.0±0.0	1023.3±341.5	230.4±69.7

Table 5: Average and standard deviation for rank of discovered exo subspace, total execution time, and decomposition time for the MDPs with nonlinear state transitions.

perform very well. They converge quickly, and they are able to match the Endo Reward Oracle’s performance. In both settings, the Baseline converges to a suboptimal value and suffers from high variance. Most shockingly, GRDS performs catastrophically and exhibits very high variance even though it discovers an exogenous subspace of the correct rank.

Now consider \mathcal{M}_3 in Figure 9c. On this problem, Simplified-GRDS and SRAS perform poorly (although still better than the baseline), while GRDS performs much better. However, none of the methods is able to match the Endo Reward Oracle. Table 5 reveals that all of the methods, but particularly Simplified-GRDS and SRAS, are failing to discover the correct exogenous subspace. This suggests that the CCC computation when applied to the simplified objective is not finding good solutions. To evaluate this possibility, we reran the \mathcal{M}_3 experiment with a larger value of $\epsilon = 0.1$ instead of its default value of 0.05. With this change, the results improve dramatically for Simplified-GRDS and SRAS, and they are able to match the performance of the Endo Reward Oracle. However, the performance of GRDS does not improve, which suggests that it is not able to find good solutions to the large manifold optimization problems that it is solving. This could be because the CCC objective is confused by the nonlinear dynamics or it could be that the optimization is trapped in local minima.

5.3.3 Combinatorial Action Spaces

A limitation of our experiments so far has been that the action space is one-dimensional. We have seen that this implies that the maximal exogenous subspace has dimension $n + m - 1$ rather than n as originally intended. In this section, we describe experiments where we introduce higher-dimensional action spaces. For example, with a 5-dimensional action space, the policy must now select one of 10 values for each of the 5 action variables. In effect, the MDP now has 10^5 primitive actions.

To design MDPs with high-dimensional action spaces, we modify the general linear setting of Section 5.2, so that the action $a_t \in \mathbb{R}^l$ is an l -D vector, and the matrix M_a multiplying a_t is in $\mathbb{R}^{m,l}$. As in the single-action setting, each action variable takes 10 possible values evenly-spaced in $[-1, 1]$. We consider 6 MDPs with a variety of different structures, which may in principle appear in real applications:

- 10-D MDP with $m = n = 5$ and $l = 5$. The action matrix M_a is *dense*, meaning that all its entries are nonzero. We sample the entries in M_a from the uniform distribution over $[0, 1)$ and subsequently normalize each row of M_a to sum to 0.99 for stability. We apply the decomposition algorithms after $L = 6000$ steps and train for a total of $N = 200000$ steps.
- 20-D MDP with $m = n = 10$ and $l = 10$. The action matrix M_a is dense, and generated as above. We set $L = 10000$ and $N = 200000$.
- 30-D MDP with $m = n = 15$ and $l = 8$. The action matrix M_a is *partial dense*, meaning that only $l = 8$ out of the $m = 15$ endogenous states are controlled, but these 8 states are controlled by all actions. M_a is generated as above, except that the rows corresponding to non-controlled endo variables are 0. We set $L = 15000$ and $N = 200000$.

Action Variables	Exo/Endo State Variables	Method	Exo Subspace Rank	Total Time (secs)	Decomposition Time (secs)
5 (dense)	5/5	Baseline	-	3576.8±293.2	-
		GRDS	7.47±0.50	4835.2±960.6	69.8±39.1
		Simplified-GRDS	7.47±0.50	4864.5±979.3	148.1±70.2
		SRAS	7.27±0.44	4914.6±1126.0	402.8±134.0
10 (dense)	10/10	Baseline	-	6162.7±478.0	-
		GRDS	15.6±0.49	7745.5±1299.4	396.5±228.8
		Simplified-GRDS	16.0±0.0	7731.9±1292.3	387.0±145.0
		SRAS	16.0±0.0	8064.7±2006.7	1546.7±483.1
8 (partial dense)	15/15	Baseline	-	8734.0±878.1	-
		GRDS	27.0±0.0	10400.0±1599.6	397.0±244.3
		Simplified-GRDS	27.0±0.0	10150.5±1452.2	556.7±121.8
		SRAS	26.93±0.25	11448.9±4052.9	3702.0±1730.1
8 (partial disjoint)	15/15	Baseline	-	8388.9±706.1	-
		GRDS	22.0±0.0	10399.5±2200.5	1136.4±433.9
		Simplified-GRDS	22.0±0.0	10362.2±1687.5	1520.7±304.4
		SRAS	22.0±0.0	10389.7±1877.7	1224.7±506.5
10 (partial disjoint sparse)	15/20	Baseline	-	12088.9±973.6	-
		GRDS	23.2±0.4	16126.3±1096.9	2799.9±473.5
		Simplified-GRDS	5.47±1.89	18627.7±3103.6	7019.8±1427.1
		SRAS	6.2±1.51	13984.1±6876.4	1976.3±1504.9
20 (partial disjoint sparse)	30/40	Baseline	-	35134.1±2877.3	-
		GRDS	50.0±0.0	43345.1±3470.3	10256.2±2719.9
		Simplified-GRDS	50.0±0.0	44187.4±3672.7	10670.1±3015.7
		SRAS	49.0±0.0	44350.5±3540.4	11691.1±2925.2

Table 6: Mean and standard deviation of the rank of the discovered exo subspace, total execution time, and decomposition time for MDPs with multiple action variables.

- 30-D MDP with $m = n = 15$ and $l = 8$. The action matrix M_a is *partial disjoint*, meaning that only $l = 8$ out of the $m = 15$ endo states are controlled but each of these 8 states is controlled by a distinct action variable. We sample the $l = 8$ nonzero entries of M_a from the uniform distribution over $[0.5, 1.5)$. We set $L = 15000$ and $N = 200000$.
- 35-D MDP with $m = 20$, $n = 15$ and $l = 10$. The action matrix M_a is *partial disjoint*, i.e., only 10 endogenous state variables are directly controlled through the 10 actions (each by a distinct action variable) whereas the remaining ones are controlled indirectly through the other endogenous states; furthermore, the endo transition matrix M_e is *sparse* with sparsity (fraction of nonzeros) 14.3%. Specifically, M_e is generated as in Section 5.2 except that only a small part of the matrix (equal to 14.3%) is initialized to nonzero values. We set $L = 20000$ and $N = 200000$.
- 70-D MDP with $m = 40$, $n = 30$ and $l = 20$. The action matrix M_a is *partial disjoint*, i.e., only 20 endogenous states are directly controlled through the 20 actions whereas the remaining ones are controlled indirectly through the other endogenous states. The endo transition matrix M_e is *sparse* with sparsity 14.3%. We set $L = 35000$ and $N = 300000$.

Figures 10a-10f plot RL performance for these 6 MDPs. We run 15 replications with different seeds and a reward regression learning rate of 0.0006. A first observation is that in all 6 settings the baseline struggles and shows very slow improvement over time (e.g., Figure 10b). Its performance appears to decay on the smallest of these MDPs (Figure 10a). The Endo Reward Oracle performs visibly better than the Baseline and is able to attain higher rewards. However, it exhibits high variance and it improves very slowly (e.g., Figure 10b).

Surprisingly, the Simplified-GRDS and SRAS methods substantially outperform the Endo Reward Oracle. It appears that our methods are able to discover additional exogenous dimensions that reduce the variance of the endogenous reward below the level of the reward oracle. Table 6 confirms that, with the exception of the 35-dimensional sparse, partial disjoint MDP, the algorithms are all discovering exogenous spaces of the expected size. For example, in the largest MDP, which has 70 dimensions and a 20-dimensional action space, GRDS and Simplified-GRDS both discover a 50-dimensional exogenous space. The algorithms are challenged by the fourth MDP ($n=15$, $m = 20$, $l = 10$). On this MDP, GRDS finds a 23.2-dimensional exo space on average, but Simplified-GRDS and SRAS only find exo spaces with an average dimension of 5.47 and 6.2, respectively. They also exhibit high variation in the number of discovered dimensions. Despite these failures, Simplified-GRDS and SRAS perform very well on all six of these MDPs. GRDS struggles on the dense MDPs, but does quite well on the sparse and partial disjoint MDPs.

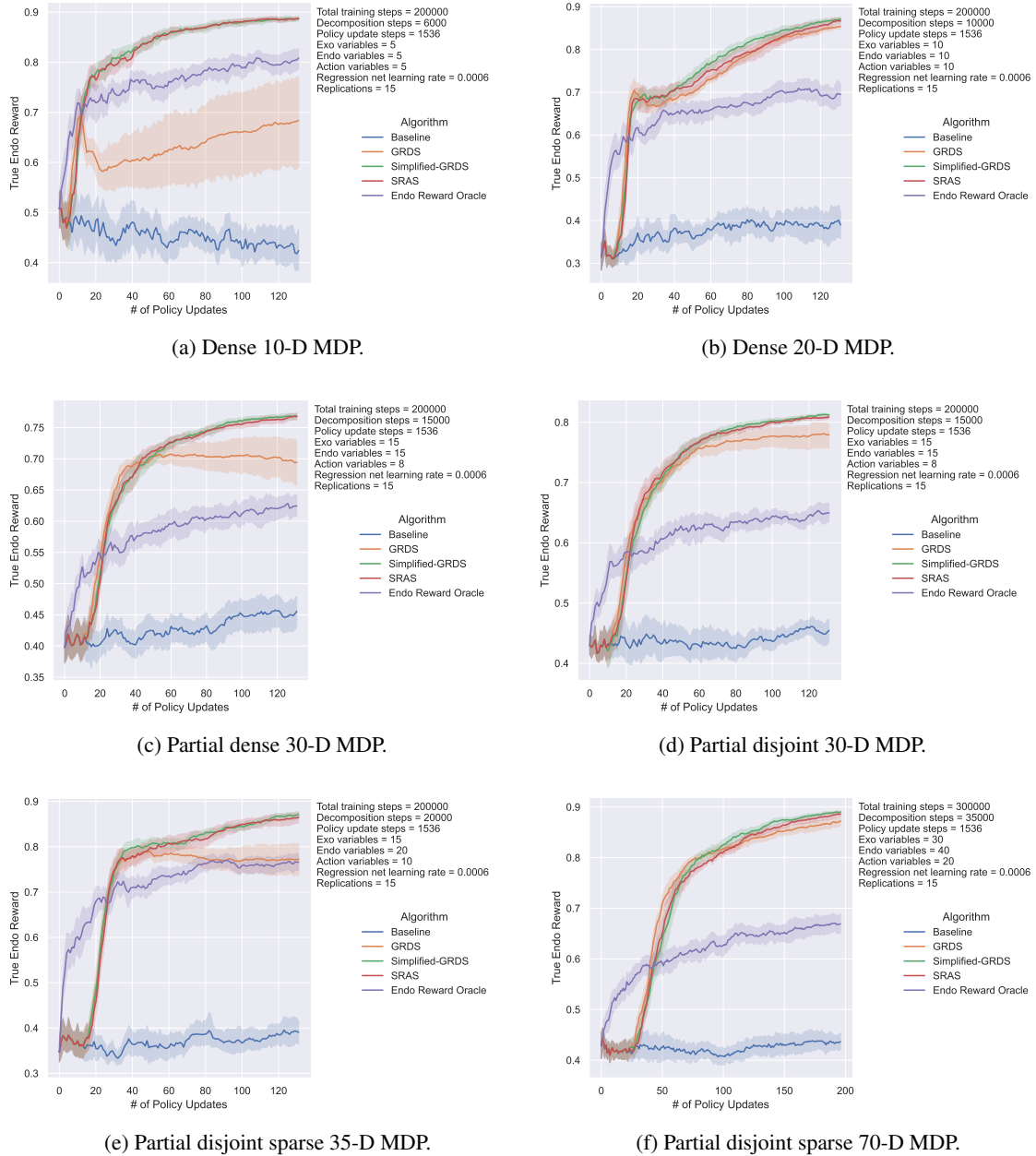


Figure 10: RL performance for MDPs with multiple action variables.

5.3.4 Discrete MDPs

The final variation in MDP structure that we studied was to create an MDP with discrete states. Figure 11 shows a simple routing problem defined on a road network. There are 9 endogenous states corresponding to the nodes of the network. This MDP is episodic; each episode starts in the starting node, v_0 , and ends in the terminal node v_8 . Each edge in the network has a corresponding traversal cost, and the goal of the agent is to reach the terminal node while minimizing the total cost. There are 4 exogenous state variables; each of them is independent of the others and evolves as $x_{t+1,i} = 0.9 \cdot x_{t,i} + \varepsilon_{exo}$, where ε_{exo} is distributed according to $\mathcal{N}(0, 1)$ and $i \in \{1, 2, 3, 4\}$. These exogenous state variables are intended to model global phenomena such as amount of automobile traffic, fog, snow, and pedestrian traffic. These quantities evolve independently of the navigation decisions of the agent, but they modify the cost of traversing the edges.

The reward function is the sum of two terms:

$$r_t = -\text{cost}(s_t \rightarrow s_{t+1}) - \sum_{i=1}^4 x_{t,i}.$$

The first term is the endogenous reward $R_{\text{end},t}$ and the second term is the exogenous reward $R_{\text{exo},t}$.

The actions at each node consist in choosing one of the outbound edges to traverse. We restrict the set of actions to move only rightward (i.e., toward states with higher subscripts). For instance, there are three available actions at node v_0 corresponding to the three outgoing edges, but only a single action at node v_4 . The cost of traversing an edge is shown by the edge weights in Figure 11. The MDP is deterministic: a given action (i.e., edge selection) at a given node always results in the same transition. The observed state consists of the 1-hot encoding for the 9 endo states plus the 4-D continuous exo state variables.

We apply episodic RL with PPO. Since the MDP is small, we modify some of the hyperparameters as follows. We set the total training steps to $N = 10000$ and the policy update steps to $K = 128$. We perform decomposition after $L = 300$ episodes instead of the default value of 3,000 steps. The PPO batch size is set to 32. Every time we update the policy, we execute 300 evaluation episodes (in a separate instance of the MDP environment). For reward regression, we compute a Single Linear Regression rather than Online Neural Net Regression (see Section 5.2.3). We perform 15 replications, each with a different random seed.

Figure 12a plots RL performance. Note that our methods perform on par with the Endo Reward Oracle and exhibit very little variance, with the exception of SRAS. On the other hand, the Baseline makes very slow progress. Table 7 reports the rank of the discovered exogenous subspace as well as the total time and decomposition time. GRDS and Simplified-GRDS discover large exogenous subspaces of rank 11 and 10, respectively. The computed exogenous subspace includes the 4 exogenous state variables we defined as well as linear combinations of the endogenous states that do not depend or have only weak dependence on the action. In contrast, SRAS discovers an exo subspace of very low rank, which explains its suboptimal performance.

The strong performance of our methods might be due to deterministic dynamics of the problem. To test this, we created a stochastic version of the road network MDP. The transition probabilities are specified as follows:

- Taking action 0 / 1 / 2 at node v_0 leads to nodes v_1, v_2, v_4 with probabilities $(0.5, 0.3, 0.2) / (0.3, 0.5, 0.2) / (0.3, 0.2, 0.5)$, respectively.
- Taking action 0 / 1 at node v_1 leads to nodes v_4, v_5 with probabilities $(0.6, 0.4) / (0.5, 0.5)$, respectively.
- Taking action 0 / 1 at node v_2 leads to nodes v_3, v_4 with probabilities $(0.5, 0.5) / (0.3, 0.7)$, respectively.
- Taking action 0 / 1 at node v_3 leads to nodes v_6, v_7 with probabilities $(0.7, 0.3) / (0.4, 0.6)$, respectively.
- Taking action 0 / 1 / 2 at node v_4 leads to nodes v_5, v_6, v_8 with probabilities $(0.6, 0.2, 0.2) / (0, 1, 0) / (0.3, 0.2, 0.5)$, respectively.
- There is only one action (action 0) available at nodes v_5, v_6, v_7 , and this leads with probability 1 to nodes v_8, v_7, v_8 , respectively.
- Node v_8 remains a terminal node.

We employ the same hyperparameters as in the deterministic setting, except that we set the total training steps $N := 20000$ and the number of decomposition episodes $L := 600$.

Figure 12b plots the RL performance over 15 trials (each with a separate random seed). We observe that Simplified-GRDS and GRDS perform only slightly worse than the Endo Reward Oracle, while SRAS exhibits slightly lower average performance and higher variance. The Baseline improves very slowly and lags far behind the other methods. Due to the stochastic transitions, all methods (and particularly the Baseline) exhibit larger variance than in the deterministic MDP in Figure 12a.

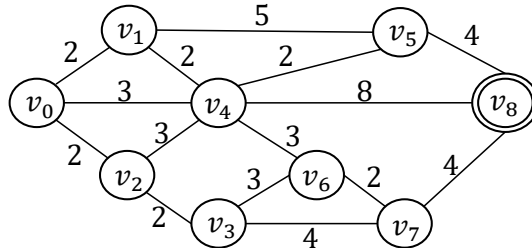


Figure 11: Graph for discrete MDP.

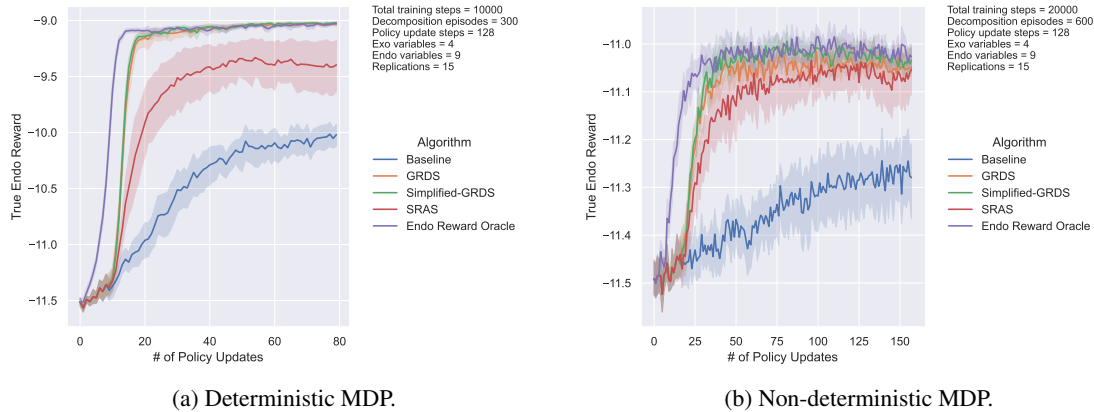


Figure 12: RL performance for discrete MDPs.

MDP	Exo/Endo State Variables	Method	Exo Subspace Rank	Total Time (secs)	Decomposition Time (secs)
Deterministic	4/9	Baseline	-	225.6±16.7	-
		GRDS	9.47±0.50	271.4±55.8	68.4±26.9
		Simplified-GRDS	11.0±0.0	229.3±18.0	10.2±1.9
		SRAS	2.13±1.63	272.9±39.2	72.3±13.5
Non-deterministic	4/9	Baseline	-	419.9±10.8	-
		GRDS	9.66±0.70	503.6±102.2	109.1±42.7
		Simplified-GRDS	11.0±0.0	446.6±21.5	15.6±2.1
		SRAS	2.8±1.38	488.0±56.0	82.7±9.7

Table 7: Average and standard deviation for rank of discovered exo subspace, total execution time, and decomposition time for the discrete MDPs.

Regarding the rank of the computed subspace, we notice from Table 7 that the ranks of the discovered exo subspaces are the same as for the deterministic MDP. This demonstrates the robustness of the algorithms. Simplified-GRDS finds the largest exogenous space with GRDS close behind. SRAS finds much smaller spaces, which partially explains its slightly poorer performance. It is important to remember that not all dimensions of the discovered exogenous subspaces may be relevant to reward regression. SRAS may only be discovering 2.8 dimensions, on average, but these are enough to give it a huge performance advantage over the Baseline.

The total CPU cost and decomposition cost are higher than the deterministic setting, which reflects the added cost of running online reward regression for twice as many steps.

In this problem, the rank-descending methods worked better than SRAS, but even SRAS gave excellent results, and the total CPU time required is not significantly higher than the Baseline.

5.3.5 RQ4 Summary

The experiments demonstrate that our methods are able to handle nonlinear rewards, combinatorial action spaces, and discrete state spaces without modification. When we introduced nonlinear transition dynamics, however, all of our methods performed poorly on at least one of the three MDPs tested. Excellent performance for Simplified-GRDS and SRAS was restored by increasing the value of ϵ , but this did not improve GRDS very much. This is additional evidence that the high dimensional manifold optimization problems that GRDS solves are difficult, particularly when the CCC is computed in a nonlinear setting.

5.4 Anti-correlated Exo and Endo Rewards

Recall in Section 2.3 we showed that if the endogenous and exogenous rewards are negatively correlated, the variance of the endogenous reward can be less than the variance of the full reward and there is no variance reduction benefit from computing the exo/endo reward decomposition. Specifically, Theorem 6 introduced the covariance condition that the variance of the exogenous reward must be greater than twice the negative covariance between the exogenous

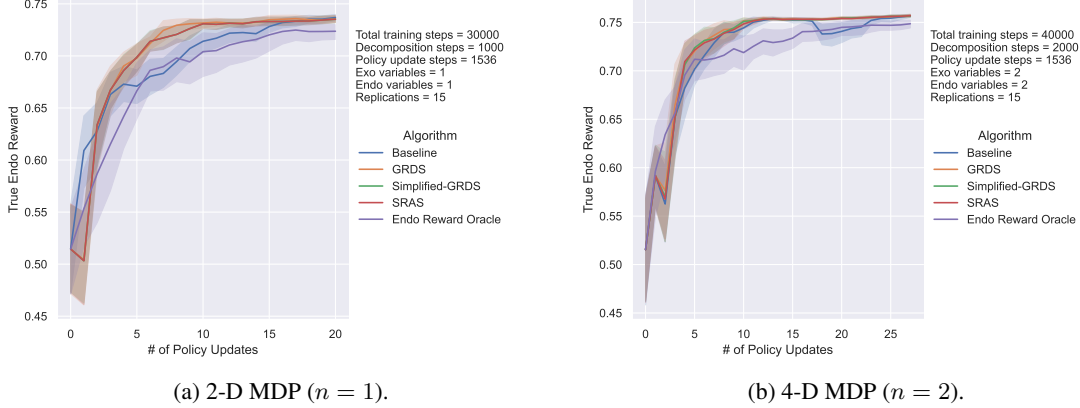


Figure 13: RL performance for MDPs with anti-correlated exo and endo rewards.

and endogenous rewards. RQ5 asks how our algorithms behave when this covariance condition is violated. Does RL performance suffer?

To study this question, we define the following family of $2n$ -D MDPs with a nonlinear exogenous reward

$$\begin{aligned}
 x_{t+1} &= 0.9 \cdot M_{exo} \cdot x_t + \varepsilon_{exo} \\
 e_{t+1} &= 0.45 \cdot M_{end} \cdot e_t + 0.55 \cdot M_{exo} \cdot x_t + M_a \cdot a_t + \varepsilon_{end} \\
 R_{end,t} &= e^{-|\text{avg}(e_t) - 2.5|/3} \\
 R_{exo,t} &= e^{-|\text{avg}(x_t) + 2.5|/3}.
 \end{aligned}$$

The endo and exo states e_t and x_t are both n -D. The matrices $M_{exo} \in \mathbb{R}^{n \times n}$ and $M_{end} \in \mathbb{R}^{n \times n}$ follow the recipe given in Section 5.2. $M_a \in \mathbb{R}^n$ is the coefficient for the action a_t , and it is set to be a vector of ones. The elements of the exogenous noise $\varepsilon_{exo} \in \mathbb{R}^n$ are distributed according to $\mathcal{N}(0, 0.16)$, while the elements of the endogenous noise $\varepsilon_{end} \in \mathbb{R}^n$ are distributed according to $\mathcal{N}(0, 0.04)$. The observed state vector $s_t \in \mathbb{R}^{2n}$ is a linear mixture of the hidden exogenous and endogenous states, as in Section 5.2.

An interesting property of this class of MDPs is that the product $M_{exo} \cdot x_t$ appears with a relatively high coefficient in both x_{t+1} and e_{t+1} . Hence, e_{t+1} and x_{t+1} will exhibit positive correlation. As a result, when $\text{avg}(e_t)$ (and thus $\text{avg}(x_t)$) is high and close to 2.5, $R_{end,t}$ will be high and $R_{exo,t}$ will be low. Conversely, when $\text{avg}(e_t)$ (and thus $\text{avg}(x_t)$) is low and close to -2.5 , $R_{end,t}$ will be low and $R_{exo,t}$ will be high. This causes the endo and exo rewards to be anti-correlated to the point that the covariance condition is violated.

To verify this, we measured the variance $\text{Var}(R_{exo,t})$ and the covariance $-2 \cdot \text{Cov}(R_{end,t}, R_{exo,t})$ for both MDPs under 2 policies: a random policy and the optimal policy. For the 2-D MDP, we find that $\text{Var}(R_{exo,t}) = 0.026$ and $-2 \cdot \text{Cov}(R_{end,t}, R_{exo,t}) = 0.04$ under a random policy, and $\text{Var}(R_{exo,t}) = 0.026$ and $-2 \cdot \text{Cov}(R_{end,t}, R_{exo,t}) = 0.037$ under the optimal policy. For the 4-D MDP, we find that $\text{Var}(R_{exo,t}) = 0.021$ and $-2 \cdot \text{Cov}(R_{end,t}, R_{exo,t}) = 0.033$ under a random policy, and $\text{Var}(R_{exo,t}) = 0.021$ and $-2 \cdot \text{Cov}(R_{end,t}, R_{exo,t}) = 0.040$ under the optimal policy. Hence, the covariance condition is violated in all cases.

Figures 13a and 13b show the RL performance for the different methods when $n = 1$ and $n = 2$, respectively. The exo subspace ranks and time costs are summarized in Table 8. Since the MDPs are rather small, for the former we set $L = 1000$ for the number of steps prior to applying the state-space decomposition methods and train for $N = 30000$. For the latter set $L = 2000$ and $N = 40000$. We perform 15 trials with different seeds.

Notice how the Endo Reward Oracle performs worse than the Baseline; this is to be expected, because the Endo Reward Oracle is forced to use the Endo reward, which has higher variance than the full reward. Our naive expectation was that our decomposition methods would exhibit the same behavior, since they seek to find the maximal exogenous subspace. However, what we observe is that all of our methods do much better than the Endo Reward Oracle and, in the case of $n = 1$, they exceed the Baseline as well.

The key to understanding what is happening is to focus on the reward regression. The loss function for the reward regression is precisely the residual variance of the predicted reward, and the residual reward is precisely our estimate of the endogenous reward. Consequently, reward regression will ignore any exogenous variables that would cause an increase in the variance of the endogenous reward. In the case of $n = 1$, the reward regression has apparently found

some component of the exogenous reward that is not anti-correlated with the endogenous reward and exploited it to reduce the variance of the endogenous reward. Consequently our methods are able to learn faster than the Baseline.

The larger result is that our algorithms can never be affected by anti-correlated rewards. In the worst case, the reward regression will ignore the exogenous variables and simply predict the mean exogenous reward. This will have no effect on the endo-MDP or the RL performance of our methods.

Exo State Variables	Endo State Variables	Method	Exo Subspace Rank	Total Time (secs)	Decomposition Time (secs)
1	1	Baseline	-	221.9±9.7	-
		GRDS	1.0±0.0	276.0±38.3	2.2±0.7
		Simplified-GRDS	1.0±0.0	276.9±36.8	2.2±0.6
		SRAS	1.0±0.0	276.6±39.6	2.3±0.8
2	2	Baseline	-	308.4±9.4	-
		GRDS	2.4±0.8	402.8±67.0	22.5±25.2
		Simplified-GRDS	3.0±0.0	394.3±55.5	6.5±0.8
		SRAS	2.26±0.93	403.8±80.6	24.0±23.1

Table 8: Average and standard deviation for rank of discovered exo subspace, total execution time, and decomposition time for the MDPs with anti-correlated exo and endo rewards.

5.5 Risks and Benefits of Simplified-GRDS

Our experimental results suggest that the Simplified-GRDS method performs very well. RQ6 asks about the risks of the Simplified-GRDS method. From a mathematical perspective, when we minimize $I(X'; A | X)$ (or the CCC approximation), we are only eliminating edges from A to X' , which are the direct effects of A . We are not excluding any indirect path by which A might affect E' , and E' might then affect X in some future time step. In the linear dynamical MDPs that we have studied, such indirect effects do not arise, and all effects of A on X' are visible immediately. Of course, because Simplified-GRDS verifies the full constraint $I(X'; [E, A] | X) < \epsilon$, Simplified-GRDS is still sound, but it may fail to find the maximal exogenous subspace in complex MDPs (as we saw in some of the modified MDPs).

This suggests that for general MDPs, we should choose GRDS rather than Simplified-GRDS. However, our experiments have also shown that there are several cases where GRDS encounters difficulty minimizing the CCC proxy of the $I(X'; [E, A] | X)$ objective. Hence, we believe additional research is needed to improve the manifold optimization process so that GRDS can overcome these challenging cases.

5.6 Practical Considerations

In this section, we switch our attention to practical aspects of our proposed methods. Our goal is to answer RQ7, which concerns how to set the hyperparameters of our method.

5.6.1 Impact of Hyperparameters on Baseline

First, we investigate the impact of hyperparameters on the Baseline. For this purpose, we consider the High-D linear setting of Section 5.2. Recall that for this setting we used the default PPO and Adam hyperparameters in stable-baselines3, summarized in Table 2. We now ask whether the performance of Baseline can be improved by using different hyperparameters. If that were the case, then a more careful hyperparameter tuning could be an alternative to our proposed algorithms.

We consider the 5-D MDP with 3 exo and 2 end variables of Figure 6a, where the Baseline fluctuates between 0.4 and 0.5 with an average of 0.45, visibly lower than all other methods. To understand whether this can be improved further, we tune 3 critical hyperparameters of PPO optimization. We let the batch size take values in $\{16, 32, 64, 128, 256, 512\}$ (Figure 14a), the learning rate take values in $\{5 \times 10^{-5}, 1 \times 10^{-4}, 5 \times 10^{-4}, 1 \times 10^{-3}, 5 \times 10^{-3}, 1 \times 10^{-2}\}$ (Figure 14b), and the number of steps per policy update K take values in $\{250, 500, 750, 1000, 2000, 3000\}$ (Figure 14c). For each experiment, all hyperparameters except for the tuned one are set to the values in Figure 6a. For Figure 14c, we perform policy evaluation every 1536 steps, instead of after each policy update, to ensure that all curves have the same number of evaluation points. We use 10 independent replications with different seeds. Finally, we increase the number of training steps to $N = 80000$ to ensure that the Baseline has enough training budget to converge.

The results demonstrate that none of the parameter combinations can raise performance significantly. Some values for the number of policy update steps manage to slightly improve the average Baseline performance to 0.5 from 0.45, but

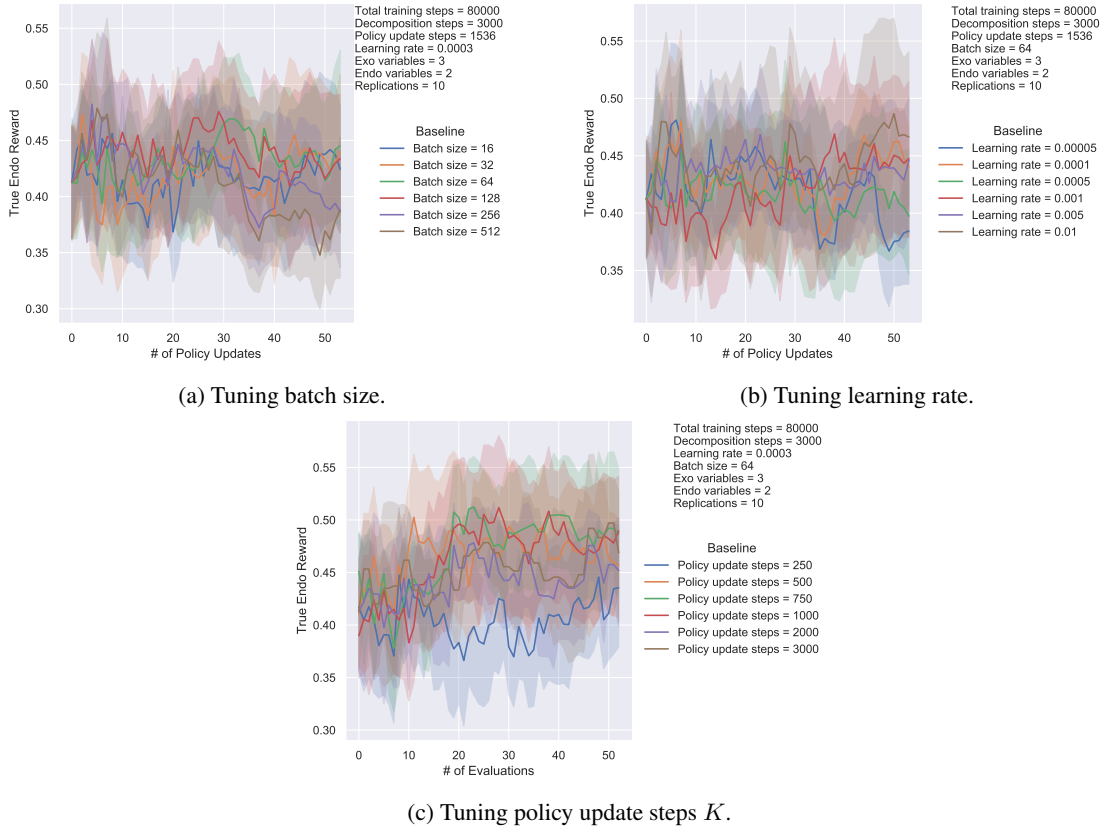
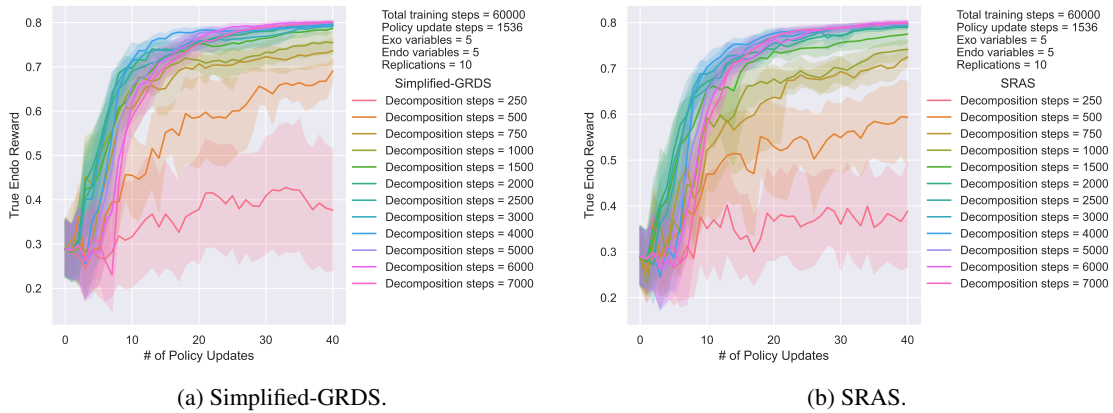


Figure 14: RL performance for Baseline of Figure 6a under various hyperparameters.

Figure 15: RL performance for varying values of L , the number of steps prior to applying the decomposition algorithms, for the 10D setting of Figure 6b.

they still suffer from significant variance. This is in sharp contrast to our algorithms and the Endo Reward Oracle in Figure 6a, which all exhibit much lower variance. Given that this experiment only tunes one hyperparameter at a time, we cannot exclude the possibility that there are combinations of hyperparameters that can achieve a higher and more stable performance for the Baseline. However, its low performance under the default hyperparameters and on a range of reasonable values provides evidence that its poor performance mainly stems from the stochasticity of the exogenous rewards and not badly-chosen hyperparameters.

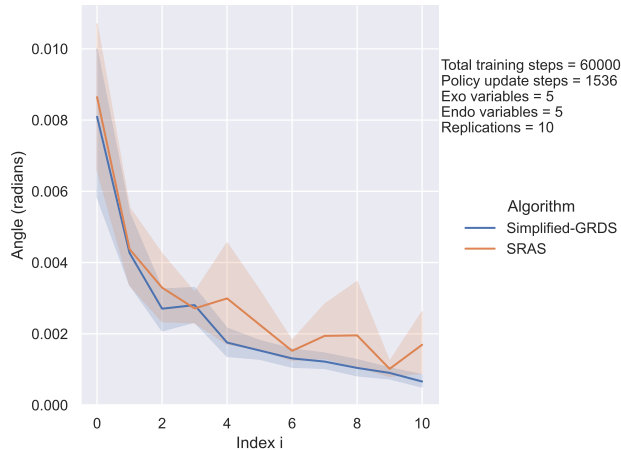


Figure 16: Angle between orthogonal complements of computed exo subspaces corresponding to L_i and L_{i+1} decomposition steps, where the index i ranges from 0 to 10.

5.6.2 Sensitivity Analysis

Recall from Section 5.1 that the main hyperparameter we need to set for our proposed methods is the number of steps L prior to applying the exogenous subspace discovery algorithms. This specifies the number of (s, a, r, s') tuples that are collected for subspace discovery. In this section, we shed light on the impact of L on RL performance. In this direction, we consider the 10-D setting with 5 exo and 5 endo variables of Figure 6b, where our methods and the Endo Reward Oracle converge to a total reward of 0.8 in $N = 50000$ steps. In contrast, the Baseline only attains a reward of around 0.3 on average. We perform sensitivity analysis by considering twelve possible values for L : 250, 500, 750, 1000, 1500, 2000, 2500, 3000, 4000, 5000, 6000, 7000. We denote each value by the increasing sequence $L_i, i \in \{0, \dots, 11\}$, where $L_0 = 250$ and $L_{10} = 7000$. We report the average RL performance for the Simplified-GRDS and SRAS methods in Figure 15(a,b), since they both perform very well. For both methods, when $L_0 = 250$, performance is barely better than the Baseline. As we increase L , performance improves steadily and almost matches the Endo Reward Oracle as soon as we reach 2000 decomposition steps. Increasing L beyond 2000 gives minor benefit and delays the time at which PPO can take advantage of the improved reward function.

This suggests that the decomposition algorithms have converged after $L = 2000$. Can we verify this? The rank of the discovered exogenous space is not informative, because it is always 9-dimensional for all 12 values of L and across all 10 replications. To get a finer-grained measure, we can take advantage of the fact that the complement of the discovered 9-dimensional exogenous space is a 1-dimensional space. This means it can be represented by a direction vector, and we can compare different solutions by computing the angles between these direction vectors.

Figure 16 depicts the angle (in radians) between the orthogonal complements of the exogenous subspaces for each consecutive pair of L_i and L_{i+1} values. If the methods had converged, these angles would be zero. They are not zero, which shows that the exogenous subspaces are continuing to change as L increases. But the angles are all very small (less than 0.5 degrees in the largest case), so these changes are not large, and they are converging (with few exceptions) monotonically toward zero. Simplified-GRDS exhibits smooth convergence, whereas SRAS shows higher variance and a few bumps.

The results suggest that manifold optimization performs very well on this problem, even with relatively small numbers of samples. What is then the reason for the different performance levels in Figure 15? The answer lies in the exogenous reward regression. Recall that after L steps, we conclude Phase 1 by computing the decomposition and then fitting the exogenous reward neural net to the L collected observations. Even though different numbers of decomposition steps result in almost identical exogenous subspaces, the subsequent exogenous reward regression can yield dramatically different exo reward models. When the value of L is very low, we have only a limited number of samples for the exo reward regression, and these might not to cover the exo state subspace adequately. As a result, the learned exo reward model may overfit the observations and fail to generalize to other subspaces. The subsequent online neural network reward regression in Phase 2 only processes each new observation once, so learning the correct exo reward model can take many steps, and cause PPO to learn slowly.

To confirm the above, we perform a second experiment. Unlike previous experiments, we decouple decomposition and exogenous reward regression. Decomposition still takes place after L_i steps. But reward regression is now performed

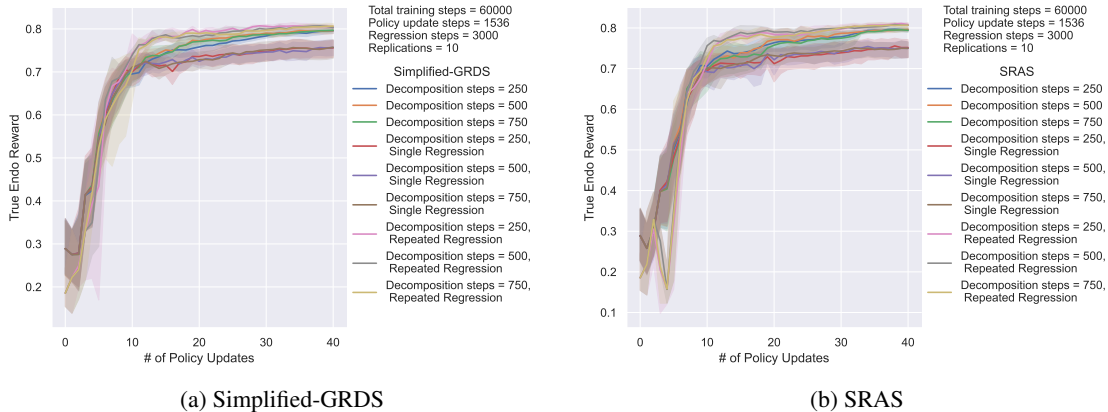


Figure 17: RL performance when computing the exo/endo decomposition at $L_i = 250, 500,$ and 750 steps. Reward regression starts at 3000 steps. Default: online neural network regression; Single Regression: single linear regression at 3000 steps; Repeated Regression: linear regression every 256 steps.

after 3000 samples have been collected (3000 is the default value for L in the high-D experiments). After learning the exogenous reward model with the 3000 samples, we proceed to Phase 2. We experiment with three options for exogenous reward regression in Phase 2: (i) standard online learning where we update the exogenous reward model every $M = 256$ steps; (ii) a single linear regression after which the exogenous reward model is never updated; and (iii) repeated linear regression where we fit a new exogenous reward model from scratch every $M = 256$ steps. We study the three lowest values for L_i ($L_0 = 250, L_1 = 500$ and $L_2 = 750$), as these were the values in Figure 15 with the worst performance.

Figure 17 plots the RL performance averaged over 10 independent trials. We make several observations. First, increasing the number of steps for learning the initial exogenous reward model from L_i to 3000 improves RL performance. With online learning, we match the Endo Reward Oracle’s average performance of 0.8. This confirms our previous hypothesis that the reason for the bad performance in Figure 15 was the poor initial exogenous reward model. With a single regression, RL performance improves (especially for $L_0 = 250$ and $L_1 = 500$), but it performs worse than online learning while having greater variance. Interestingly, learning a new linear regression model every $M = 256$ steps performs the best and slightly outperforms online neural network regression. A plausible reason for this is that online regression only performs a single pass over the data, so it may adapt to the changing state and reward distribution more slowly. On the other hand, repeated linear regression requires 10 times as much computation time as online regression for the settings in Figures 17a and 17b.

5.6.3 Practical Guidelines For State Decomposition and Exo Reward Regression

This sensitivity analysis suggests the following procedure for computing state space decompositions and reward regressions. Start with a small number for L (e.g., 250) and compute the corresponding exo subspace after L steps. Then, every ΔL steps (e.g., 250), recompute the exo subspace until the discovered exo subspace stops changing. This can be detected when (i) the rank of the subspace does not change, and (ii) the largest principal angle between consecutive subspaces is close to 0 [Björck and Golub, 1973].

As soon as we have an initial exo subspace, we can fit the exogeneous reward model, and each time we recompute the subspace, we can re-fit the model. These initial fits could be performed with linear regression or neural network regression. Once the exogenous subspace as converged, we can switch to online neural network regression, because the regression inputs will have stabilized.

Application constraints may suggest alternative procedures. If each step executed in the MDP is very expensive, then the cost of the multiple decomposition and reward regression computations is easy to justify. However, if MDP transitions are cheap, then we need to take a different approach. If many similar MDPs will need to be optimized, we can use this full procedure on a few of them to determine the value of L at which the exo space converges. We then just use that value to trigger exo/endo decomposition and perform neural network reward regression starting at step L and continuing online. If there is only one MDP to be solved, L could be selected using a simulation of the MDP. In all of our experiments, we have followed this procedure for setting L .

A last question concerns the value for the CCC threshold ϵ . In theory, we should use very low values to minimize the chance of discovering an invalid exo/endo state decomposition, but this could come at the cost of having to perform more steps in GRDS and SRAS. We lack theoretical guidance for making this decision. In principle, one could start with a somewhat large value for ϵ (e.g., 0.1) and perform multiple runs (in simulation or on a sample of MDPs) with progressively smaller values of ϵ until either the discovered exo subspace converges or RL performance stabilizes.

5.7 Discussion

Let us review the research questions and our results.

- RQ1: Do our methods speed up reinforcement learning in terms of sample complexity? In terms of total CPU time? We found that our methods yield dramatic speedups for reinforcement learning both in terms of the number of MDP transitions observed and in terms of clock time. The improvements are so dramatic that we were not able to run the Baseline method long enough for it to match the level of RL performance achieved by our methods, so we estimated this by linear extrapolation.
- RQ2: Do our methods discover the correct maximal exogenous subspaces? Our methods surprised us by finding exogenous subspaces that were larger than we had naively expected. Analysis showed that these subspaces did indeed have maximal dimension. Our experiments measured the correctness of the subspaces by the resulting RL performance. In nearly all cases, our methods matched the performance of the Endo Reward Oracle that was told the correct subspace for the endogenous reward. In the 2-D covariance condition experiment, our methods did better than the Endo Reward Oracle.
- RQ3: What is the best approach to reward regression? Single linear, repeated linear, or online neural network regression? We found that online neural network regression worked best and was more stable, even in cases where the reward function was linear.
- RQ4: How do the algorithms behave when the MDPs are changed to have different properties: (a) rewards are nonlinear, (b) transition dynamics are nonlinear, (c) action space is combinatorial, and (d) states and actions are discrete? Our methods, combined with neural network regression, handled the nonlinear rewards well. When the transition dynamics are nonlinear, our methods sometimes struggled, but we found that they worked well if we increased the ϵ parameter to allow the CCC objective to be substantially nonzero. Our methods worked very well in combinatorial action spaces and in discrete MDPs.
- RQ5: How do the algorithms behave when the covariance condition is violated? When the covariance condition is violated, our methods still give excellent results. This is because reward regression minimizes the variance of the endogenous reward, so it only fits that aspect of the exogenous reward that can be removed without increasing the variance of the endogenous reward.
- RQ6: What are the risks and benefits of using the simplified objective in SRAS and Simplified-GRDS? The Simplified-GRDS method gave the best overall RL performance. It provides a nice balance of computational efficiency and optimization performance while remaining sound.
- RQ7: How should hyperparameters be set? How many training tuples should be collected before performing exogenous subspace discovery? When should reward regression begin, and on what schedule? We found that the default values of the hyperparameters worked well, and we developed a tuning procedure for determining the training set size K for exogenous subspace discovery. It starts with $K = 250$ and repeatedly adds 250 tuples until the exo space stabilized. Small values of K worked surprisingly well.

The benefits of our algorithms are not necessarily limited to linear MDPs. We observed strong performance with general nonlinear exo reward functions, and often on MDPs with nonlinear exo/endo transition dynamics but where the state space could be linearly decomposed into the exo and endo subspaces. This showed that our CCC objective can provide good results even in these nonlinear cases. An alternative to our CCC-based linear approach would be to enforce the exo/endo decomposition using cross-covariance operators on a Reproducing Kernel Hilbert Space (RKHS). However, RKHS computations can be computationally challenging and are difficult to scale to high-dimensional spaces [Fukumizu et al., 2008].

6 Related Work

In this section, we review prior work on reinforcement learning with exogenous information that is not covered elsewhere in the paper. Efroni et al. [2022b] introduce the Exogenous Block Markov Decision Process (EX-BMDP) setting to model environments with exogenous noise. Under the assumption that the endogenous state transition is near deterministic, they propose the Path Predictive Elimination (PPE) algorithm. PPE learns a form of multi-step

inverse dynamics [Paster et al., 2021]. It can recover the latent endogenous model while being both sample efficient and computationally efficient. PPE runs in a reward-free setting and does not make any assumptions about the reward function. In their follow-up work, Efroni et al. [2022a] introduce the ExoMDP setting, which is a finite state-action variant of the EX-BMPD where the state directly decomposes into a set of endogenous and exogenous factors, while the reward only depends on the endogenous state. They propose ExoRL, an algorithm that learns a near-optimal policy for the ExoMDP with sample complexity polynomial in the number of endogenous state variables and logarithmic in the number of exogenous components. Because the reward does not depend on the exogenous state variables, those variables are not only exogenous but irrelevant, and they can be ignored during reinforcement learning. In our work, in contrast, the exogenous variables can still be important for the policy, so the RL algorithm must consider them as inputs when learning the policy.

In a different thread of work, Chitnis and Lozano-Pérez [2020] address the problem of learning a compact model of an MDP with endogenous and exogenous components for the purpose of planning. They consider only reducing the exogenous part of the state, given that is the part that induces the most noise, and assume that the reward function decomposes into a sum over the individual effects of each exogenous state variable. They introduce an algorithm based on the mutual information among the exogenous state variables that generates a compact representation, and they provide conditions for the optimality of their method. Our assumption of additive reward decomposition is weaker than their per-state-variable assumption.

Another line of work related to exogenous information concerns curiosity-driven exploration by Pathak et al. [2017], where the goal is to learn a reward to enable the agent to explore its environment better in the presence of very sparse extrinsic rewards. It falls under the well-studied class of methods with intrinsic rewards [Bellemare et al., 2016, Haber et al., 2018, Houthoofd et al., 2016, Oh et al., 2015, Ostrovski et al., 2017, Badia et al., 2020] This work employs a self-supervised inverse dynamics model, which encodes the states into representations that are trained to predict the action. As a result, the learned representations do not include environmental features that cannot influence or are not influenced by the agent’s actions. Based on these representations, the agent can learn an exploration strategy that removes the impact of the uncontrollable aspects of the environment. Note that the inverse dynamics objective is generally not sufficient for control and does not typically come with theoretical guarantees [Rakelly et al., 2021]. Finally, we mention that reinforcement learning with exogenous information has also been studied from a more empirical standpoint in real problems such as learning to drive [Chen et al., 2021].

Finally, our work shares similarities with other work on modeling the controllable aspects in the environment [e.g., Choi et al., 2019, Song et al., 2020, Burda et al., 2019, Bellemare et al., 2012, Corcoll et al., 2022, Thomas et al., 2018]. The main difference is that in exo/endo MDPs, we capture the controllable versus uncontrollable aspects via the exo/endo factorization, where endo (resp., exo) states correspond to the controllable (resp. uncontrollable) aspects. Combining the two families of approaches could be an avenue for future research. We also note the work by Yang et al. [2022], which proposes the dichotomy of control for return-conditioned supervised learning. This is accomplished by conditioning the policy on a latent variable representation of the future and introducing two conditional mutual information constraints that remove any information from the latent variable that has to do with randomness in the environment. However, unlike ours, their work is not concerned with exogenous state variables and decompositions.

7 Concluding Remarks

In this paper, we proposed a causal theory of exogeneity in reinforcement learning and showed that in causal models satisfying the full and diachronic two-step DBN structures, the exogenous variables are causally exogenous. We introduced exogenous-state MDPs with additively decomposable rewards and proved that such MDPs can be decomposed into an exogenous Markov reward process and an endogenous MDP such that any optimal policy for the endogenous MDP is an optimal policy for the original MDP. We studied the properties of valid exo/endo decompositions and proved that there is a maximal exogenous subspace that contains all other exogenous subspaces. We also showed that not all subsets of the maximal exogenous subspace define valid exo/endo decompositions.

Given an exogenous-state MDP, we wish to discover a useful exogenous subspace of its state space. We explored several optimization formulations based on conditional mutual information for discovering the exogenous state variables and estimating the exogenous reward. We developed two practical algorithms, GRDS and SRAS, for the case when the exogenous space is a linear projection of the full state space. Our algorithms use the conditional correlation coefficient (CCC) as a measure for conditional independence and rely on solving a manifold optimization problem. Under the assumption that the exploration policy visits all states and tries all actions infinitely often, we showed that GRDS discovers the maximal exogenous subspace. Furthermore, under the assumption of faithfulness, the exogenous subspace we discover is guaranteed to contain only causally-exogenous components. We also introduced Simplified-GRDS, which employs a simplified CCC objective and then checks the solution to see if it satisfies the full CCC objective.

Our experiments on a variety of high-dimensional linear dynamical MDPs demonstrated that our algorithms, particularly Simplified-GRDS and SRAS, can greatly accelerate reinforcement learning. Additional experiments showed that these methods can also give excellent performance on MDPs with nonlinear rewards, nonlinear transition dynamics, combinatorial action spaces, and discrete state spaces. The methods are robust to hyperparameter settings and do not require delicate hyperparameter tuning.

There are several important directions for future research. First, we lack a deep theoretical understanding of the manifold optimization problem corresponding to the CCC. It would be helpful to shed light on its sample complexity and on its loss landscape, which may contain local minima. It is also critical to elucidate the conditions under which the CCC can capture conditional independence, at least for linearly decomposable MDPs. Second, we lack a rigorous theory of the impact of exogenous reward regression on RL convergence. Such knowledge could help us design better exogenous reward regression methodologies. Third, in our work we constrain the exogenous rewards to be additive. However, it is possible that in real settings exogenous rewards are non-additive (e.g., multiplicative), and our decomposition theorem will not hold. Investigating non-additive decompositions would be valuable. Fourth, a more precise mathematical analysis of the simplified objective that we employ in the Simplified-GRDS and SRAS algorithms might help explain their strong empirical performance. Fifth, it would be nice to study nonlinear exo/endo decompositions, especially in the presence of nonlinear transition dynamics. Can efficient, general strategies be discovered? Finally, are there alternatives to the assumptions (admissible MDP, fully-randomized policy, and faithfulness) that we adopted to prove causal exogeneity of the subspaces discovered by GRDS?

Acknowledgments

We would like to acknowledge support for this project from the National Science Foundation (NSF grant IIS-9988642), the Multidisciplinary Research Program of the Department of Defense (MURI N00014-00-1-0637), and a gift to the Oregon State University Foundation from Huawei. We thank Yuvraj Sharma for porting our implementation to Python and assisting with some of the experiments.

A Additional Theory on Exogenous State Variables

Definition 1 for causal exogeneity is inherently structural: it defines causal exogeneity as a property of the structure of the causal graph. In this appendix, we exploit this to structurally characterize causally exogenous state variables (Appendix A.1) as well as the causal graphs with causally exogenous state variables (Appendix A.2).

A.1 Structural Characterization of Causally-Exogenous State Variables

We begin by providing a general structural condition in terms of the unrolled DBN of an MDP that guarantees causal exogeneity. To this goal, we introduce the structural notion of *action-disconnected states*; we subsequently show that action-disconnected state variables are causally exogenous.

Definition 8 (Action-Disconnected State Variables). *A state variable C is action-disconnected, if the unrolled decision diagram contains no directed chain of the form $A_t \rightarrow \dots \rightarrow C_\tau, \forall t \in \{0, \dots, H-1\}, \forall \tau \in \{t+1, \dots, H\}$.*

To visualize action-disconnected state variables, consider the 3-state MDP of Figure 18a and assume a horizon $H = 2$. The unrolled diagram for that value of H is depicted in Figure 18b. State variables S_1 and S_2 are action-disconnected, whereas S_3 is not due to the presence of the directed chains $A \rightarrow S'_3 \rightarrow S''_3 \rightarrow S'''_3, A' \rightarrow S''_3 \rightarrow S'''_3$, and $A'' \rightarrow S'''_3$.

Theorem 9. *If a state variable C is action-disconnected, then C is causally exogenous.*

Proof. Let \mathcal{G} be the graph corresponding to the unrolled decision diagram of the MDP from timestep 0 to timestep H . Define a trail as a loop-free and undirected (i.e., all edge directions are ignored) path between two nodes. We will make use of the d -separation theory with trails [see Pearl, 1988, 2009]. Furthermore, recall Rule 3 of the do-calculus for any causal graph \mathcal{G}

$$P(F \mid \text{do}(G), \text{do}(H), J) = P(F \mid \text{do}(G), J), \text{ if } F \perp\!\!\!\perp H \mid G \cup J \text{ in } \tilde{\mathcal{G}},$$

where $\tilde{\mathcal{G}}$ is the graph obtained by first deleting all edges pointing into G and then deleting all arrows pointing into H from nodes that are not ancestors of J . According to Definition 1, in order to show that C must be exogenous, we must prove that

$$P(C_{t+1}, \dots, C_H \mid C_t, \text{do}(A_t)) = P(C_{t+1}, \dots, C_H \mid C_t).$$

We will prove this statement by applying Rule 3 of the do-calculus above. For this purpose, we set $F \leftarrow C_{t+1}, \dots, C_H$, $G \leftarrow \emptyset$, $H \leftarrow A_t$, and $J \leftarrow C_t$. Given G is the empty set and A_t cannot have incoming edges from any ancestor of C_t ,

the graph $\tilde{\mathcal{G}}$ will be identical to \mathcal{G} except that the incoming edges to A_t are deleted. To show exogeneity, it then suffices to show that

$$C_{t+1}, \dots, C_H \perp\!\!\!\perp A_t \mid C_t \text{ in } \tilde{\mathcal{G}}.$$

Indeed, consider any trail P connecting node A_t to node $C_{t+\tau}$ in $\tilde{\mathcal{G}}$. Since C is action-disconnected, we know that there can be no directed chain from A_t to $C_{t+\tau}$ of the form $A_t \rightarrow \dots \rightarrow C_{t+\tau}$. We argue that this then implies that P must necessarily contain a collider node Z of the form $\rightarrow Z \leftarrow$. To see why, notice that the first link in P has the form $A_t \rightarrow \dots$. If all subsequent links in P are of the form $\dots \rightarrow \dots$, then P would be a directed chain, which is a contradiction. Hence, the edge directionality at P must change at some node, which implies there must be some collider node Z in P . The following two cases are then possible:

1. If Z is not C_t or an ancestor of C_t , then the P is d -separated and thus does not violate the causal Definition 1.
2. Otherwise, assume that Z is either C_t or an ancestor of C_t . By the structure of the causal graph, it is not hard to see that in order for this assumption to hold, P must contain a link $V_t \leftarrow U_{t-1}$ from some state or action variable U_{t-1} at time step $t-1$ to some state variable V_t at time step t . Consider the sub-trail up to node U_{t-1} , which will have the form $A_t \rightarrow \dots V_t \leftarrow U_{t-1}$. The sub-trail must contain a collider node \tilde{Z} ; furthermore, \tilde{Z} has time index t or higher, so it cannot be C_t or an ancestor of C_t . But this shows that trail P is also d -separated and, hence, does not violate the causal exogeneity Definition 1. □

According to Corollary 5, state variables S_1 and S_2 in the MDP of Figure 9 are causally exogenous. What about the reverse direction? We show that it is a natural implication of Definition 1 for causal exogeneity.

Theorem 10. *If state variable C is causally exogenous, then C must be action-disconnected in the corresponding causal graph \mathcal{G} .*

Proof. Assume C is not action-disconnected. Then there must exist some directed chain $A_t \rightarrow \dots \rightarrow C_{t+\tau}$ connecting A_t to some future state $C_{t+\tau}$. This chain cannot go through C_t due to the structure of \mathcal{G} . In that case, A_t and $C_{t+\tau}$ are not d -separated by C_t in graph $\tilde{\mathcal{G}}$, where $\tilde{\mathcal{G}}$ is identical to \mathcal{G} except that the incoming edges to A_t are deleted. As a result, we cannot apply Rule 3 of the do-calculus to simplify expression $P(C_{t+\tau} \mid \text{do}(A_t), C_t)$ to $P(C_{t+\tau} \mid C_t)$. The property $P(C_{t+\tau} \mid \text{do}(A_t), C_t) = P(C_{t+\tau} \mid C_t)$ cannot thus hold as a result of the DAG structure of \mathcal{G} . Intuitively, the existence of chain $A_t \rightarrow \dots \rightarrow C_{t+\tau}$ in $\tilde{\mathcal{G}}$ means that there is a path through which an intervention $\text{do}(A_t)$ on A_t can influence $C_{t+\tau}$, which implies that state variable C cannot be causally exogenous. □

It is not hard to see that Theorems 9 and 10 also hold, when C is a set of causally exogenous state variables. Taken together, Theorems 9 and 10 imply the next result.

Corollary 5. *The set of causally exogenous state variables is identical to the set of action-disconnected variables.*

Proof. Theorem 9 establishes the forward direction, while Theorem 10 establishes the reverse direction. □

The previous result allows us to prove two basic properties of causally exogenous state variables.

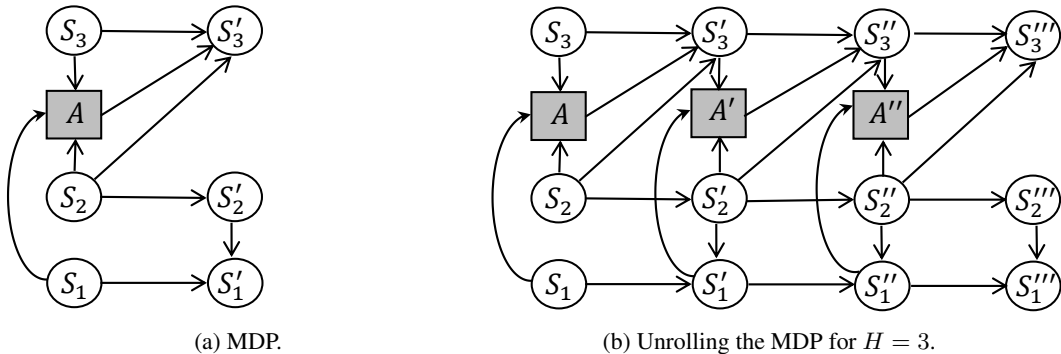


Figure 18: An MDP with 3 state variables S_1, S_2, S_3 , where S_1 and S_2 are exogenous.

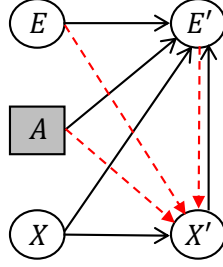


Figure 19: State transition diagram for an MDP with all links (black and dashed red) present. Links to the action node A from E and X are missing for fully randomized policies.

Theorem 11. *Consider any MDP with causally exogenous state variables.*

1. *Assume that the two sets of state variables $X_1 = S[\mathcal{I}_1]$ and $X_2 = S[\mathcal{I}_2]$ are causally exogenous. Then the union set $X = S[\mathcal{I}_1 \cup \mathcal{I}_2]$ is also causally exogenous.*
2. *Assume $X = S[\mathcal{I}]$ is a set of causally exogenous state variables. Any subset $\tilde{X} \subseteq X$ is then also causally exogenous.*

Proof. We trivially have from Corollary 5:

1. Any state variable in X_1 or X_2 must be action-disconnected, so the union $X_1 \cup X_2$ can only contain action-disconnected state variables.
2. Any state variable in X must be action-disconnected, hence state variables in $\tilde{X} \subseteq X$ must be action-disconnected.

□

Finally, we remark that defining exogeneity in causal terms as in Definition 1 is the most natural choice. To see why, consider the MDP in Figure 18a. For this MDP, S_1 and S_2 are exogenous, since their evolution does not depend on the action. Indeed, both S_1 and S_2 are exogenous by Corollary 5, since it is easy to verify that they are both action-disconnected in the unrolled diagram. In particular, S_1 will satisfy the causal definition $P(S'_1 | S_1, \text{do}(A)) = P(S'_1 | S_1)$. On the other hand, it may not be true that $P(S'_1 | S_1, A)$ equals $P(S'_1 | S_1)$. This is because of the trail $A \leftarrow S_2 \rightarrow S'_2 \rightarrow S'_1$, which could make S'_1 conditionally dependent on A given S_1 even though S'_1 is not causally dependent on A .

A.2 Characterization of Causally-Exogenous Causal Graphs with the Complete Exogenous Set

Theorem 7 establishes conditions under which the discovered set X of a full or diachronic exo/endo decomposition is causally exogenous. In particular, under these conditions, the maximal exo set will contain causally exogenous state variables only. A natural question then arises: does the maximal exo set contain *all* causally exogenous state variables? Notice that the union property (e.g., in Corollary 1 or Lemma 1) only allows us to take the union of exo/endo decompositions, not the union of arbitrary sets of exogenous state variables. So, it is not immediately obvious whether the maximal exo set will contain all exo state variables.

To answer this question, we first introduce the concept of the complete exogenous set, which we then use to characterize the structure of all possible causal graphs with causally exogenous state variables.

Definition 9 (Complete Exogenous Set). *The complete exogenous set X_f of an MDP is defined as the set of all causally exogenous state variables. Its complement $E_f = X_f^c$ is called the complete endogenous set.*

Obviously, E_f can only contain state variables that are not causally exogenous. Our next result is central and characterizes all possible causal graphs with causally exogenous state variables.

Theorem 12. *Consider any stationary MDP with causally exogenous state variables. Its underlying causal graph can only have two possible forms: (i) the full exo DBN of Figure 2 with $X = X_f$, or (ii) a special class of DAGs where all directed paths in the unrolled DBN from A to state variables in E_f terminate at a timestep equal to the horizon H .*

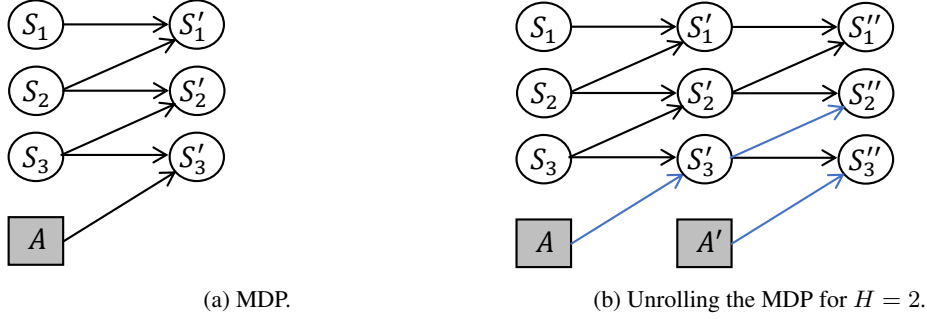


Figure 20: An edge case for Theorem 12, where the MDP does not accept any full exo/endo decomposition, even for the maximal exo state space.

Proof. Consider the complete exo set X_f . By Corollary 5, we know that X_f must be action-disconnected. Furthermore, state variables in E_f must not be action-disconnected, or else they would be causally exogenous and thus belong to X_f ; the latter is impossible since X_f by definition contains *all* causally exogenous state variables. As a result, for each state variable E_i in E_f , there must be at least one $E_{t,i}$ with $t \in \{1, \dots, H\}$ so that there is a directed path from some $A_\tau, \tau \in \{0, t-1\}$ to $E_{t,i}$. Let's now consider the state partition (E_f, X_f) in causal graph \mathcal{G} . The unrestricted state transition diagram will contain all links (black and dashed red) in Figure 19. In order to show that (E_f, X_f) matches the causal full exo DBN of Figure 2, we must show that it must be missing all the red dashed links. We separately consider the 3 links:

1. The link $A \rightarrow X'$ must not be present because it would trivially give a directed path from A_t to X_{t+1} , which violates the exogeneity of X_j according to Corollary 5.
2. The link $E' \rightarrow X'$ must also not be present. Indeed, assume there is some link $E'_i \rightarrow X'_j$. By the observation above, there is a directed path from some A_τ to $E_{t,i}$. But then we can extend this path to get a directed path from A_τ to $X_{t,j}$ using the link $E'_i \rightarrow X'_j$, which violates the exogeneity of X_j according to Corollary 5.
3. We finally discuss the link $E \rightarrow X'$. Assume there is such a link $E_i \rightarrow X'_j$. Given E_i is not exogenous, there is a directed path from some A_k to $E_{t,i}$. We can then extend that path to $X_{t+1,j}$ to get a directed path from A_k to $X_{t+1,j}$ using the link $E_i \rightarrow X'_j$, which violates the exogeneity of X_j according to Corollary 5.

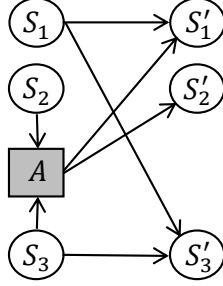
There is only one special edge case we need to consider for point (3). If there is a single directed path from A to E_i that terminates at $E_{H,i}$, then it is not possible to extend that path to $X_{H+1,j}$, since we cannot go beyond time horizon H . \square

Figure 20 depicts a graph where case (ii) of Theorem 12 applies. Consider the MDP in Figure 20a with 3 state variables and a horizon of $H = 2$. We depict the unrolling process over H in Figure 20b. Directed paths starting from action nodes are shown in blue color. Notice that S_1 is the only action-disconnected state variable, and according to Corollary 5, it will be the only causally exogenous state variable. Hence, the maximal exo set will simply be $X_f = \{S_1\}$ with corresponding $E_f = \{S_2, S_3\}$. Notice, however, the link from S_2 to S'_1 ; since this link originates from E_f to X'_f , the corresponding state partition (E_f, X_f) does not abide by the full causally exogenous DBN of Figure 2.

Theorem 12 has important implications in practice. Assume any admissible MDP with a fully randomized exploration policy. Under faithfulness, any MDP with exogenous state variables will generally accept a full exo/endo (statistical) decomposition $S = (E, X)$, namely, the one where X is the full exo set X_f containing all exogenous state variables. Hence, the full exo DBN is not just a convenient tool based on the 2-timestep dynamics, but a powerful abstraction that can usually capture the maximal exo set X_m under certain conditions. However, edge cases exist according to Theorem 12: for instance, in the MDP of Figure 20 there is no valid full exo/endo decomposition even though the maximal exo set is nonempty, under the standard conditions. This answers the question we asked at the beginning of Appendix A.2.

B The Simplified Objective

Our experiments showed that the Simplified-GRDS and SRAS algorithms often give excellent performance. Both of these algorithms employ the simplified information theoretic objective $I(X'; A | X) = 0$ in place of either the

Figure 21: MDP with 3 endogenous state variables S_1, S_2, S_3 .

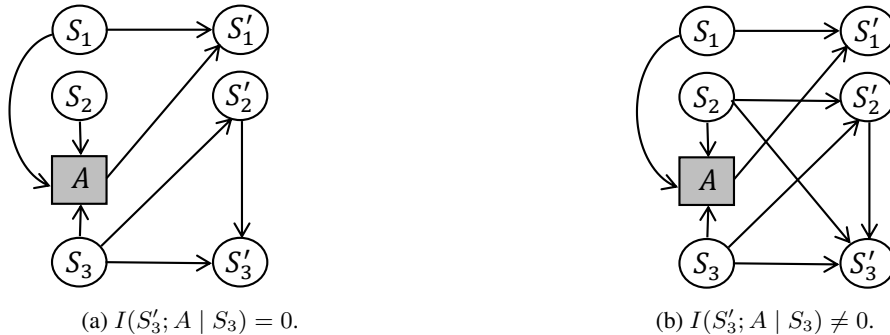
diachronic objective $I(X'; A, E, E' | X) = 0$ or the full objective $I(X'; A, E | X) = 0$. In this appendix, we analyze the properties of the simplified objective.

It is easy to find examples where the simplified objective fails. Consider the DBN in Figure 21 of an MDP with the state variables S_1, S_2 and S_3 . The policy determining the action depends only on S_2 and S_3 but not on S_1 . All state variables can be endogenous (S_1 and S_2 directly, and S_3 indirectly through its dependence on S_1). However, the MDP satisfies the condition $I(S'_3; A | S_3) = 0$. Hence, we cannot use the simplified objective to safely conclude whether a state variable is exogenous or not when analyzing the 2-timestep DBN.

As we would expect, the simplified setting does not necessarily lead to valid full or diachronic exo/endo decompositions. In this direction, first note that even when the simplified objective returns a set X of variables that are causally exogenous, X and its complement $E = X^c$ may not correspond to a valid exo/endo decomposition (E, X) . Consider for example $X = \{S_3\}$ in Figure 22a, which satisfies $I(X'; A | X) = 0$ but X and the corresponding $E = \{S_1, S_2\}$ are not a valid full exo/endo decomposition because S'_3 depends on S'_2 . This is not the case when using the full or diachronic objectives. Furthermore, it is possible for a state variable X to be exogenous, even though it fails to satisfy $I(X'; A | X) = 0$. Consider $X = \{S_3\}$ in Figure 22b. It may not satisfy $I(S'_3; A | S_3) = 0$ due to the trail $A \leftarrow S_2 \rightarrow S'_3$ from A to S'_3 .

Despite the fact that the simplified objective $I(X'; A | X) = 0$ is not sufficient to identify exogenous variables, it can be used as a simpler proxy for the full objective $I(X'; [E, A] | X) = 0$. Any set of state variables X that satisfies the full objective must necessarily satisfy the simplified objective, since the latter has fewer constraints than the former. Of course, the simplified objective may return an over-estimate of the set of exogenous state variables, possibly contaminated with endogenous components. For this reason, it is always important to check the decomposition $(E = X^c, X)$ that satisfies the simplified objective against the full (or diachronic) objective.

The shortcomings of the simplified objective result from attempting to apply it within the framework of the 2-timestep DBN. If we unroll the DBN and consider the H -horizon MDP, then the simplified objective corresponds to directly checking that all variables in X are disconnected from A and therefore X is causally exogenous. The next theorem resembles Theorem 7 for full or diachronic factorizations.

Figure 22: State transition diagrams for two MDPs. In both MDPs, S_2 and S_3 are exogenous.

Theorem 13. Assume that an H -horizon MDP is admissible, data D has been collected by executing a fully-randomized policy for n steps, and the faithfulness assumption holds for the causal graph \mathcal{G} describing the MDP. If

$$\lim_{n \rightarrow \infty} \hat{I}(X_\tau; A_t | X_t) = 0, \forall t \leq H-1, t+1 \leq \tau \leq H, \quad (31)$$

then X is causally exogenous.

Proof. (sketch) Equation (31) is equivalent to the statement that $P(X_\tau | X_t, A_t) = P(X_\tau | X_t)$ for all t and τ . Under the faithfulness assumption, we can infer that there is no directed path from any A_t to any X_τ . Hence, X is action-disconnected in the causal graph \mathcal{G} , and it follows from Theorem 9 that X is causally exogenous. \square

The reverse direction is trivial. If X is causally exogenous and the faithfulness assumption holds, then the simplified condition must hold between each A_t and every X_τ . It follows that in the unrolled MDP, the simplified objective will detect exactly the exogenous variables (under the assumptions of the theorem).

Theorem 13 has the drawback that it must consider all long-range dependencies, and this requires estimating $P(X_t, X_\tau, A_t)$ for all $t \leq H-1$ and all τ such that $t+1 \leq \tau \leq H$. This makes much less effective use of the data set D . In practical applications, it might be fruitful to explore approximate variants of this theorem that make use of a small number F of forward steps. In this case, we could enforce just F constraints per timestep, i.e., $I(X_{t+k}; A_t | X_t) = 0, \forall 1 \leq k \leq F$, where F is a small number.

C Dynamic Program for the Covariance Condition

Theorem 14. The variance of the H -step return $B^\pi(s; H)$ can be computed as the solution to the following dynamic program:

$$V^\pi(s; 0) := 0; \quad \text{Var}[B^\pi(s; 0)] := 0 \quad (32)$$

$$V^\pi(s; h) := m(s, \pi(s)) + \gamma \mathbb{E}_{s' \sim P(s' | s, \pi(s))} [V^\pi(s'; h-1)] \quad (33)$$

$$\begin{aligned} \text{Var}[B^\pi(s; h)] &:= \sigma^2(s, \pi(s)) - V^\pi(s; h)^2 + \\ &\quad \gamma^2 \mathbb{E}_{s' \sim P(s' | s, \pi(s))} [\text{Var}[B^\pi(s'; h-1)]] + \\ &\quad \mathbb{E}_{s' \sim P(s' | s, \pi(s))} [m(s, \pi(s)) + \gamma V^\pi(s'; h-1)]^2 \end{aligned} \quad (34)$$

Equations (33) and (34) apply for all $h > 0$.

Proof. Sobel (1982) analyzed the variance of infinite horizon discounted MDPs with deterministic rewards. We modify his proof to handle a fixed horizon and stochastic rewards. We proceed by induction on h . To simplify notation, we omit the dependence on π .

Base Case: $H = 0$. This is established by Equations (32).

Inductive Step: $H = h$. Write

$$B(s; h) = R(s) + \gamma B(s'; h-1),$$

where the rhs involves the three random variables $R(s)$, S' , and $B(s'; h-1)$ (with samples $s' \sim S'$). To obtain Equation (33), compute the expected value

$$V(s; h) = \mathbb{E}_{B(s; h)} [B(s; h)] = \mathbb{E}_{s', R(s), B(s'; h-1)} [R(s) + \gamma B(s'; h-1)],$$

and take each expectation in turn. To obtain the formula for the variance, write the standard formula for the variance:

$$\text{Var}[B(s; h)] = \mathbb{E}_{B(s; h)} [B(s; h)^2] - \mathbb{E}_{B(s; h)} [B(s; h)]^2.$$

Substitute $R(s) + \gamma B(s'; h-1)$ in the first term and simplify the second term to obtain

$$\mathbb{E}_{s', R(s), B(s'; h-1)} [\{R(s) + \gamma B(s'; h-1)\}^2] - V(s; h)^2.$$

Expand the square in the first term:

$$\mathbb{E}_{s', R(s), B(s'; h-1)} [R(s)^2 + 2R(s)\gamma B(s'; h-1) + \gamma^2 B(s'; h-1)^2] - V(s; h)^2.$$

Distribute the two innermost expectations over the sum:

$$\mathbb{E}_{s'} [\mathbb{E}_{R(s)} [R(s)^2] + 2m(s)\gamma V(s'; h-1) + \gamma^2 \mathbb{E}_{B(s'; h-1)} [B(s'; h-1)^2]] - V(s; h)^2.$$

Apply the definition of variance in reverse to terms 1 and 3 in brackets:

$$\mathbb{E}_{s'}[\text{Var}[R(s)] + m(s)^2 + 2m(s)\gamma V(s'; h-1) + \gamma^2 \text{Var}[B(s; h-1)] + \gamma^2 V(s'; h-1)^2] - V(s; h)^2$$

Factor the quadratic involving terms 1, 3, and 4:

$$\mathbb{E}_{s'}[\sigma^2(s) + [m(s) + \gamma V(s'; h-1)]^2 + \gamma^2 \text{Var}[B(s'; h-1)]] - V(s; h)^2.$$

Finally, distribute the expectation with respect to s' to obtain Equation (34). \square

Theorem 15. *The covariance between the exogenous H -step return $B_x^\pi(x; H)$ and the endogenous H -step return $B_e^\pi(e, x; H)$ can be computed via the following dynamic program:*

$$\text{Cov}[B_x^\pi(x; 0), B_e^\pi(e, x; 0)] := 0 \tag{35}$$

$$\begin{aligned} \text{Cov}[B_x^\pi(x; h), B_e^\pi(e, x; h)] := & \\ & \gamma^2 \mathbb{E}_{e' \sim P(e'|e, x), x' \sim P(x'|x)} \{ \text{Cov}[B_x^\pi(x'; h-1), B_e^\pi(e', x'; h-1)] + \\ & [m_x(x) + \gamma V_x(x'; h-1)] \times [m_e(e, x, \pi(e, x)) + \gamma V_e^\pi(e', x'; h-1)] \} \\ & - V_x^\pi(x; h) V_e^\pi(e, x; h). \end{aligned} \tag{36}$$

Equation (36) applies for all $h > 0$.

Proof. By induction. The base case is established by Equation (35). For the inductive case, we begin with the formula for non-centered covariance:

$$\text{Cov}[B_x(x; h), B_e(e, x; h)] = \mathbb{E}_{B_x(x; h), B_e(e, x; h)}[B_x(x; h)B_e(e, x; h)] - V_x(x; h)V_e(e, x; h).$$

Replace $B_x(x; h)$ by $R_x(x) + \gamma B_x(x'; h-1)$ and $B_e(e, x; h)$ by $R_e(e, x) + \gamma B_e(e', x'; h-1)$ and replace the expectations wrt $B_x(x; h)$ and $B_e(e, x; h)$ by expectations wrt the six variables $\{e' \sim E', x' \sim X', R_x(x), R_e(e, x), B_x(x'; h-1), B_e(e', x'; h-1)\}$. We will use the following abbreviations for these variables: $s' = \{e', x'\}$, $r = \{R_e(x), R_e(e, x)\}$, and $B = \{B_x(x'; h-1), B_e(e', x'; h-1)\}$.

$$\begin{aligned} \text{Cov}[B_x(x; h), B_e(e, x; h)] = & -V_x(x; h)V_e(e, x; h) + \\ & \mathbb{E}_{s', r, B}[(R_x(x) + \gamma B_x(x'; h-1))(R_e(e, x) + \gamma B_e(e', x'; h-1))]. \end{aligned}$$

We will focus on the expectation term. Multiply out the two terms and distribute the expectations wrt r and B :

$$\begin{aligned} \mathbb{E}_{s'}[m_x(x)m_e(e, x) + \gamma m_x(x)V_e(e', x'; h-1) + \gamma m_e(e, x)V_x(x'; h-1) + \\ \gamma^2 \mathbb{E}_B[B_x(x'; h-1)B_e(e', x'; h-1)]]]. \end{aligned}$$

Apply the non-centered covariance formula “in reverse” to term 4.

$$\begin{aligned} \mathbb{E}_{s'}[m_x(x)m_e(e, x) + \gamma m_x(x)V_e(e', x'; h-1) + \gamma m_e(e, x)V_x(x'; h-1) + \\ \gamma^2 V_x(x'; h-1)V_e(e', x'; h-1) + \gamma^2 \text{Cov}[B_x(x'; h-1)B_e(e', x'; h-1)]]]. \end{aligned}$$

Distribute expectation with respect to s' :

$$\begin{aligned} m_x(x)m_e(e, x) + \gamma m_x(x)\mathbb{E}_{s'}[V_e(e', x'; h-1)] + \gamma m_e(e, x)\mathbb{E}_{s'}[V_x(x'; h-1)] + \\ \gamma^2 \mathbb{E}_{s'}[V_x(x'; h-1)]\mathbb{E}_{s'}[V_e(e', x'; h-1)] + \gamma^2 \text{Cov}[B_x(x'; h-1)B_e(e', x'; h-1)] \end{aligned}$$

Obtain Equation (36) by factoring the first four terms, writing the expectations explicitly, and including the $-V_x(x; h)V_e(e, x; h)$ term. \square

To gain some intuition for this theorem, examine the three terms on the right-hand side of Equation (36). The first is the “recursive” covariance for $h-1$. The second is the one-step non-centered covariance, which is the expected value of the product of the backed-up values for V_e^π and V_x^π . The third term is the product of V_e^π and V_x^π for the current state, which re-centers the covariance.

References

- P.-A. Absil, R. Mahony, and R. Sepulchre. *Optimization Algorithms on Matrix Manifolds*. Princeton University Press, Princeton, NJ, USA, 2007.
- Alexander Alemi, Ben Poole, Ian Fischer, Joshua Dillon, Rif A. Saurous, and Kevin Murphy. Fixing a broken ELBO. In *Proceedings of the 35th International Conference on Machine Learning*, volume 80, pages 159–168, 2018.
- Lynton Ardizzone, Jakob Kruse, Carsten Rother, and Ullrich Köthe. Analyzing inverse problems with invertible neural networks. In *International Conference on Learning Representations*, 2019.
- Kunihiro Baba, Ritei Shibata, and Masaaki Sibuya. Partial correlation and conditional correlation as measures of conditional independence. *Australian & New Zealand Journal of Statistics*, 46(4):657–664, 2004.
- Francis R. Bach and Michael I. Jordan. Kernel independent component analysis. *J. Mach. Learn. Res.*, 3:1–48, 2003.
- Adrià Puigdomènech Badia, Pablo Sprechmann, Alex Vitvitskiy, Daniel Guo, Bilal Piot, Steven Kapturowski, Olivier Tieleman, Martin Arjovsky, Alexander Pritzel, Andrew Bolt, and Charles Blundell. Never give up: Learning directed exploration strategies. In *International Conference on Learning Representations*, 2020.
- David Barber and Felix Agakov. The im algorithm: A variational approach to information maximization. In *Proceedings of the 16th International Conference on Neural Information Processing Systems*, page 201–208, 2003.
- Jens Behrmann, Paul Vicol, Kuan-Chieh Wang, Roger Grosse, and Joern-Henrik Jacobsen. Understanding and mitigating exploding inverses in invertible neural networks. In *Proceedings of The 24th International Conference on Artificial Intelligence and Statistics*, volume 130 of *Proceedings of Machine Learning Research*, pages 1792–1800. PMLR, 2021.
- Mohamed Ishmael Belghazi, Aristide Baratin, Sai Rajeshwar, Sherjil Ozair, Yoshua Bengio, Aaron Courville, and Devon Hjelm. Mutual information neural estimation. In *Proceedings of the 35th International Conference on Machine Learning*, volume 80, pages 531–540. PMLR, 2018.
- Marc Bellemare, Sriram Srinivasan, Georg Ostrovski, Tom Schaul, David Saxton, and Remi Munos. Unifying count-based exploration and intrinsic motivation. In *Advances in Neural Information Processing Systems*, volume 29, 2016.
- Marc G. Bellemare, Joel Veness, and Michael Bowling. Investigating contingency awareness using atari 2600 games. In *Proceedings of the Twenty-Sixth AAAI Conference on Artificial Intelligence*, AAAI’12, page 864–871, 2012.
- James Bergstra and Yoshua Bengio. Random search for hyper-parameter optimization. *J. Mach. Learn. Res.*, 13: 281–305, 2012.
- Åke Björck and Gene H. Golub. Numerical methods for computing angles between linear subspaces. *Mathematics of Computation*, 27(123):579–594, 1973.
- David M. Blei, Alp Kucukelbir, and Jon D. McAuliffe. Variational inference: A review for statisticians. *Journal of the American Statistical Association*, 112(518):859–877, 2017.
- Robert Bray. Markov decision processes with exogenous variables. *Management Science*, 65(10):4598–4606, 2019.
- Greg Brockman, Vicki Cheung, Ludwig Pettersson, Jonas Schneider, John Schulman, Jie Tang, and Wojciech Zaremba. Openai gym, 2016.
- Lars Buitinck, Gilles Louppe, Mathieu Blondel, Fabian Pedregosa, Andreas Mueller, Olivier Grisel, Vlad Niculae, Peter Prettenhofer, Alexandre Gramfort, Jaques Grobler, Robert Layton, Jake VanderPlas, Arnaud Joly, Brian Holt, and Gaël Varoquaux. API design for machine learning software: experiences from the scikit-learn project. In *ECML PKDD Workshop: Languages for Data Mining and Machine Learning*, pages 108–122, 2013.
- Yuri Burda, Harrison Edwards, Amos Storkey, and Oleg Klimov. Exploration by random network distillation. In *International Conference on Learning Representations*, 2019.
- Dian Chen, Vladlen Koltun, and Philipp Krähenbühl. Learning to drive from a world on rails. In *2021 IEEE/CVF International Conference on Computer Vision (ICCV)*, pages 15570–15579, 2021.
- Rohan Chitnis and Tomás Lozano-Pérez. Learning compact models for planning with exogenous processes. In *Proceedings of the Conference on Robot Learning*, volume 100 of *Proceedings of Machine Learning Research*, pages 813–822, 2020.
- Jongwook Choi, Yijie Guo, Marcin Moczulski, Junhyuk Oh, Neal Wu, Mohammad Norouzi, and Honglak Lee. Contingency-aware exploration in reinforcement learning. In *International Conference on Learning Representations*, 2019.

- Oriol Corcoll, Youssef Sherif Mansour Mohamed, and Raul Vicente. Did i do that? blame as a means to identify controlled effects in reinforcement learning. *Transactions on Machine Learning Research*, 2022.
- Thomas Dietterich, George Trimponias, and Zhitang Chen. Discovering and removing exogenous state variables and rewards for reinforcement learning. In *Proceedings of the 35th International Conference on Machine Learning*, volume 80, pages 1262–1270. PMLR, 2018.
- M. D. Donsker and S. R.S. Varadhan. Asymptotic evaluation of certain markov process expectations for large time. iv. *Communications on Pure and Applied Mathematics*, 36(2):183–212, 1983.
- Alan Edelman, Tomás A. Arias, and Steven T. Smith. The geometry of algorithms with orthogonality constraints. *SIAM J. Matrix Anal. Appl.*, 20(2):303–353, 1999.
- Yonathan Efroni, Dylan J Foster, Dipendra Misra, Akshay Krishnamurthy, and John Langford. Sample-efficient reinforcement learning in the presence of exogenous information. In *Proceedings of Thirty Fifth Conference on Learning Theory*, volume 178, pages 5062–5127, 2022a.
- Yonathan Efroni, Dipendra Misra, Akshay Krishnamurthy, Alekh Agarwal, and John Langford. Provably filtering exogenous distractors using multistep inverse dynamics. In *International Conference on Learning Representations*, 2022b.
- Raphael Fonteneau, Susan A Murphy, Louis Wehenkel, and Damien Ernst. Batch mode reinforcement learning based on the synthesis of artificial trajectories. *Annals of Operations Research*, 208(1):383–416, 2012. doi: 10.1007/s10479-012-1248-5.
- Stephen H. Friedberg, Arnold J. Insel, and Lawrence E. Spence. *Linear algebra*. Pearson Education, 4th ed. edition, 2002.
- Kenji Fukumizu, Francis R Bach, and Michael I Jordan. Dimensionality reduction for supervised learning with reproducing kernel hilbert spaces. *Journal of Machine Learning Research*, 5(Jan):73–99, 2004.
- Kenji Fukumizu, Arthur Gretton, Xiaohai Sun, and Bernhard Schölkopf. Kernel measures of conditional dependence. In *Advances in neural information processing systems*, pages 489–496, 2008.
- Nick Haber, Damian Mrowca, Stephanie Wang, Li F Fei-Fei, and Daniel L Yamins. Learning to play with intrinsically-motivated, self-aware agents. In *Advances in Neural Information Processing Systems*, volume 31, 2018.
- Yanjun Han, Jiantao Jiao, Tsachy Weissman, and Yihong Wu. Optimal rates of entropy estimation over Lipschitz balls. *The Annals of Statistics*, 48(6):3228 – 3250, 2020.
- R. Devon Hjelm, Alex Fedorov, Samuel Lavoie-Marchildon, Karan Grewal, Philip Bachman, Adam Trischler, and Yoshua Bengio. Learning deep representations by mutual information estimation and maximization. In *7th International Conference on Learning Representations, ICLR*, 2019.
- Rein Houthoofd, Xi Chen, Xi Chen, Yan Duan, John Schulman, Filip De Turck, and Pieter Abbeel. Vime: Variational information maximizing exploration. In *Advances in Neural Information Processing Systems*, volume 29, 2016.
- Bo Jiang and Yu-Hong Dai. A framework of constraint preserving update schemes for optimization on stiefel manifold. *Math. Program.*, 153(2):535–575, 2015.
- Kirthevasan Kandasamy, Akshay Krishnamurthy, Barnabys Póczos, Larry Wasserman, and James M. Robins. Non-parametric von mises estimators for entropies, divergences and mutual informations. In *Proceedings of the 28th International Conference on Neural Information Processing Systems - Volume 1*, page 397–405, 2015.
- Diederik P. Kingma and Jimmy Ba. Adam: A method for stochastic optimization. In *ICLR*, 2015.
- Ivan Kobyzev, Simon J.D. Prince, and Marcus A. Brubaker. Normalizing flows: An introduction and review of current methods. *IEEE Transactions on Pattern Analysis and Machine Intelligence*, 43(11):3964–3979, 2021.
- Niklas Koenen, Marvin N. Wright, Peter Maass, and Jens Behrmann. Generalization of the change of variables formula with applications to residual flows. In *ICML Workshop on Invertible Neural Networks, Normalizing Flows, and Explicit Likelihood Models*, 2021.
- Daphne Koller and Nir Friedman. *Probabilistic Graphical Models: Principles and Techniques*. The MIT Press, Cambridge, MA, 2009.
- Alexander Kraskov, Harald Stögbauer, and Peter Grassberger. Estimating mutual information. *Phys. Rev. E*, 69, 2004.
- David McAllester and Karl Stratos. Formal limitations on the measurement of mutual information. In *Proceedings of the Twenty Third International Conference on Artificial Intelligence and Statistics*, volume 108, pages 875–884. PMLR, 2020.
- Sean McGregor, Rachel Houtman, Claire Montgomery, Ronald Metoyer, and Thomas G. Dietterich. Factoring Exogenous State for Model-Free Monte Carlo. *arXiv 1703.09390*, 2017.

- Kevin R. Moon, Kumar Sricharan, and Alfred O. Hero. Ensemble estimation of mutual information. In *2017 IEEE International Symposium on Information Theory (ISIT)*, pages 3030–3034, 2017.
- XuanLong Nguyen, Martin J Wainwright, and Michael Jordan. Estimating divergence functionals and the likelihood ratio by penalized convex risk minimization. In *Advances in Neural Information Processing Systems*, volume 20, 2007.
- Sebastian Nowozin, Botond Cseke, and Ryota Tomioka. F-gan: Training generative neural samplers using variational divergence minimization. In *Proceedings of the 30th International Conference on Neural Information Processing Systems*, page 271–279, 2016.
- Junhyuk Oh, Xiaoxiao Guo, Honglak Lee, Richard Lewis, and Satinder Singh. Action-conditional video prediction using deep networks in atari games. In *Proceedings of the 28th International Conference on Neural Information Processing Systems - Volume 2*, page 2863–2871, 2015.
- Georg Ostrovski, Marc G. Bellemare, Aäron van den Oord, and Rémi Munos. Count-based exploration with neural density models. In *Proceedings of the 34th International Conference on Machine Learning - Volume 70*, page 2721–2730, 2017.
- Keiran Paster, Sheila A. McIlraith, and Jimmy Ba. Planning from pixels using inverse dynamics models. In *International Conference on Learning Representations*, 2021.
- Adam Paszke, Sam Gross, Francisco Massa, Adam Lerer, James Bradbury, Gregory Chanan, Trevor Killeen, Zeming Lin, Natalia Gimelshein, Luca Antiga, Alban Desmaison, Andreas Kopf, Edward Yang, Zachary DeVito, Martin Raison, Alykhan Tejani, Sasank Chilamkurthy, Benoit Steiner, Lu Fang, Junjie Bai, and Soumith Chintala. Pytorch: An imperative style, high-performance deep learning library. In *Advances in Neural Information Processing Systems 32*, pages 8024–8035, 2019.
- Deepak Pathak, Pulkit Agrawal, Alexei A. Efros, and Trevor Darrell. Curiosity-driven exploration by self-supervised prediction. In *Proceedings of the 34th International Conference on Machine Learning - Volume 70*, page 2778–2787, 2017.
- Judea Pearl. *Probabilistic Reasoning in Intelligent Systems: Networks of Plausible Inference*. Morgan Kaufmann Publishers Inc., San Francisco, CA, USA, 1988.
- Judea Pearl. *Causality: Models, Reasoning and Inference*. Cambridge University Press, USA, 2nd edition, 2009.
- Ben Poole, Sherjil Ozair, Aaron Van Den Oord, Alex Alemi, and George Tucker. On variational bounds of mutual information. In *Proceedings of the 36th International Conference on Machine Learning*, volume 97, pages 5171–5180. PMLR, 2019.
- Martin L. Puterman. *Markov Decision Processes: Discrete Stochastic Dynamic Programming*. John Wiley & Sons, Inc., New York, NY, USA, 1st edition, 1994.
- Antonin Raffin, Ashley Hill, Adam Gleave, Anssi Kanervisto, Maximilian Ernestus, and Noah Dormann. Stable-baselines3: Reliable reinforcement learning implementations. *Journal of Machine Learning Research*, 22(268):1–8, 2021.
- Kate Rakelly, Abhishek Gupta, Carlos Florensa, and Sergey Levine. Which mutual-information representation learning objectives are sufficient for control? In *Advances in Neural Information Processing Systems*, volume 34, pages 26345–26357, 2021.
- Danilo Rezende and Shakir Mohamed. Variational inference with normalizing flows. In *Proceedings of the 32nd International Conference on Machine Learning*, volume 37 of *Proceedings of Machine Learning Research*, pages 1530–1538. PMLR, 2015.
- Shashank Singh and Barnabás Póczos. Nonparanormal information estimation. In *Proceedings of the 34th International Conference on Machine Learning*, volume 70 of *Proceedings of Machine Learning Research*, pages 3210–3219, 2017.
- Matthew J. Sobel. The Variance of Discounted Markov Decision Processes. *Journal of Applied Probability*, 19(4): 394–402, 1982.
- Yuhang Song, Jianyi Wang, Thomas Lukasiewicz, Zhenghua Xu, Shangdong Zhang, Andrzej Wojcicki, and Mai Xu. Mega-reward: Achieving human-level play without extrinsic rewards. *Proceedings of the AAAI Conference on Artificial Intelligence*, 34(04):5826–5833, 2020.
- P. Spirtes, C. Glymour, and R. Scheines. *Causation, Prediction, and Search*. MIT press, 2nd edition, 2000.
- E. Stiefel. Richtungsfelder und fernparallelismus in n-dimensionalen mannigfaltigkeiten. *Commentarii Mathematici Helvetici*, 8(1):305–353, 1935.

- Richard S. Sutton and Andrew G. Barto. *Introduction to Reinforcement Learning*. MIT Press, Cambridge, MA, USA, 1st edition, 1998.
- Valentin Thomas, Emmanuel Bengio, William Fedus, Jules Pongard, Philippe Beaudoin, Hugo Larochelle, Joelle Pineau, Doina Precup, and Yoshua Bengio. Disentangling the independently controllable factors of variation by interacting with the world. *CoRR*, abs/1802.09484, 2018.
- Andrey N. Tikhonov and Vasiliy Y. Arsenin. *Solutions of ill-posed problems*. V. H. Winston & Sons, Washington, D.C.: John Wiley & Sons, New York, 1977.
- James Townsend, Niklas Koep, and Sebastian Weichwald. Pymanopt: A python toolbox for optimization on manifolds using automatic differentiation. *Journal of Machine Learning Research*, 17(137):1–5, 2016.
- L.W. Tu. *An Introduction to Manifolds*. Universitext. Springer New York, 2010.
- Aaron van den Oord, Yazhe Li, and Oriol Vinyals. Representation learning with contrastive predictive coding. *CoRR*, abs/1807.03748, 2018. URL <http://arxiv.org/abs/1807.03748>.
- Mengjiao Yang, Dale Schuurmans, Pieter Abbeel, and Ofir Nachum. Dichotomy of Control: Separating What You Can Control from What You Cannot. *arXiv*, 2210.13435(v1):1–19, 2022. URL <http://arxiv.org/abs/2210.13435>.
- Xianli Zeng, Yingcun Xia, and Howell Tong. Jackknife approach to the estimation of mutual information. *Proceedings of the National Academy of Sciences*, 115(40):9956–9961, 2018.